

NASA TECHNICAL NOTE



NASA TN D-4322

c.1

LOAN COPY: RE
AFWL (WL)
KIRTLAND AFB



NASA TN D-4322

STATIC AND DYNAMIC
LONGITUDINAL STABILITY DERIVATIVES
OF A POWERED 0.18-SCALE MODEL
OF A FAN-IN-WING VTOL AIRCRAFT

by Joseph R. Chambers and Sue B. Grafton

Langley Research Center

Langley Station, Hampton, Va.



STATIC AND DYNAMIC LONGITUDINAL STABILITY DERIVATIVES
OF A POWERED 0.18-SCALE MODEL OF A
FAN-IN-WING VTOL AIRCRAFT

By Joseph R. Chambers and Sue B. Grafton

Langley Research Center
Langley Station, Hampton, Va.

NATIONAL AERONAUTICS AND SPACE ADMINISTRATION

For sale by the Clearinghouse for Federal Scientific and Technical Information
Springfield, Virginia 22151 - CFSTI price \$3.00

STATIC AND DYNAMIC LONGITUDINAL STABILITY DERIVATIVES
OF A POWERED 0.18-SCALE MODEL OF A
FAN-IN-WING VTOL AIRCRAFT

By Joseph R. Chambers and Sue B. Grafton
Langley Research Center

SUMMARY

An investigation was conducted to determine the static and dynamic longitudinal stability derivatives of a powered fan-in-wing V/STOL aircraft model for trimmed level flight at an angle of attack of 0° . The model had a lift fan located in each wing panel and a smaller fan located in the nose for pitch control. The investigation covered a range of values of thrust condition and oscillatory frequencies for the model with the horizontal tail both on and off.

The results of the investigation indicate that the model was statically unstable with respect to angle of attack and was statically stable with respect to velocity for the lower speeds for fan-powered flight; these trends tended to reverse as the transition to conventional wingborne flight progressed. The model had positive damping in pitch (negative values of the damping-in-pitch parameter) throughout the ranges of test conditions investigated.

INTRODUCTION

The interest in fan-in-wing V/STOL aircraft has become so substantial that there now exists a need to obtain detailed force-test data for stability and performance analysis of this type of vehicle. The present investigation was therefore undertaken to provide some experimentally measured static and dynamic longitudinal stability derivatives of a 0.18-scale model of a fan-in-wing aircraft. The results of free-flight tests of the model are presented in reference 1.

The investigation of the fan-powered flight conditions covered an angle-of-attack range from -20° to 20° and a range of louver deflection angles from 0° (louvers positioned for hovering flight) to 40° (louvers positioned for fan-powered forward flight). Tests were made for several thrust conditions and oscillatory frequencies for the model with the horizontal tail both on and off. In addition to these power-on tests for hovering flight

and transition flight, power-off tests were conducted with the fan inlet and exit closures closed to acquire similar data for conventional wingborne forward flight.

SYMBOLS AND NOMENCLATURE

All quantities with the exception of lift and drag are presented with respect to the system of body axes shown in figure 1. Inasmuch as conventional nondimensional coefficients lose their significance and tend to become infinite as the airspeed approaches zero, a major portion of the damping data is presented in dimensional form. Dimensional values are given both in U.S. Customary Units and in the International System of Units (SI). Factors relating the two systems are given in reference 2. Included in each presentation of data are the values of nondimensionalizing parameters required for converting the data to standard coefficient form.

\bar{c}	mean aerodynamic chord, feet (meters)
F_X	force along X body axis, pounds (newtons)
F_Z	force along Z body axis, pounds (newtons)
f	frequency of oscillation, cycles per second
I_Y	moment of inertia about Y body axis, slug-feet ² (kilogram-meters ²)
i_t	tail incidence angle, degrees
k	reduced-frequency parameter, $\omega\bar{c}/2V$
L_0	value of lift for longitudinal acceleration equal to zero at an angle of attack of 0°, pounds (newtons)
M_Y	pitching moment, foot-pounds (meter-newtons)
q	pitching velocity, radians per second
q_∞	free-stream dynamic pressure, $\rho V^2/2$, pounds per square foot (newtons per square meter)
S	wing area, square feet (square meters)

V	free-stream velocity, feet per second (meters per second)
W	weight, pounds (newtons)
W/S	wing loading, pounds per square foot (newtons per square meter)
X,Y,Z	body reference axes (see fig. 1)
α	angle of attack, degrees or radians
δ_a	aileron droop angle (both ailerons down), degrees
δ_f	flap deflection, degrees
δ_L	exit-louver deflection angle, degrees
ρ	air density, slugs per cubic foot (kilograms per cubic meter)
ω	angular velocity, $2\pi f$, radians per second

$$C_X = \frac{F_X}{q_\infty S} \quad C_Z = \frac{F_Z}{q_\infty S} \quad C_m = \frac{M_Y}{q_\infty S \bar{c}}$$

$$C_D = \frac{\text{Drag}}{q_\infty S} \quad C_L = \frac{\text{Lift}}{q_\infty S} \quad C_{m_{i_t}} = \frac{\partial C_m}{\partial i_t}$$

$$M_{Y_V} = \frac{\partial M_Y}{\partial V} \quad F_{X_V} = \frac{\partial F_X}{\partial V} \quad F_{Z_V} = \frac{\partial F_Z}{\partial V}$$

$$F_{X_\alpha} = \frac{\partial F_X}{\partial \alpha} \quad F_{Z_\alpha} = \frac{\partial F_Z}{\partial \alpha} \quad M_{Y_\alpha} = \frac{\partial M_Y}{\partial \alpha}$$

$$F_{X_{\dot{\alpha}}} = \frac{\partial F_X}{\partial \dot{\alpha}} \quad F_{Z_{\dot{\alpha}}} = \frac{\partial F_Z}{\partial \dot{\alpha}} \quad M_{Y_{\dot{\alpha}}} = \frac{\partial M_Y}{\partial \dot{\alpha}}$$

$$F_{X_q} = \frac{\partial F_X}{\partial q} \quad F_{Z_q} = \frac{\partial F_Z}{\partial q} \quad M_{Y_q} = \frac{\partial M_Y}{\partial q}$$

$$F_{X_{\dot{q}}} = \frac{\partial F_X}{\partial \dot{q}} \quad F_{Z_{\dot{q}}} = \frac{\partial F_Z}{\partial \dot{q}} \quad M_{Y_{\dot{q}}} = \frac{\partial M_Y}{\partial \dot{q}}$$

$$\begin{array}{ccc}
C_{X\alpha} = \frac{\partial C_X}{\partial \alpha} & C_{Z\alpha} = \frac{\partial C_Z}{\partial \alpha} & C_{m\alpha} = \frac{\partial C_m}{\partial \alpha} \\
C_{X\dot{\alpha}} = \frac{\partial C_X}{\partial \frac{\dot{\alpha}\bar{c}}{2V}} & C_{Z\dot{\alpha}} = \frac{\partial C_Z}{\partial \frac{\dot{\alpha}\bar{c}}{2V}} & C_{m\dot{\alpha}} = \frac{\partial C_m}{\partial \frac{\dot{\alpha}\bar{c}}{2V}} \\
C_{Xq} = \frac{\partial C_X}{\partial \frac{q\bar{c}}{2V}} & C_{Zq} = \frac{\partial C_Z}{\partial \frac{q\bar{c}}{2V}} & C_{mq} = \frac{\partial C_m}{\partial \frac{q\bar{c}}{2V}} \\
C_{X\dot{q}} = \frac{\partial C_X}{\partial \frac{\dot{q}\bar{c}^2}{4V^2}} & C_{Z\dot{q}} = \frac{\partial C_Z}{\partial \frac{\dot{q}\bar{c}^2}{4V^2}} & C_{m\dot{q}} = \frac{\partial C_m}{\partial \frac{\dot{q}\bar{c}^2}{4V^2}}
\end{array}$$

A dot over a symbol represents a derivative with respect to time.

In the present investigation the term "in-phase derivative" refers to any one of the oscillatory derivatives that is based on the components of forces and moments in phase with the angle of pitch produced in the oscillatory tests. The term "out-of-phase derivative" refers to any one of the stability derivatives that is based on the components of forces and moments 90° out of phase with the angle of pitch. The oscillatory derivatives of the present investigation were measured in the following combinations:

Nondimensional

In phase	Out of phase
$C_{m\alpha} - k^2 C_{m\dot{q}}$	$C_{mq} + C_{m\dot{\alpha}}$
$C_{Z\alpha} - k^2 C_{Z\dot{q}}$	$C_{Zq} + C_{Z\dot{\alpha}}$
$C_{X\alpha} - k^2 C_{X\dot{q}}$	$C_{Xq} + C_{X\dot{\alpha}}$

Dimensional

In phase	Out of phase
$M_{Y\alpha} - \omega^2 M_{Y\dot{q}}$	$M_{Yq} + M_{Y\dot{\alpha}}$
$F_{Z\alpha} - \omega^2 F_{Z\dot{q}}$	$F_{Zq} + F_{Z\dot{\alpha}}$
$F_{X\alpha} - \omega^2 F_{X\dot{q}}$	$F_{Xq} + F_{X\dot{\alpha}}$

TEST EQUIPMENT AND TECHNIQUE

Tunnel

The tests were made in the 30- by 60-foot (9.1- by 18.3-meter) open-throat test section of the Langley full-scale tunnel with the model mounted about 10 feet (3.05 meters) above a ground board. No corrections for flow angularity or blockage have been applied to the data since these effects were believed to be negligible.

Model

Photographs of the fan-in-wing model used in the investigation are presented in figure 2. A three-view sketch showing some of the more important model dimensions is presented in figure 3. Geometric characteristics of the model are listed in table I.

The model had a geometrically scaled lift fan located in each wing panel and a smaller fan located in the nose for pitch control (see fig. 2). The doors beneath the nose fan were used to control, or modulate, the thrust of the nose fan. Exit vanes (or louvers) were located beneath each wing fan and were used to deflect the fan efflux rearward and thereby impart forward thrust to the aircraft. Each wing fan incorporated closure doors to seal the wing-fan inlets during simulation of conventional jet-powered flight. The doors remained in the open position during the fan-powered tests and were closed for the power-off tests.

The model fans were driven by tip turbines powered by compressed air supplied through flexible plastic tubing. The tubing was attached to the model as close as possible to the moment center to minimize air pressure inputs to the data. Additional information regarding the model may be found in reference 1.

Apparatus

Both the static and dynamic force tests were made with a single-strut support system and a strain-gage balance. This setup is illustrated in figure 4. The model and the strain-gage balance, which joined the model to the steel channel of the yoke-pivot assembly, were mounted so that the moment reference center of both was on the vertical axis of the yoke-pivot assembly. A single degree of oscillatory motion was imparted to the model by means of a flywheel that was driven by a 3-horsepower (2.2-kilowatt) variable-speed electric motor and a system of push rods and bell cranks. The amplitude of the oscillatory motion (limited to $\pm 30^\circ$) was adjusted by varying the location of the lower pivot point of the vertical connecting rod along the radius of the flywheel. The frequency of the oscillatory motion (limited to about 2 cycles per second) was varied by changing the speed of the electric motor.

A precision sine-cosine potentiometer, which generated voltage signals proportional to the sine and cosine of the flywheel rotation angle, was coupled directly to the flywheel shaft and provided electrical signals proportional to the angular displacement and angular velocity of the model. These signals were used in the data readout procedure, which is described in detail in reference 3.

The compressed air supply was varied remotely and pressure regulators were used to hold a constant power input. The position of the wing-fan exit louvers and nose-fan modulator doors was also controlled remotely.

Test Procedures

The test procedure used in the investigation can best be explained by describing a typical test. The static tests for each condition were first conducted to determine trim conditions. This was accomplished by setting the model at an angle of attack of 0° ($\Delta\alpha = 0^{\circ}$, nonoscillatory) and bringing the tunnel airspeed up to the desired test velocity. The strain-gage return signals were switched to the static readout equipment, and the compressed airpower for the fans was then increased until the net longitudinal force was zero for that particular exit-louver angle. The position of the nose-fan modulator doors was then varied until the net pitching moment was zero; in other words, the model was trimmed with respect to both longitudinal force and pitching moment. The model power was then held constant and angle of attack was varied to determine stability with respect to angle of attack. After the static tests, the oscillatory-drive mechanism was started and a dynamic force test was conducted. By testing in this manner, similar test conditions were insured for both static and dynamic force tests; this fact becomes important for powered models with several surface settings and at low forward speeds such as were used in these tests. Variation of the thrust condition was accomplished by varying tunnel speed while maintaining power equal to that for the trim condition.

TESTS

Fan-Powered Tests

The power-on static and oscillatory force tests were made for an angle-of-attack range from -20° to 20° for exit-louver angles of 10° , 20° , 30° , and 40° . The tests were conducted by setting the louver deflection angle and first varying angle of attack while holding a constant airspeed and a constant power input. The objective of this first series of tests was to determine the angle-of-attack stability of the configuration. During a second series of tests, tunnel airspeed was varied while power was held constant to determine the speed stability of the model. In all tests for fan-powered flight, the flaps were deflected 45° and the ailerons were drooped 15° . The variation of tail-incidence

angle and nose-fan modulator-door position with exit-louver deflection angle is shown in figure 5. The tail incidence was chosen to correspond to positions used on the full-scale airplane and the nose-door position was dictated by pitch trim requirements. Additional information regarding the nose doors and their effectiveness may be found in reference 1. The landing gear remained on the model for all fan-powered tests. The forced-oscillation tests were made for an oscillation amplitude of $\pm 5^\circ$. On the basis of the flight tests of reference 1, the range of reduced-frequency parameter k (0.05 to 0.26) is believed to be representative of the frequency of the oscillations of the model in this flight range.

Static and dynamic tests were also conducted for a louver angle of 0° to determine static and dynamic stability derivatives for the configuration in hovering flight. The static tests for this condition consisted of determination of the variation of forces and moments with velocity perturbations about the hovering condition.

Power-Off Tests

Static and dynamic tests were also conducted to determine the longitudinal stability derivatives of the model for conventional wingborne flight. For these tests, the nose-fan and wing-fan inlets were sealed, the nose-fan exit doors were closed, and the wing-fan exit louvers were rotated rearward until they were fully closed and flush with the lower wing surface to provide a smooth wing contour. Tests were conducted with and without the landing gear on the model. With the landing gear on, the model was tested with the flaps deflected 45° and the ailerons drooped 15° ; with the landing gear off, the model was tested with the flaps and ailerons deflected 0° . The effects of the horizontal tail, the horizontal-tail incidence, and the oscillatory frequency were investigated.

RESULTS AND DISCUSSION

Presentation of Results

The results of the tests are discussed individually as static stability characteristics (figs. 6 to 18), in-phase oscillatory derivatives (figs. 19 to 33), out-of-phase oscillatory derivatives (figs. 34 to 39), and stability characteristics in transition (figs. 50 and 51). An outline of the contents of the data figures is as follows:

	Figures
Static stability characteristics:	
Fan-powered tests	6 to 14
Power-off tests	15 to 18

In-phase oscillatory derivatives:

Fan-powered tests 19 to 26 and 29 to 32
 Power-off tests 27, 28, and 33

Out-of-phase oscillatory derivatives:

Fan-powered tests 34 to 42 and 44 to 47
 Power-off tests 43, 48, and 49

Stability characteristics in transition 50 and 51

Static Stability Characteristics

The data presented in figure 6 for the hovering configuration indicate that the model had positive stability with respect to speed (positive value of M_{YV}), positive translational damping (negative value of F_{XV}), and negligible variation of vertical force with horizontal velocity (near zero values of F_{ZV}). These trends are characteristic of most propeller or fan-powered VTOL aircraft in hovering flight, and these parameters are the important stability derivatives defining the unstable control-fixed oscillation which occurred during the hovering flight tests. (See ref. 1.) In addition, the data indicate that the forces and moments depend very little on angle of attack for small velocity perturbations. The data for an angle of attack of -90° indicate that the model had positive damping of vertical motion in hovering flight. The results for variations of F_X and M_Y with vertical velocity ($\alpha = -90^\circ$) are not plotted because no systematic variation was obtained.

The data of figures 7 to 10 for louver deflection angles corresponding to transition flight conditions indicate that the model was statically unstable with respect to angle of attack for the lower values of exit-louver deflection (that is, at low airspeeds). However, as the louver angle increased (and trimmed forward speed increased), the instability became less, and for $\delta_L = 40^\circ$ the model was about neutrally stable. Full-scale data for similar configurations (refs. 4 and 5) indicate that the nose-fan modulator doors were the primary cause of the angle-of-attack instability. Evidently the flow from the pitch fan is deflected into the region of the horizontal tail, which reduces the stabilizing contribution of the tail. It should be noted that the instability probably was caused by the particular type of longitudinal control system used on the configuration and may not be characteristic of most lift-fan powered aircraft. The configuration had speed stability (positive M_{YV}) for an exit-louver angle of 10° , but the trend of the data is toward speed instability at the highest louver angle ($\delta_L = 40^\circ$). The data indicate no large change of angle-of-attack stability with thrust condition (that is, with airspeed) as has been found

for other V/STOL types – for example, the tilt-wing configurations (ref. 3). The data of figures 11 to 14 show that as the louver deflection angle increased (trim velocity increases) the horizontal tail became progressively more effective, although the model was only neutrally stable for a louver angle of 40° .

The power-off data of figures 15 to 18 indicate that the model was statically stable for the test conditions investigated. The pitching-moment variation with angle of attack was approximately linear up to the stall. The all-movable horizontal tail was quite effective as evidenced by a sizable value of tail effectiveness ($C_{m_{i_t}} \approx -0.02$ per degree). (See figs. 17 and 18.)

In-Phase Oscillatory Derivatives

The in-phase oscillatory stability derivatives for the complete model presented in figures 19 to 22 generally confirm the results of the static tests. This fact is emphasized by the data of figures 23 to 28 where the in-phase derivatives for a range of oscillation frequencies are compared with slopes taken from the static data. The data of figures 23 to 28 also show that there was very little effect of oscillation frequency on the in-phase derivatives for the range of frequencies covered in the tests.

The data presented in figures 29 to 33 indicate that the horizontal tail produced a stabilizing contribution to static longitudinal stability at low and negative angles of attack, but that the tail was destabilizing at high positive angles of attack. This result of the oscillation tests is in qualitative agreement with the results of the static tests, but the tail contribution seemed more destabilizing in the oscillation tests. This fact is evidently the result of lag effects on the in-phase derivative $M_{Y_\alpha} - \omega^2 M_{Y_q}$.

Out-of-Phase Derivatives

The damping-in-pitch data for the hovering configuration presented in figure 34 show that the model had positive damping, but the magnitude of the damping is small. The addition of the horizontal tail increases the damping somewhat, as does an increase in frequency.

The magnitude of the damping in pitch increases somewhat as the transition from hovering flight to conventional flight progresses. (See figs. 35 to 38.) The variation of damping in pitch with thrust condition is quite systematic, but the derivative combinations $F_{Z_q} + F_{Z_{\dot{\alpha}}}$ and $F_{X_q} + F_{X_{\dot{\alpha}}}$ both vary irregularly with thrust. The addition of the horizontal tail contributes at least one-half the value of damping in pitch, even at the lower louver angles (that is, at the lower airspeeds). (See figs. 39 to 43.) Increase in speed from trimmed flight increases the contribution of the horizontal tail to the total damping.

The test results presented in figures 44 to 49 show that, in general, there was little effect of oscillatory frequency on the damping-in-pitch parameter. The major effect of the reduced-frequency parameter seems to be on the derivative $F_{Zq} + F_{Z\dot{\alpha}}$. However, the effects of this derivative on the longitudinal dynamic stability have been found to be negligible for conventional aircraft, and preliminary calculations indicate the same conclusion for fan-in-wing V/STOL aircraft.

Stability Characteristics During Transition

Some of the results of the investigation for trimmed level flight at an angle of attack of 0° are summarized by the data of figures 50 and 51. Figure 50 presents the variation of exit-louver deflection required for equilibrium flight and figure 51 presents the longitudinal stability characteristics of a full-scale airplane as functions of forward velocity from hovering to conventional forward flight. These parameters were obtained by scaling the model data. The dimensional damping-in-pitch model data were scaled by multiplying by the fourth power of the scale factor (5.5^4) and by the ratio of full-scale speed to model speed. The full-scale airplane was assumed to have a wing loading of 40 lb/ft^2 (1915 N/m^2) and a moment of inertia in pitch I_Y of $15\,000 \text{ slug-ft}^2$ ($20\,337 \text{ kg-m}^2$) on the basis of estimated full-scale values.

Figure 50 presents the exit-louver angle required for trimmed forward flight at various speeds. Based on these data, the full-scale airplane would have a maximum fan-powered forward speed at 40° louver deflection of about 82 knots. The variation of the static stability parameter $M_{Y\alpha} - \omega^2 M_{Y\dot{q}}$ presented in figure 51 shows the airplane to be statically unstable with respect to angle of attack over the fan-powered flight regime except for $V = 0$ and 82 knots, where it is neutrally stable with respect to angle of attack. The variation of the damping-in-pitch parameter $M_{Yq} + M_{Y\dot{\alpha}}$ shows that the damping in pitch increases with increasing forward speed.

CONCLUSIONS

An investigation of the static and dynamic longitudinal stability derivatives of a 0.18-scale model of a fan-in-wing V/STOL aircraft indicated the following conclusions:

1. The model was statically unstable with respect to angle of attack for fan-powered flight, but this instability diminished at high transition speeds.
2. The model possessed speed stability for low-speed fan-powered flight, but as forward speed increased, the trend was toward speed instability.

3. The model had positive damping in pitch (negative values of the damping-in-pitch parameter) for all test conditions.

Langley Research Center,
National Aeronautics and Space Administration,
Langley Station, Hampton, Va., May 11, 1967,
721-01-00-26-23.

REFERENCES

1. Kirby, Robert H.; and Chambers, Joseph R.: Flight Investigation of Dynamic Stability and Control Characteristics of a 0.18-Scale Model of a Fan-in-Wing VTOL Airplane. NASA TN D-3412, 1966.
2. Mechtly, E. A.: The International System of Units – Physical Constants and Conversion Factors. NASA SP-7012, 1964.
3. Chambers, Joseph R.; and Grafton, Sue B.: Static and Dynamic Longitudinal Stability Derivatives of a Powered 1/9-Scale Model of a Tilt-Wing V/STOL Transport. NASA TN D-3591, 1966.
4. Cook, Woodrow L.; and Hickey, David H.: Comparison of Wind-Tunnel and Flight-Test Aerodynamic Data in the Transition-Flight Speed Range for Five V/STOL Aircraft. Conference on V/STOL and STOL Aircraft, NASA SP-116, 1966, pp. 447-467.
5. Kirk, Jerry V.; Hickey, David H.; and Hall, Leo P.: Aerodynamic Characteristics of a Full-Scale Fan-In-Wing Model Including Results in Ground Effect With Nose-Fan Pitch Control. NASA TN D-2368, 1964.

TABLE I.- GEOMETRIC CHARACTERISTICS OF THE MODEL

Fans:	
Nose-fan diameter	0.54 ft (16.46 cm)
Wing-fan diameter	0.94 ft (28.65 cm)
Wing:	
Area	8.47 ft ² (0.79 m ²)
Span	5.40 ft (1.65 m)
Chord -	
Root	2.17 ft (66.14 cm)
Outboard end of center section	1.64 ft (49.99 cm)
Theoretical tip	0.65 ft (19.81 cm)
Mean aerodynamic chord	1.68 ft (51.21 cm)
Aspect ratio	3.44
Airfoil section	NACA 65-210 (modified)
Sweepback (quarter chord) -	
Center section	15°
Outer section	28°
Dihedral angle -	
Center section	0°
Outer section	-6°
Geometric twist (washout) -	
Center section	0°
Outer section	3°
Ailerons (each) -	
Chord (percentage wing chord)	25.00
Area	0.38 ft ² (0.04 m ²)
Flap (each) -	
Type	Single slotted
Chord	0.38 ft (11.58 cm)
Area	0.89 ft ² (0.08 m ²)
Vertical tail:	
Area	1.65 ft ² (0.15 m ²)
Span	1.40 ft (42.67 cm)
Chord -	
Root	1.51 ft (46.02 cm)
Tip	0.81 ft (24.69 cm)
Aspect ratio	1.18
Taper ratio	0.52
Airfoil section	NACA 64 ₁ A012
Sweepback (quarter chord)	30°
Rudder -	
Root chord	0.26 ft (7.92 cm)
Tip chord	0.18 ft (5.49 cm)
Area	0.20 ft ² (0.02 m ²)
Horizontal tail:	
Area	1.64 ft ² (0.15 m ²)
Span	2.22 ft (67.67 cm)
Chord -	
Root	0.99 ft (30.18 cm)
Tip	0.49 ft (14.94 cm)
Aspect ratio	3.00
Taper ratio	0.50
Airfoil section	NACA 64 ₁ A012
Sweepback (quarter chord)	13.70°

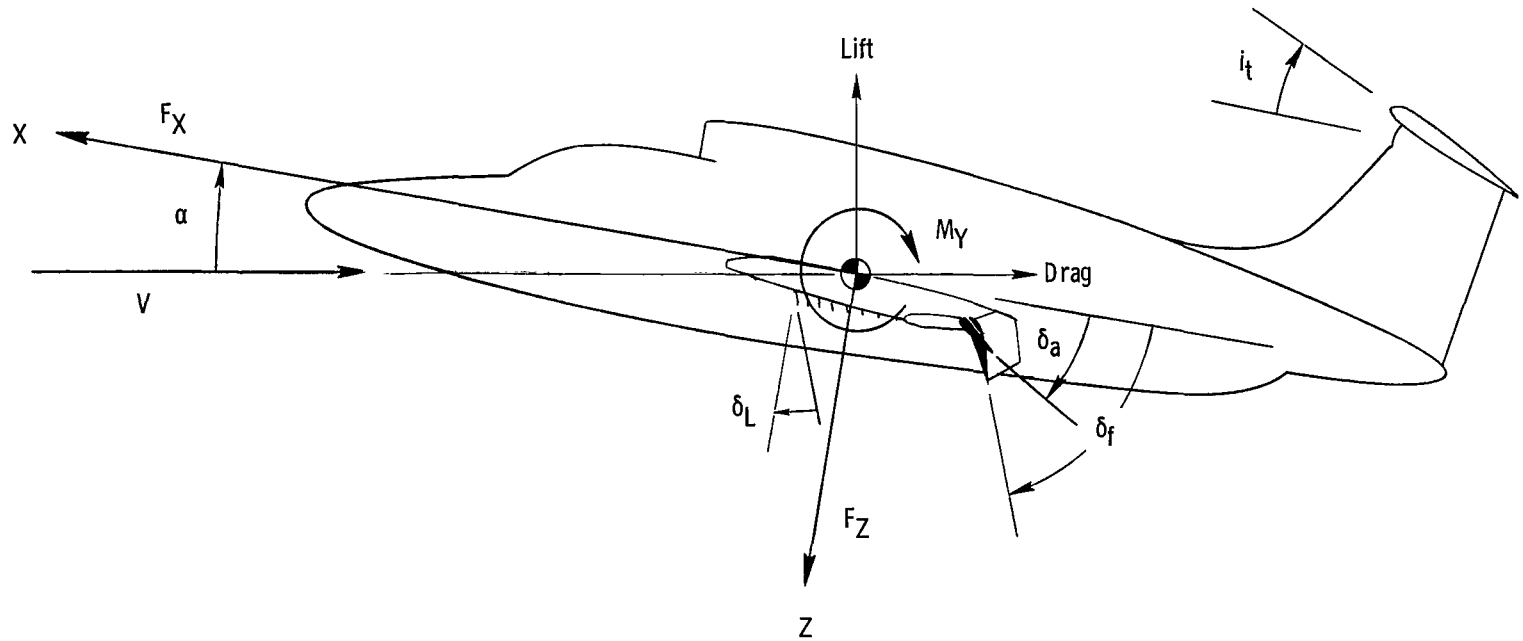
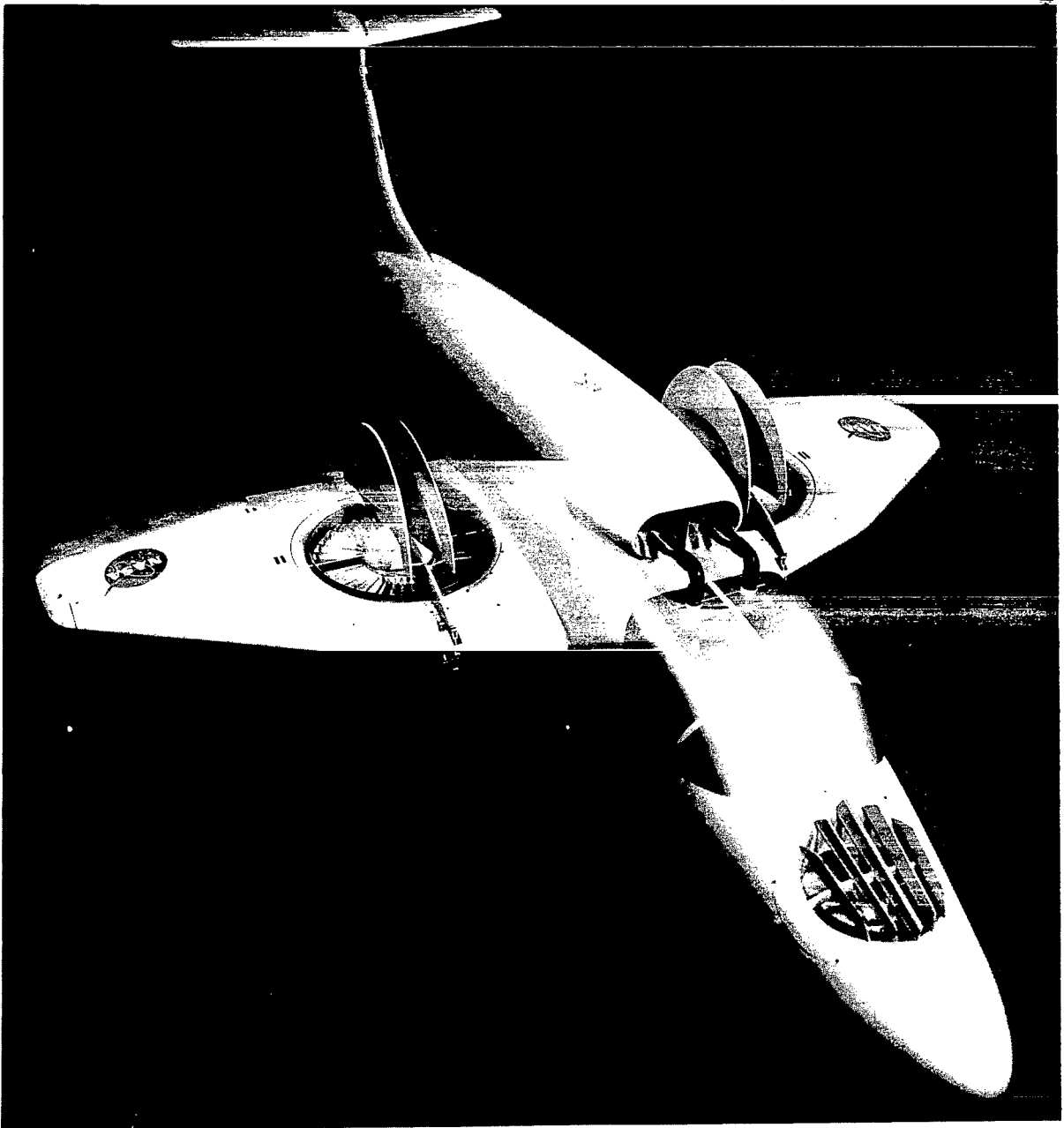


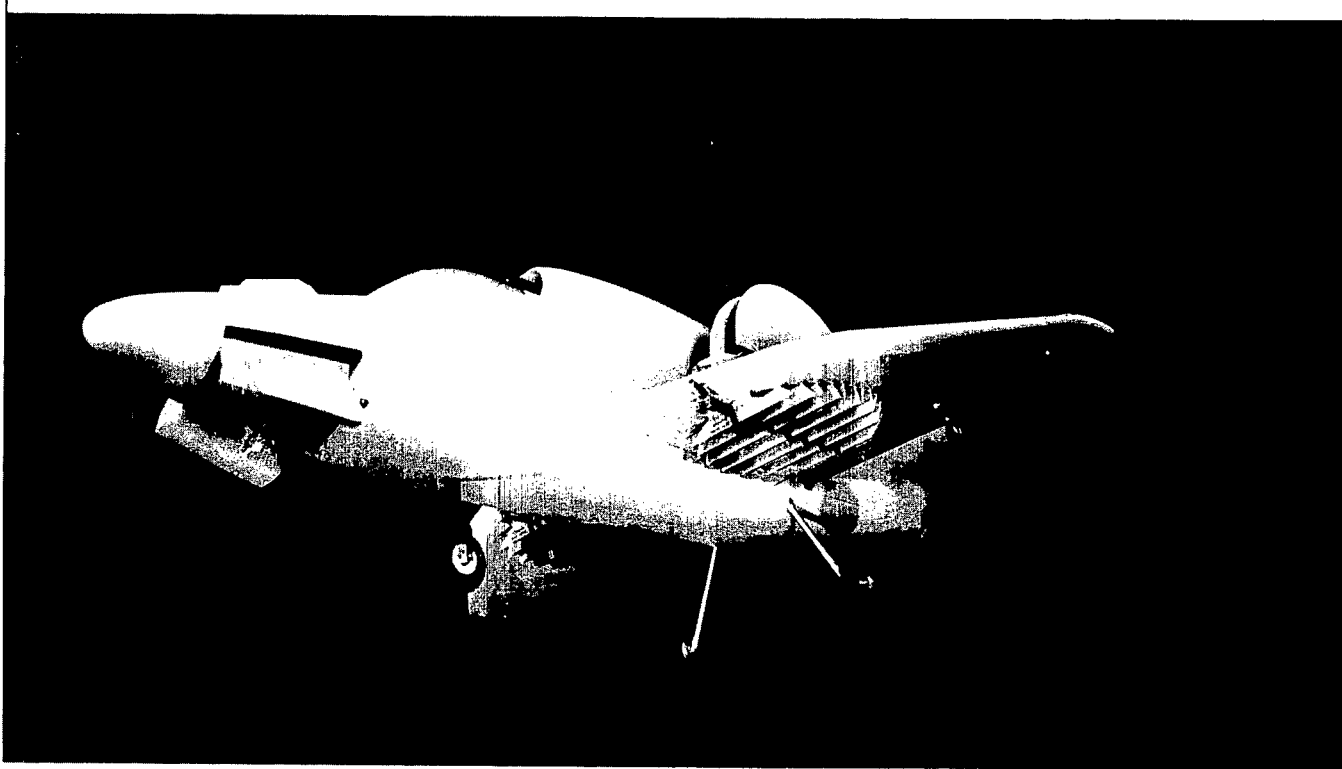
Figure 1.- Body system of axes. Positive senses of forces and moments are indicated.



(a) Top view of model.

L-62-9775

Figure 2.- Photographs of model.



(b) Bottom view of model.

L-62-9773

Figure 2.- Concluded.

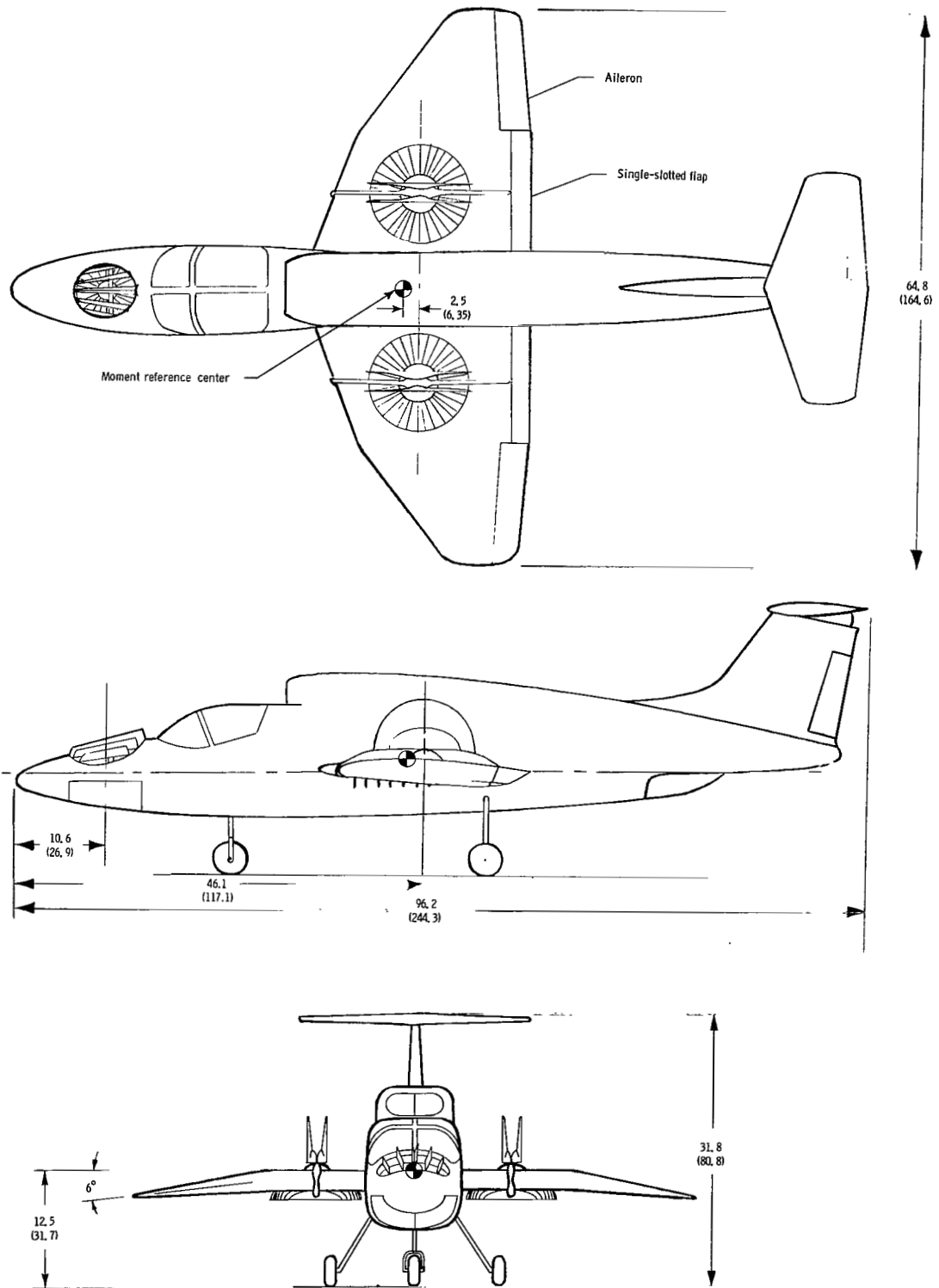


Figure 3.- Three-view sketch of model. Dimensions are given first in inches and parenthetically in centimeters.

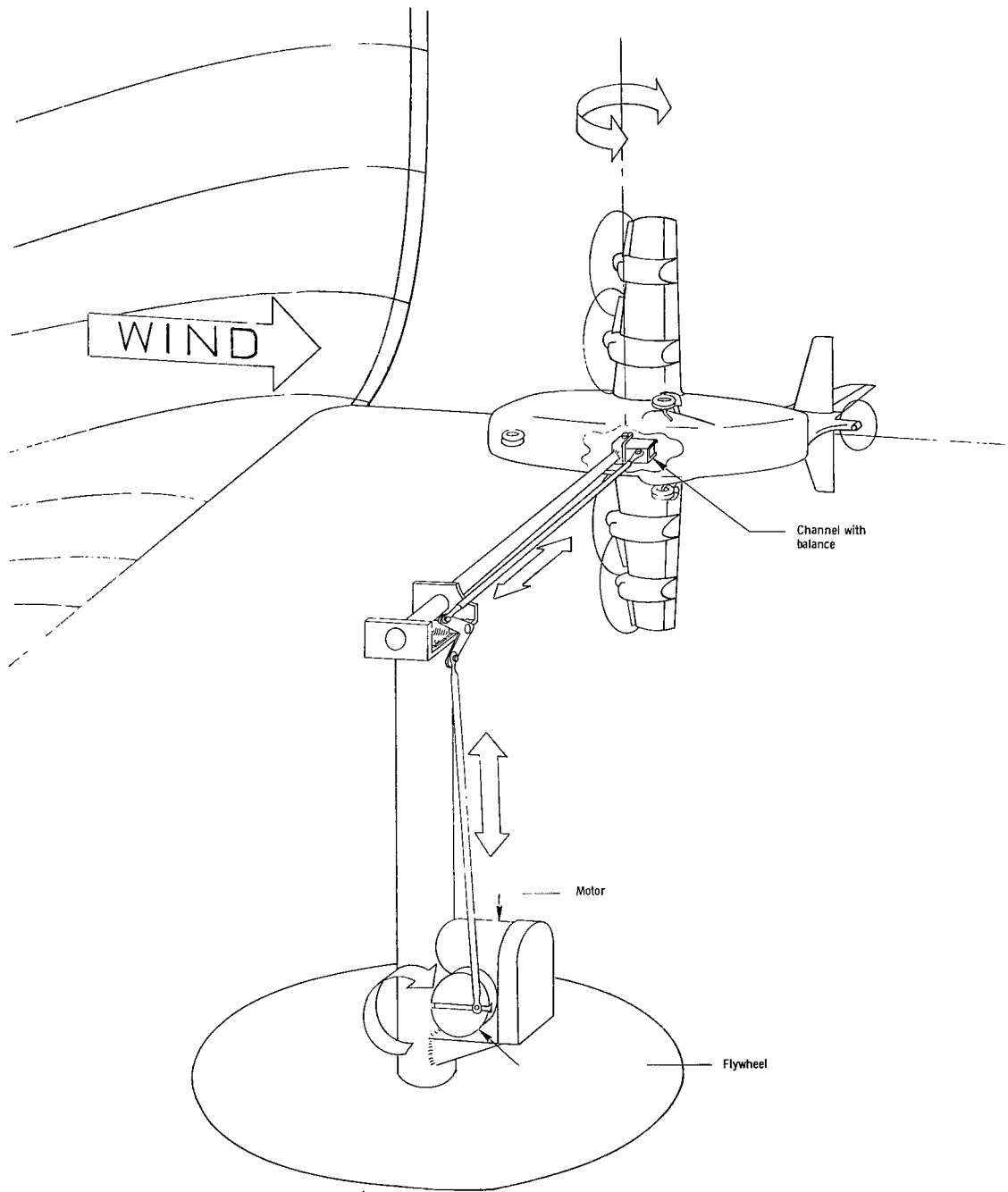


Figure 4.- Sketch of the test setup for oscillatory force tests.

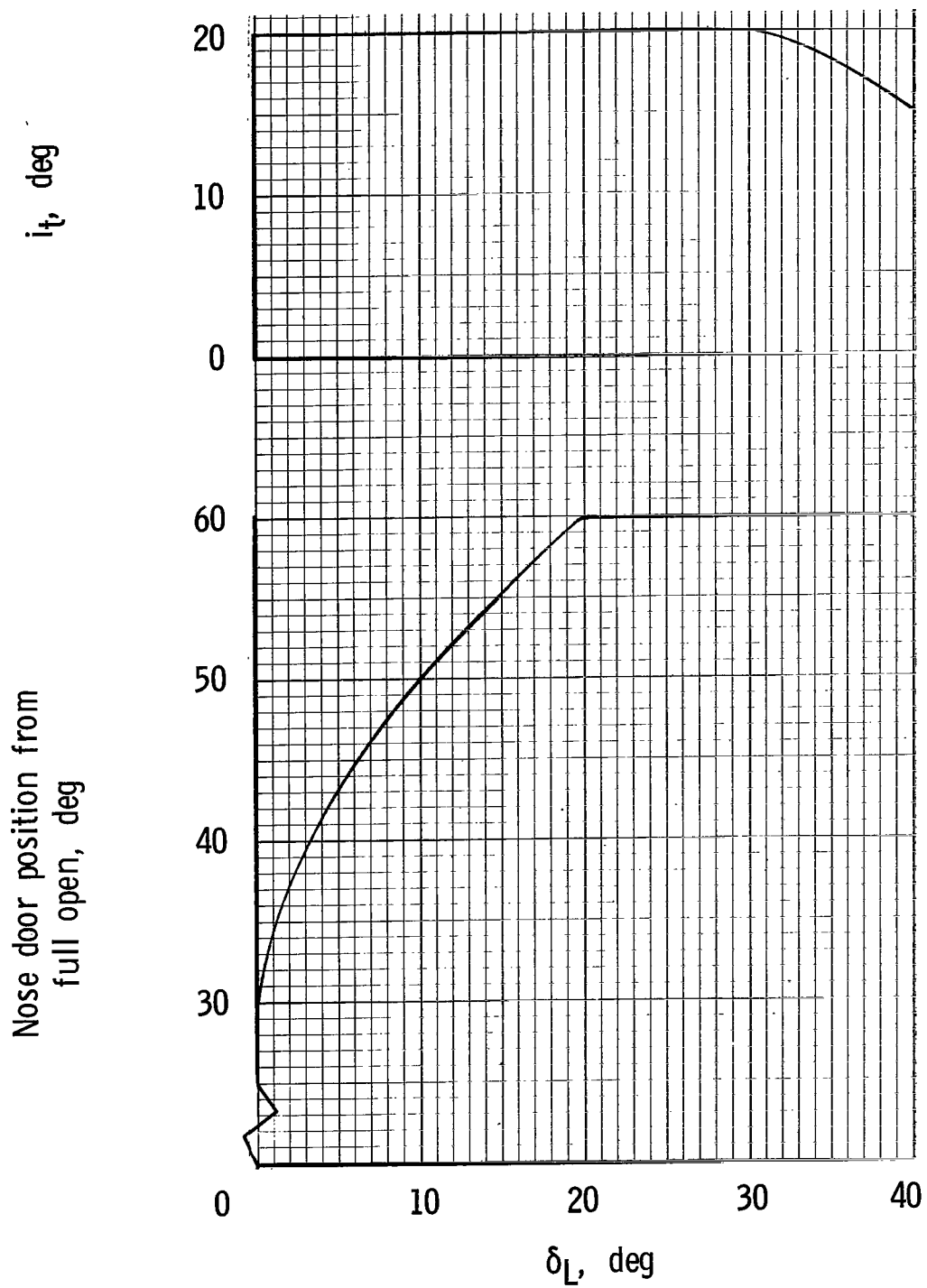


Figure 5.- Horizontal-tail incidence and nose-door position.

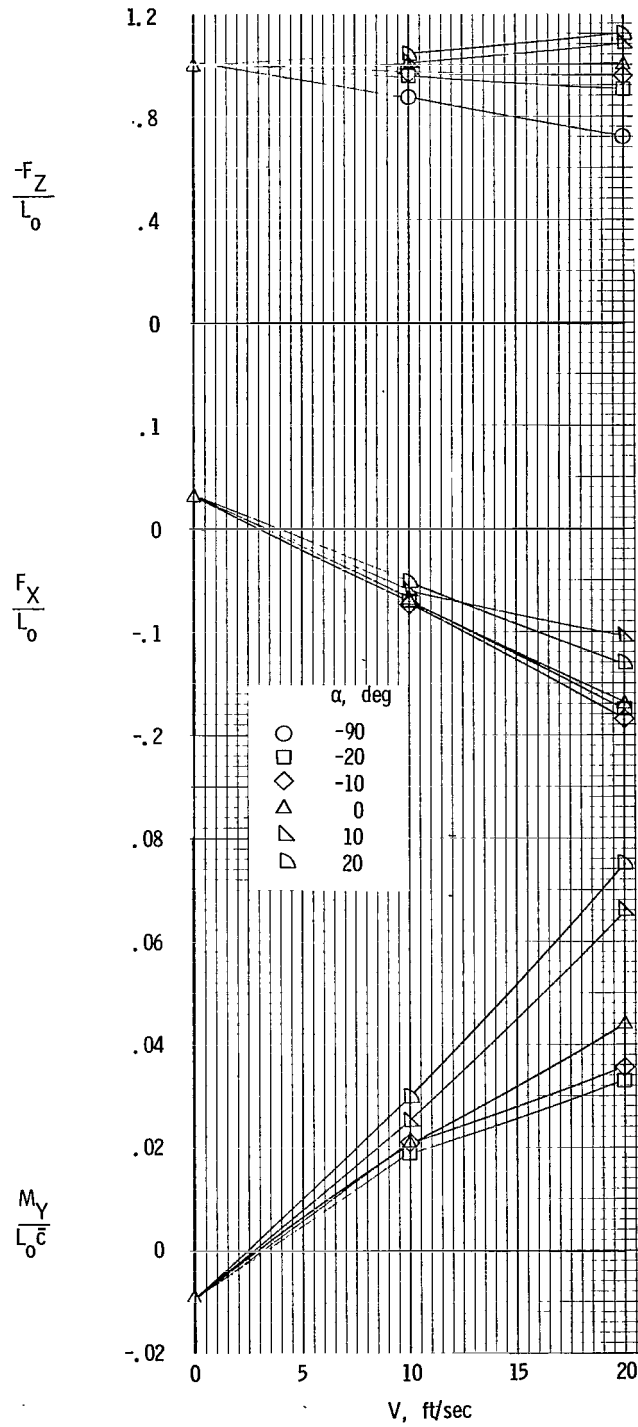


Figure 6.- Variation of forces and moments with velocity for hovering configuration. $\delta_L = 0^\circ$; $L_0 = 50.39$ pounds (224.15 N).

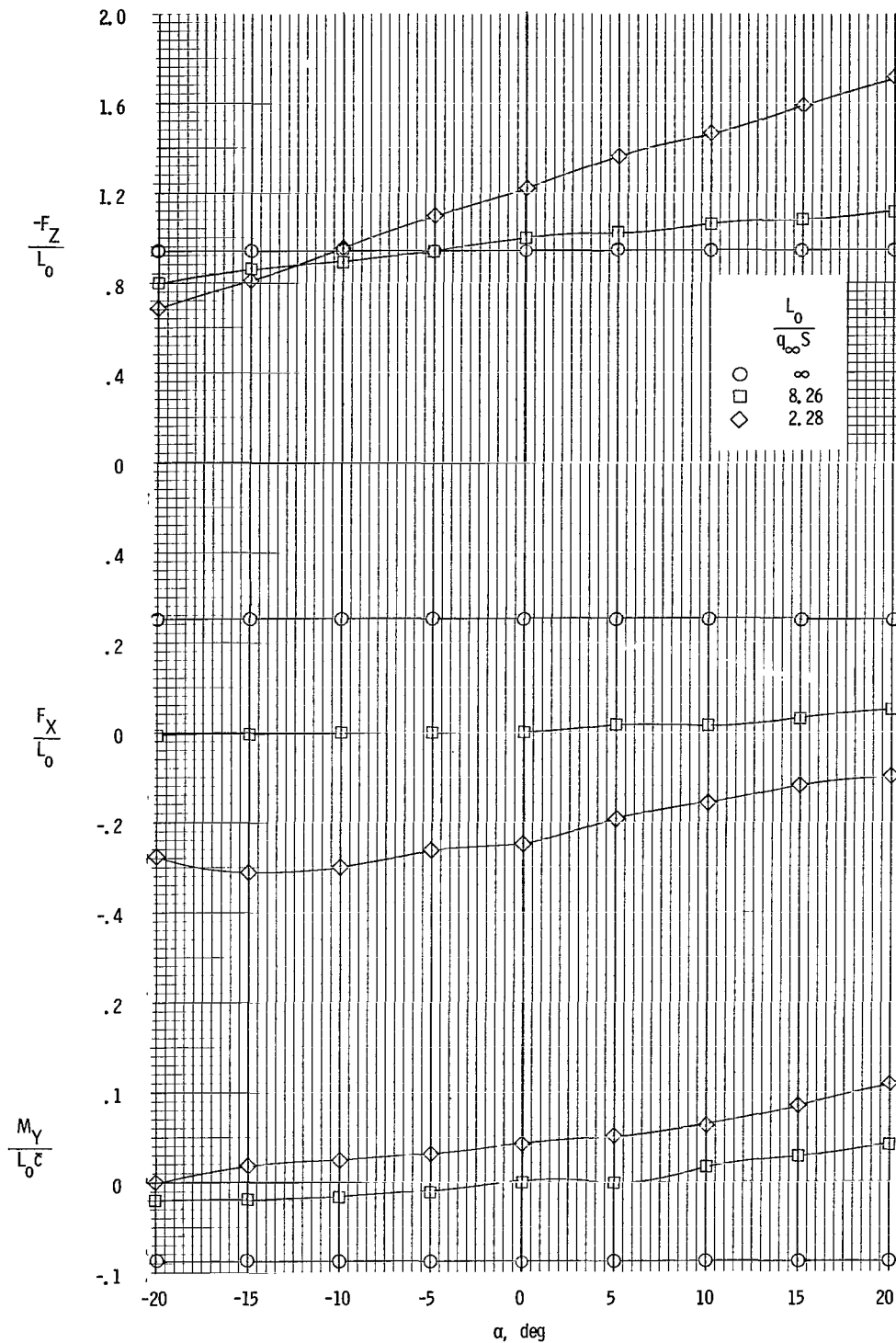


Figure 7.- Variation of forces and moments with angle of attack. $\delta_L = 10^\circ$; $i_t = 20^\circ$.

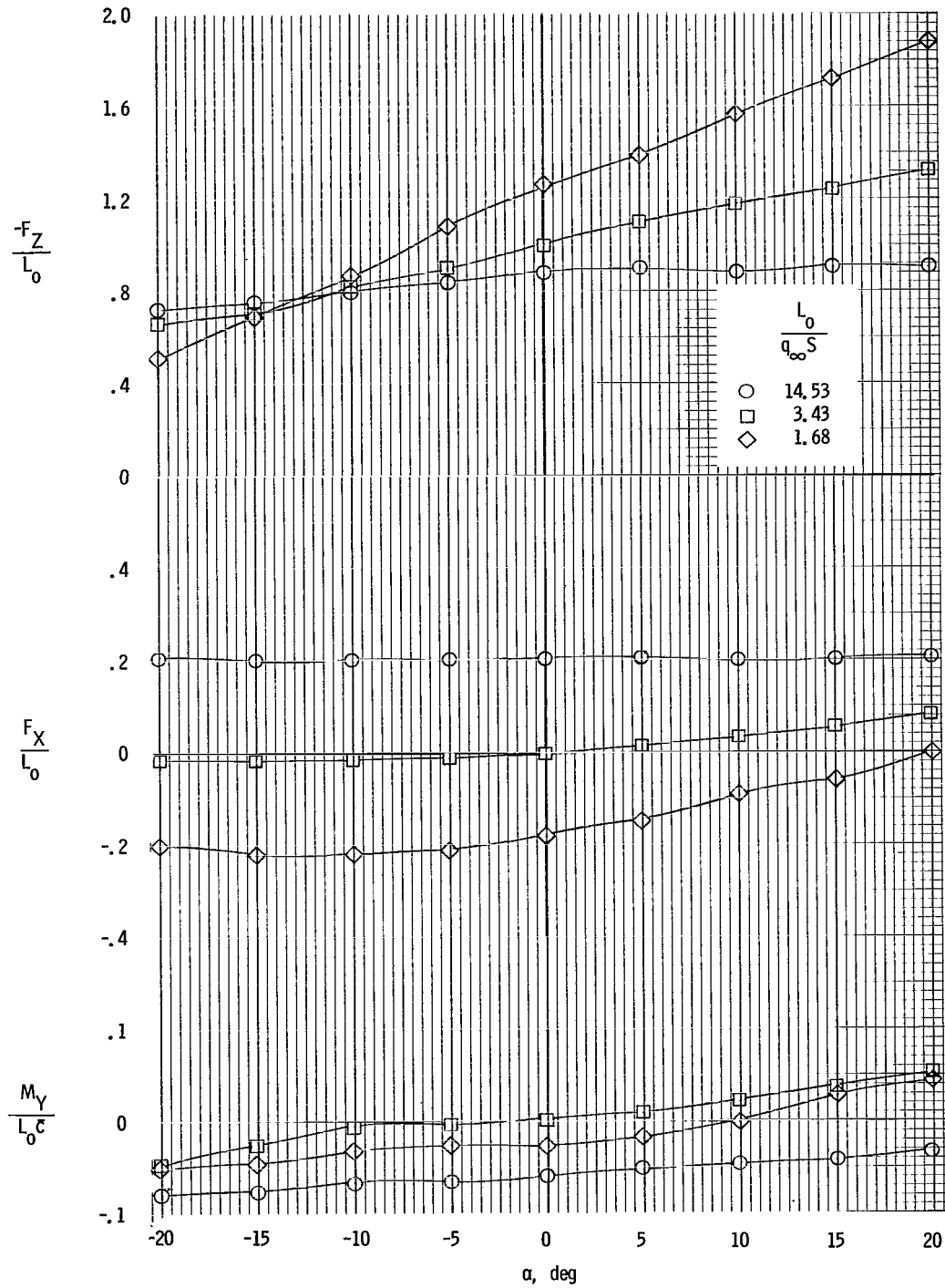


Figure 8.- Variation of forces and moments with angle of attack. $\delta_L = 20^\circ$; $i_t = 20^\circ$.

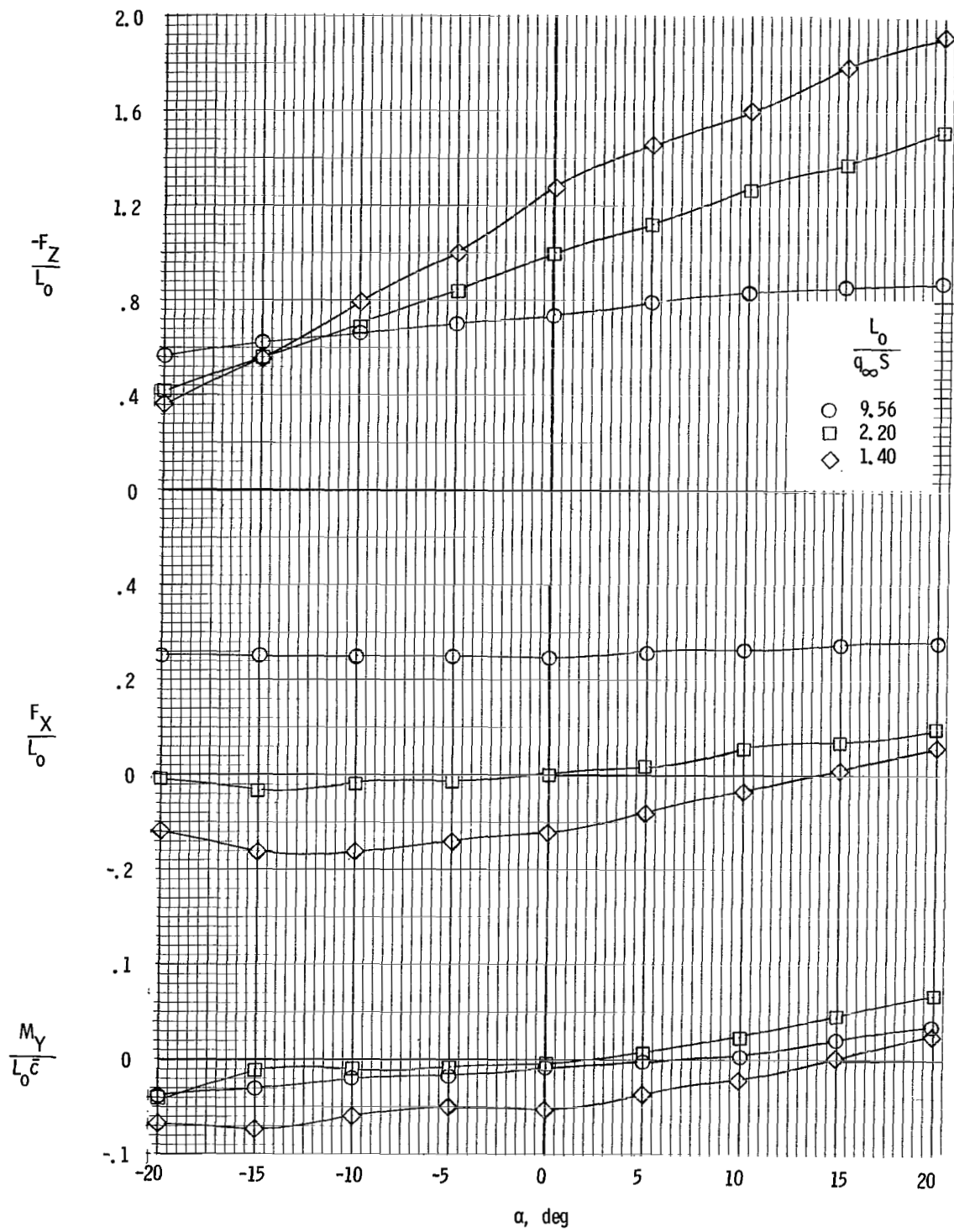


Figure 9.- Variation of forces and moments with angle of attack. $\delta_L = 30^\circ$; $i_t = 20^\circ$.

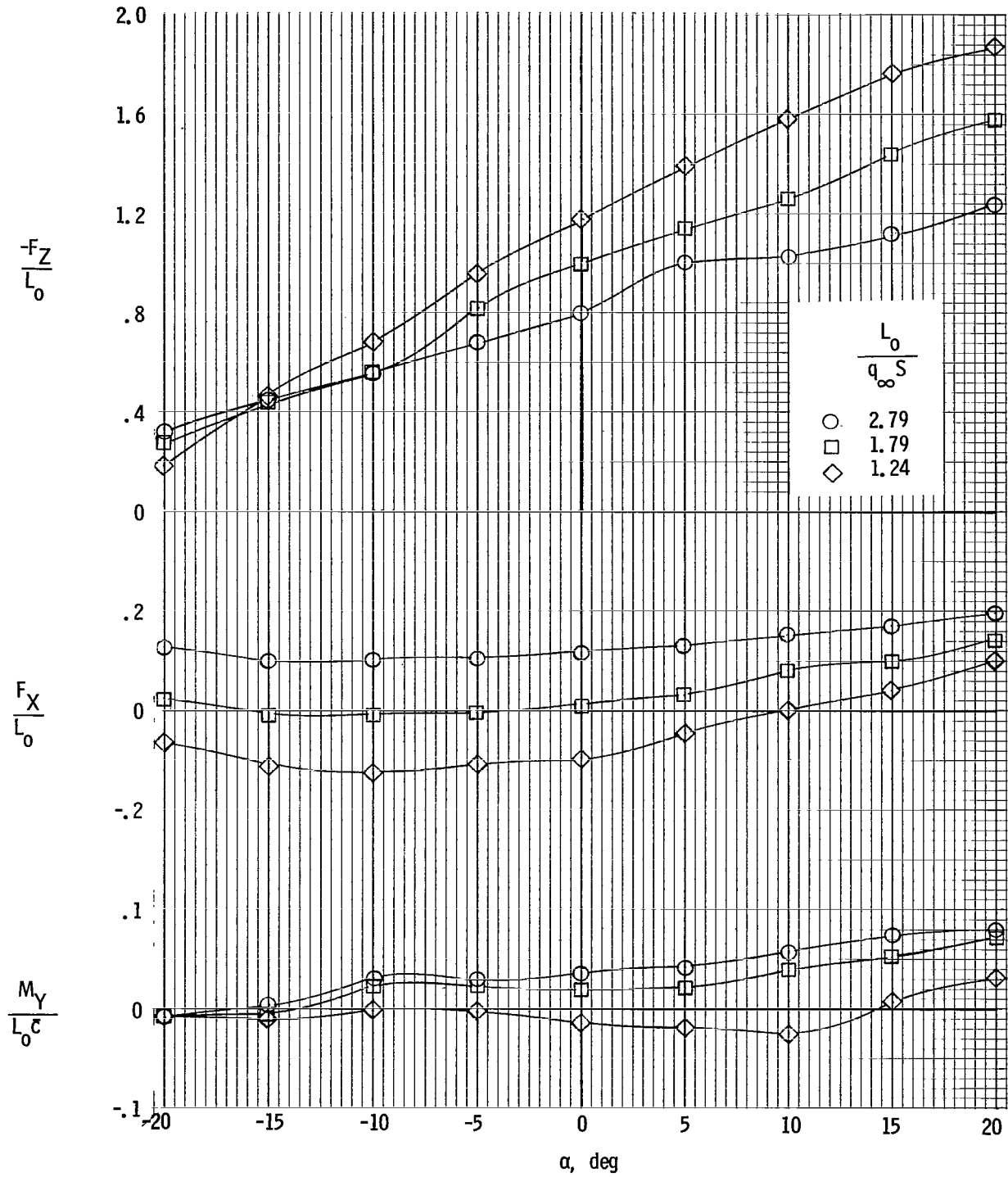


Figure 10.- Variation of forces and moments with angle of attack. $\delta_L = 40^\circ$; $i_t = 15^\circ$.

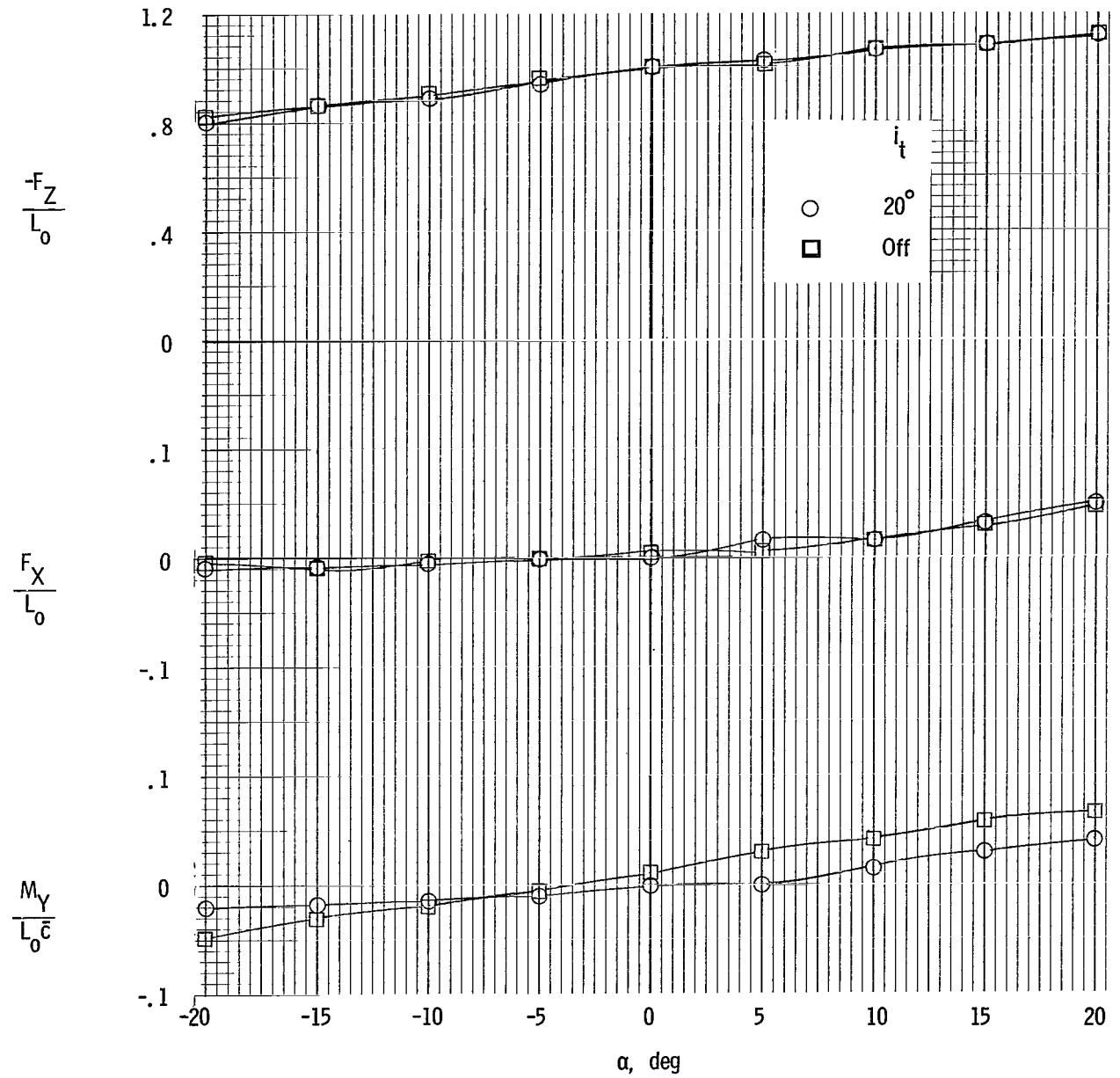


Figure 11.- Effect of horizontal tail on the static longitudinal data. $\delta_L = 10^\circ$; $\frac{L_0}{q_\infty S} = 8.26$.

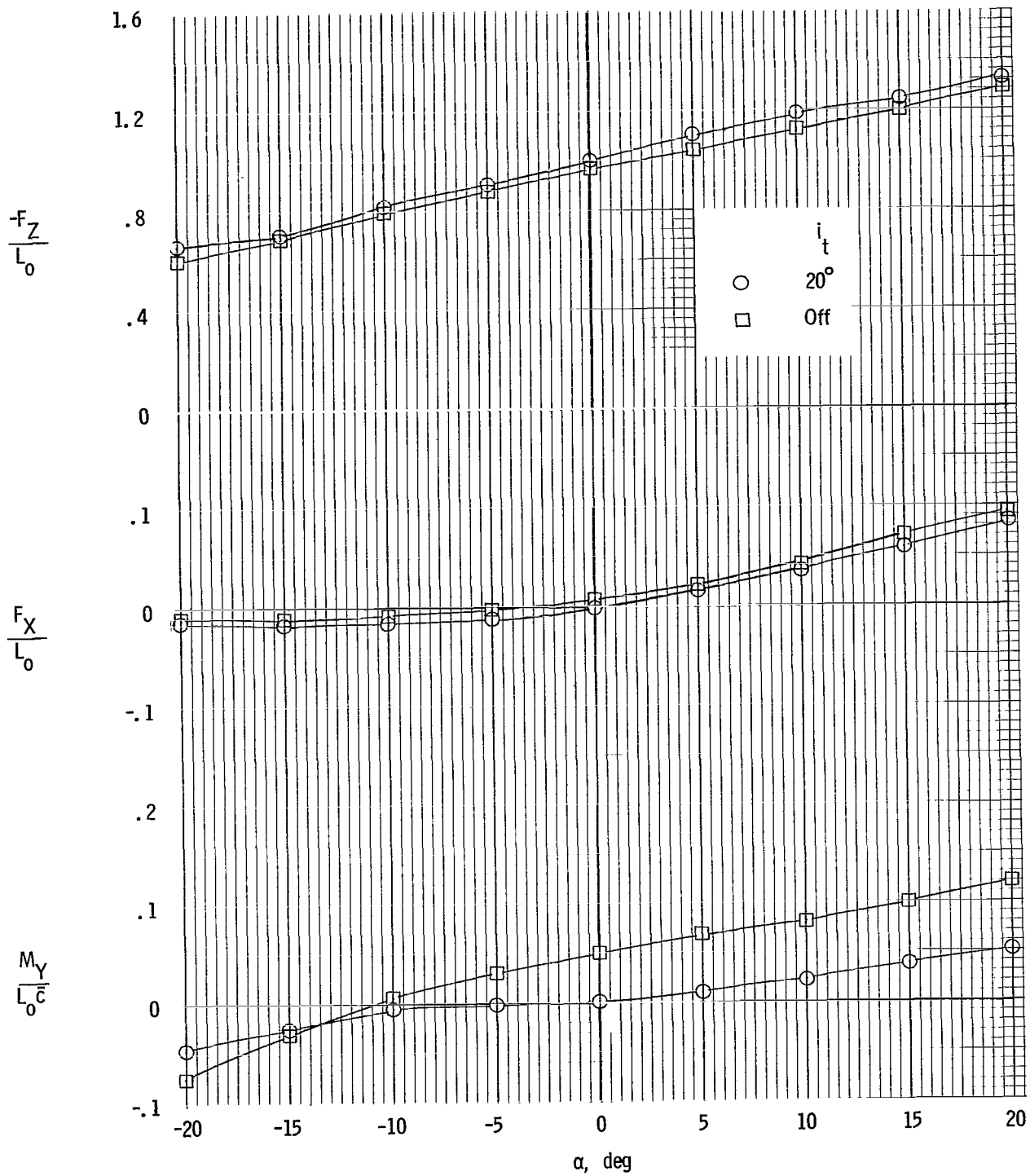


Figure 12.- Effect of horizontal tail on the static longitudinal data. $\delta_L = 20^\circ$; $\frac{L_0}{q_\infty S} = 3.43$.

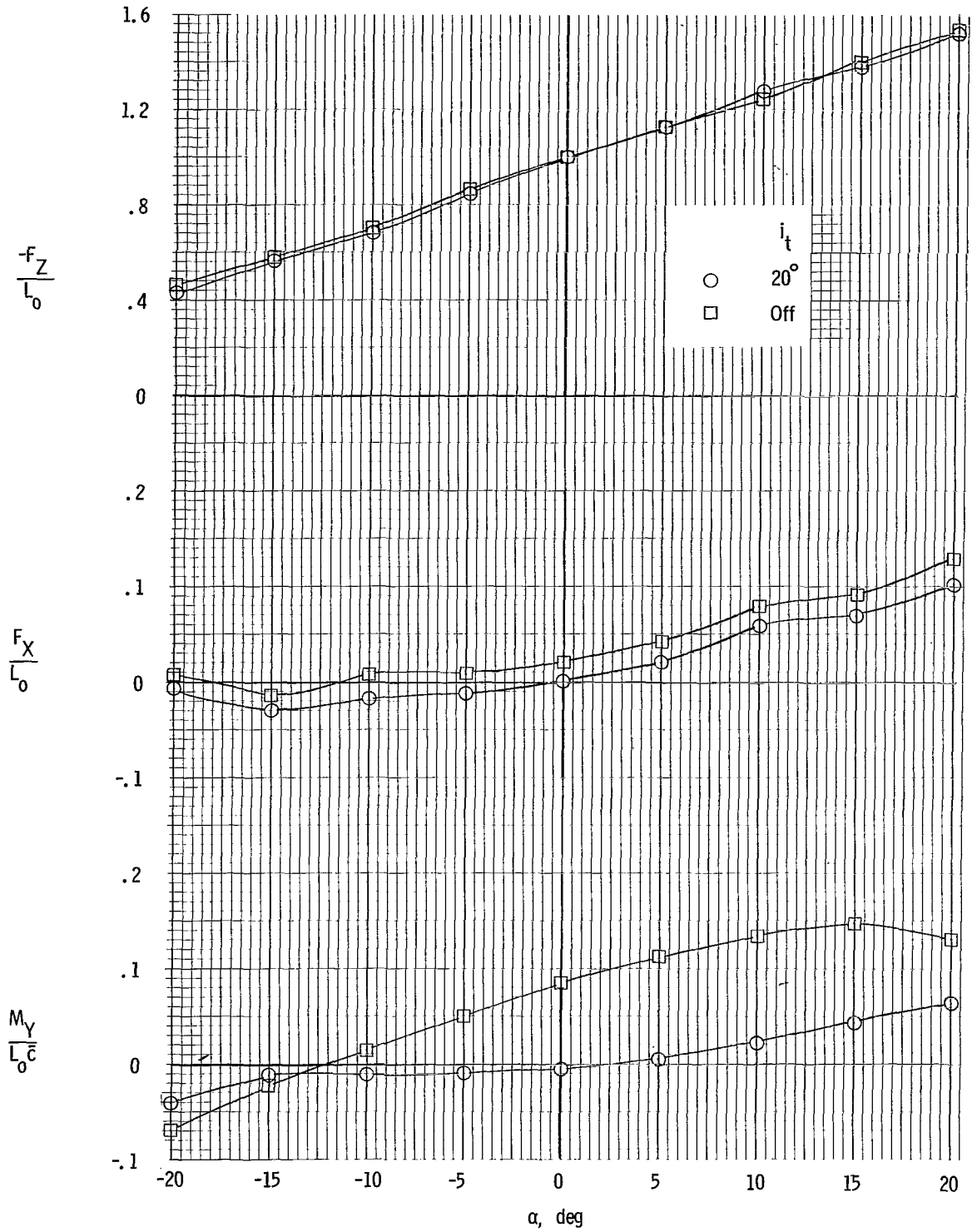


Figure 13.- Effect of horizontal tail on the static longitudinal data. $\delta_L = 30^\circ$; $L_0/q_\infty S = 2.20$.

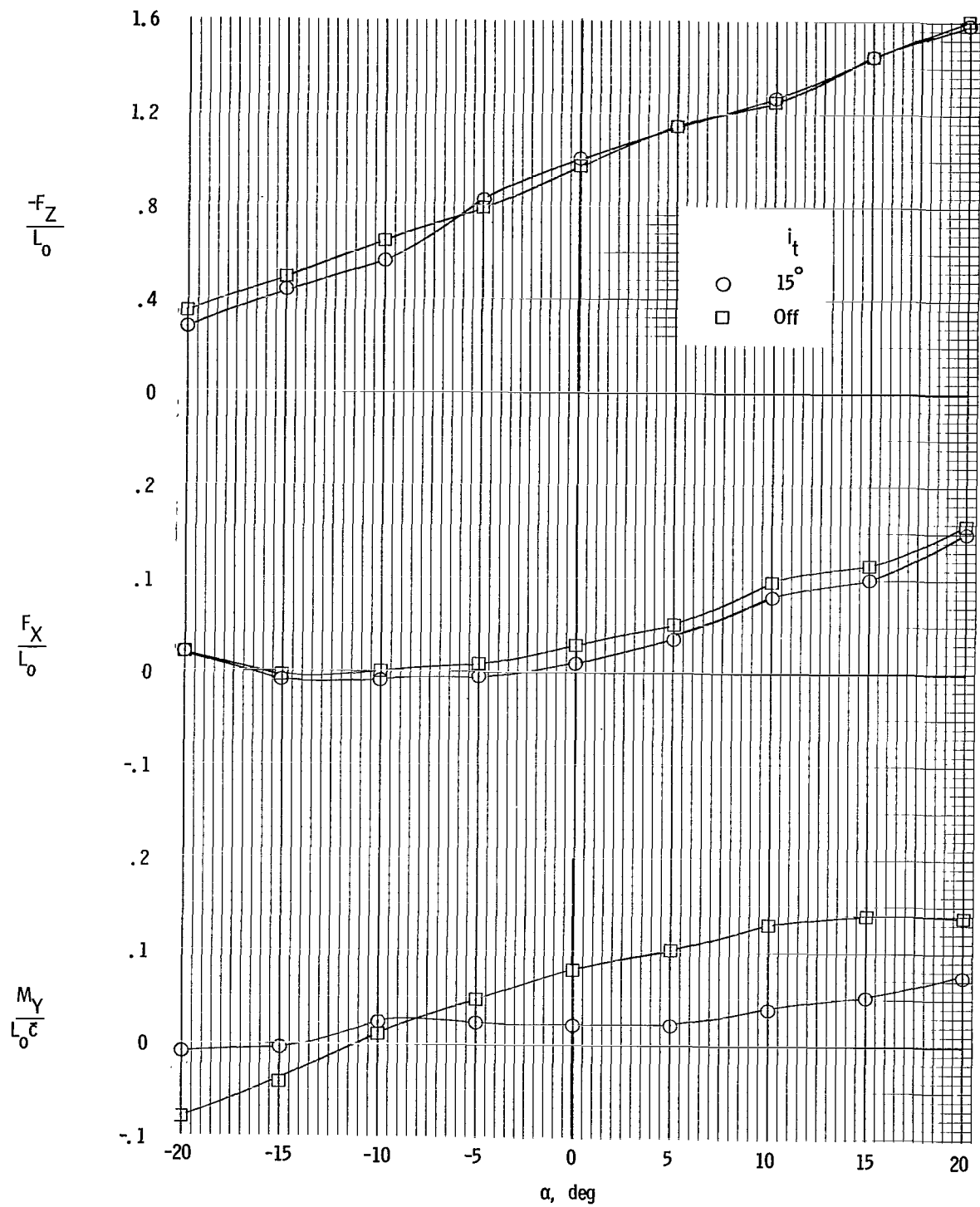


Figure 14.- Effect of horizontal tail on the static longitudinal data. $\delta_L = 40^\circ$; $\frac{L_0}{q_\infty S} = 1.79$.

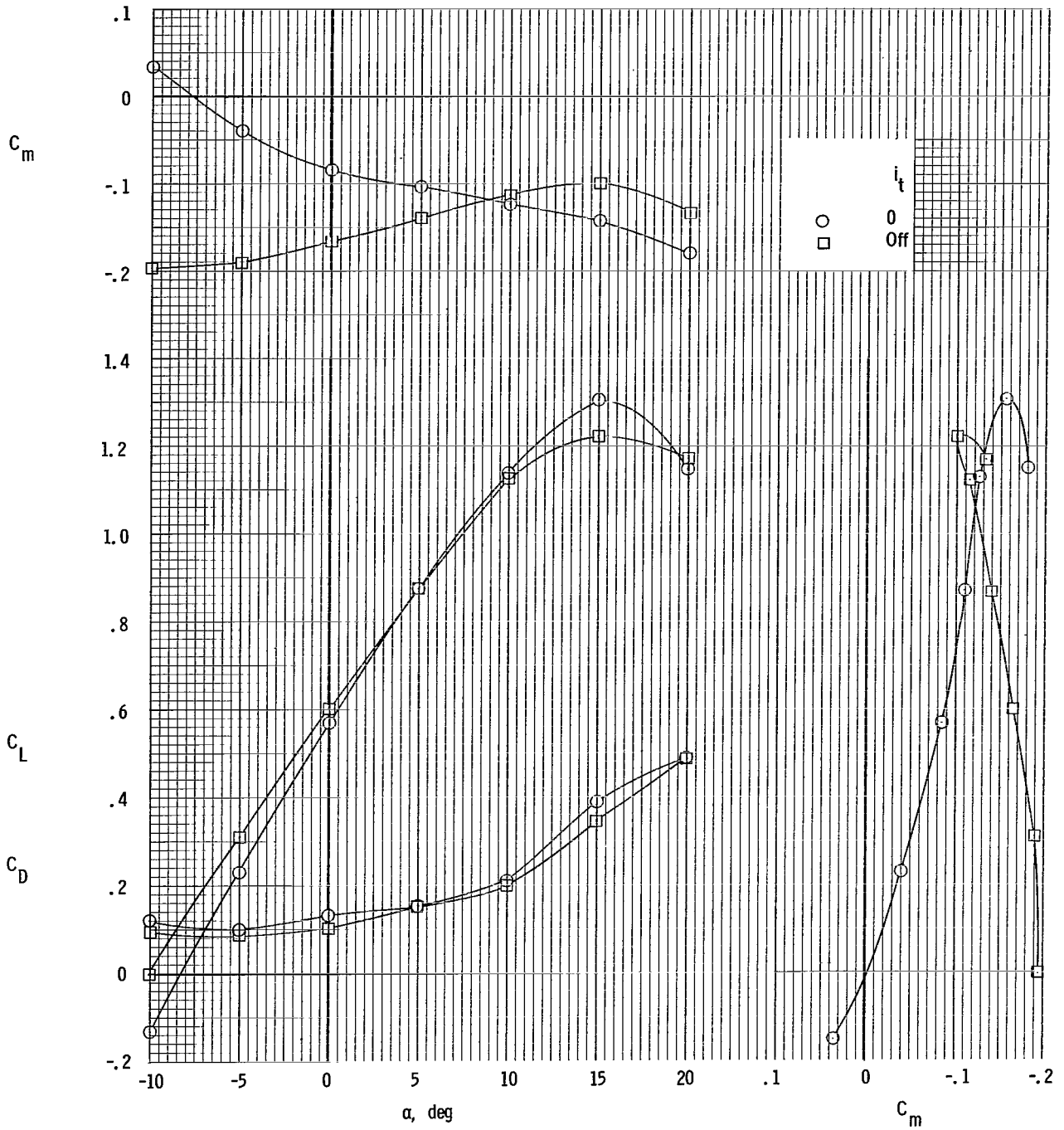


Figure 15.- Variation of the aerodynamic coefficients with angle of attack. Power off; $\delta_f = 45^\circ$; $\delta_a = 15^\circ$; $q_\infty = 6.0 \text{ lb/ft}^2$ (287.28 N/m^2); landing gear on.

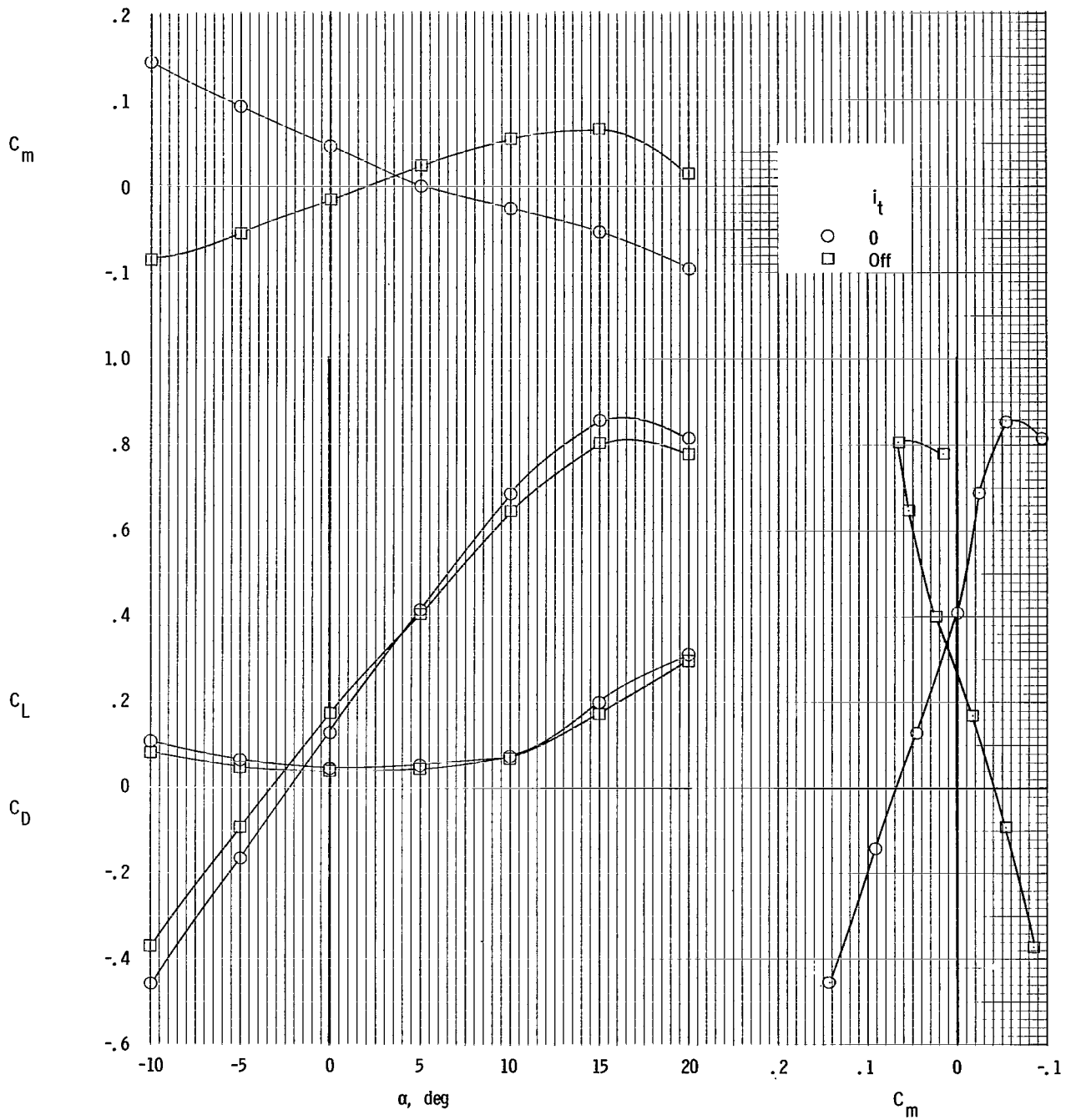


Figure 16.- Variation of the aerodynamic coefficients with angle of attack. Power off; $\delta_f = 0^\circ$; $\delta_a = 0^\circ$; $q_\infty = 6.0 \text{ lb/ft}^2$ (287.28 N/m^2), landing gear off.

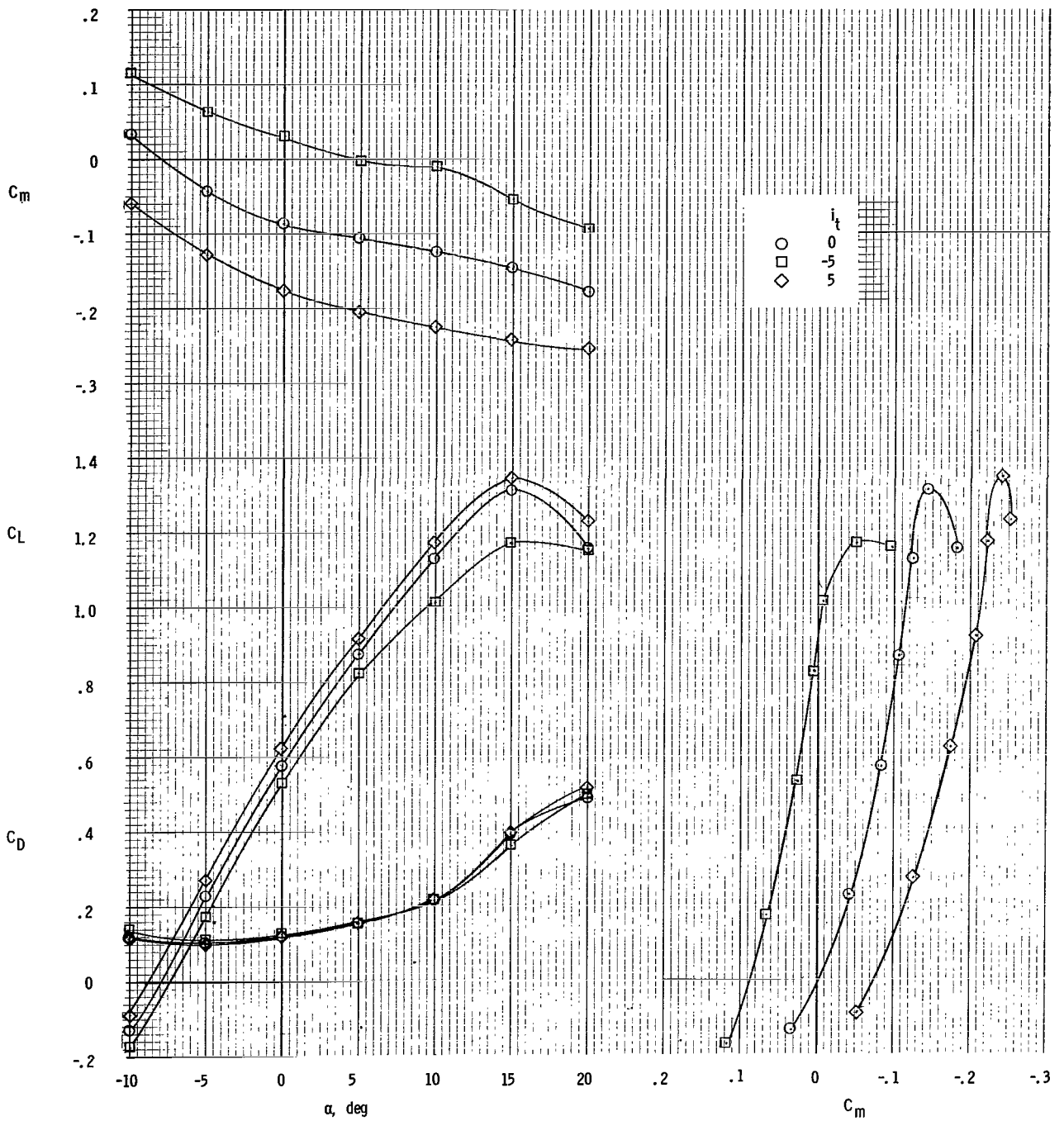


Figure 17.- Effect of horizontal-tail incidence on static longitudinal characteristics. Power off; $\delta_f = 45^\circ$; $\delta_a = 15^\circ$.

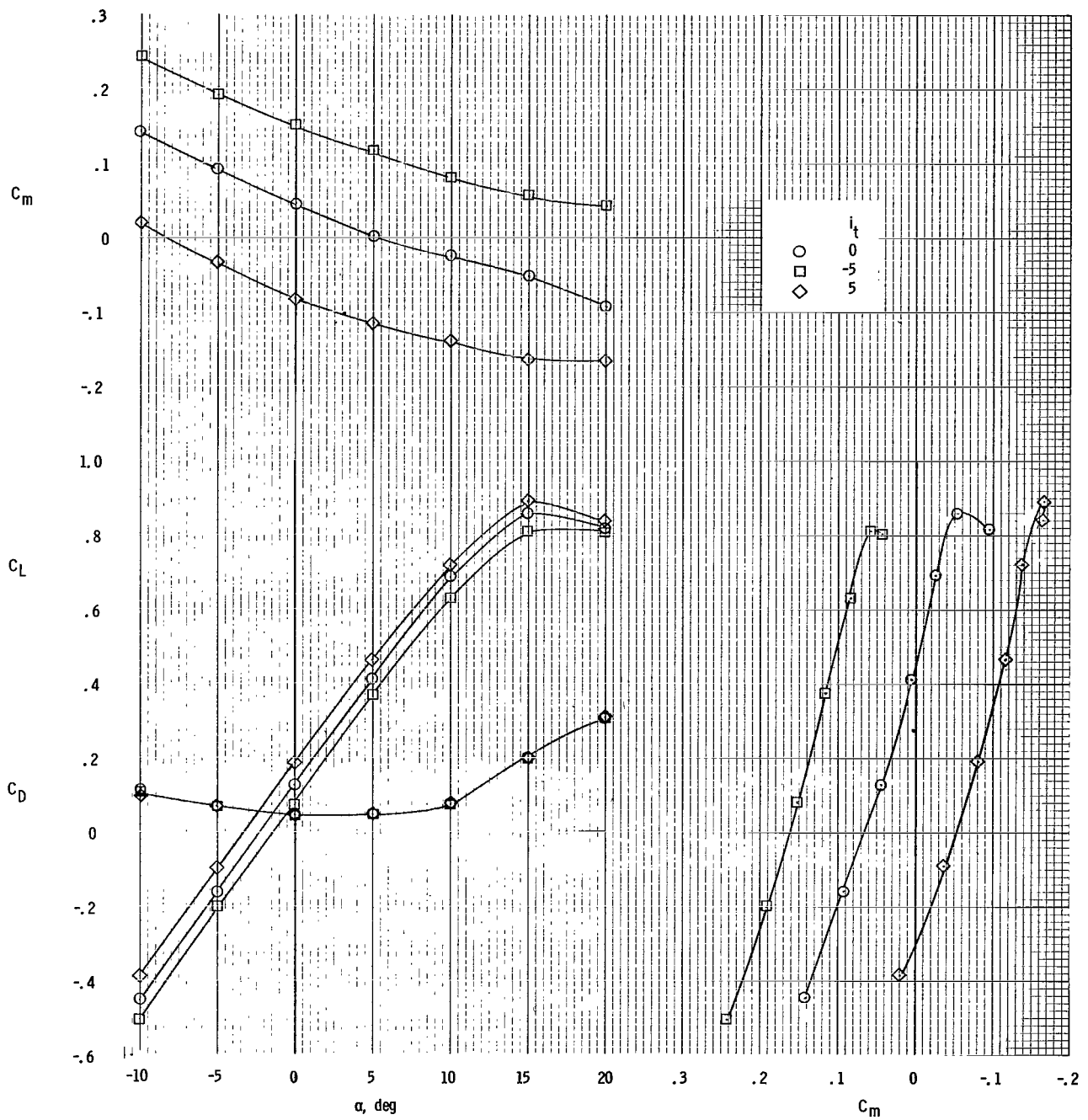


Figure 18.- Effect of horizontal-tail incidence on static longitudinal characteristics. Power off; $\delta_f = 0^\circ$; $\delta_a = 0^\circ$.

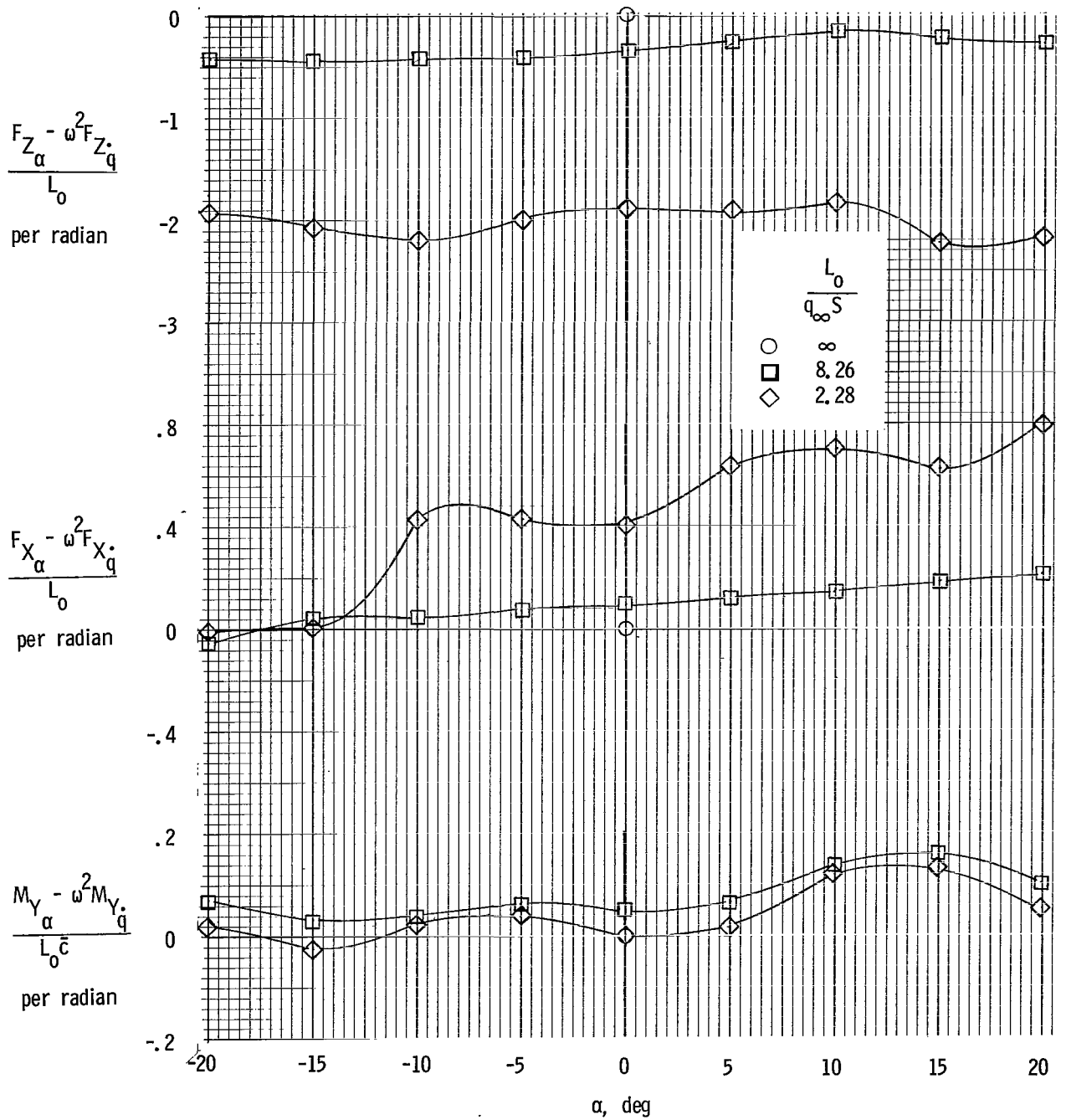


Figure 19.- Variation of the in-phase oscillatory derivatives with angle of attack. $\delta_L = 10^\circ$; $i_t = 20^\circ$.

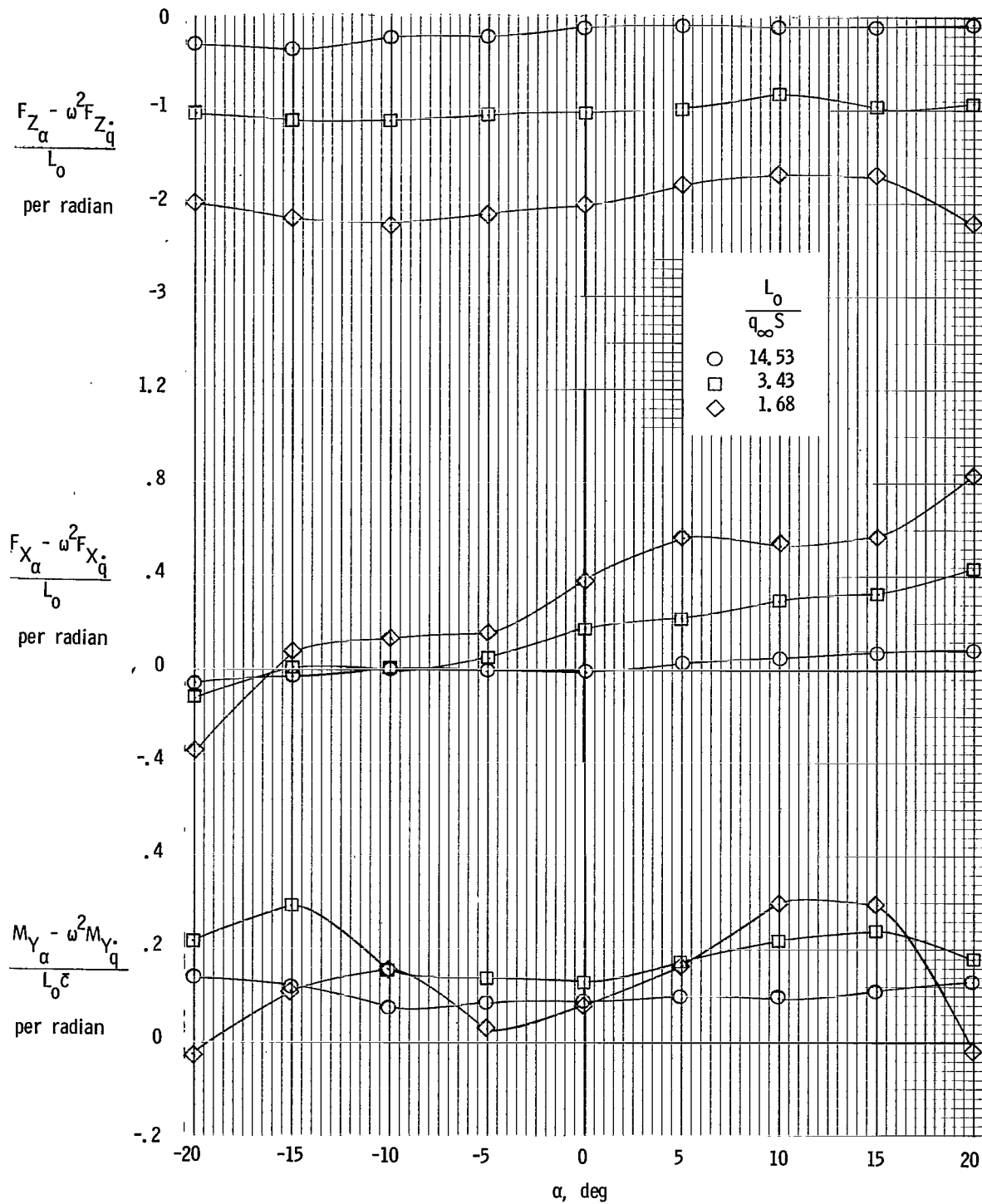


Figure 20.- Variation of the in-phase oscillatory derivatives with angle of attack. $\delta_L = 20^\circ$; $i_t = 20^\circ$.

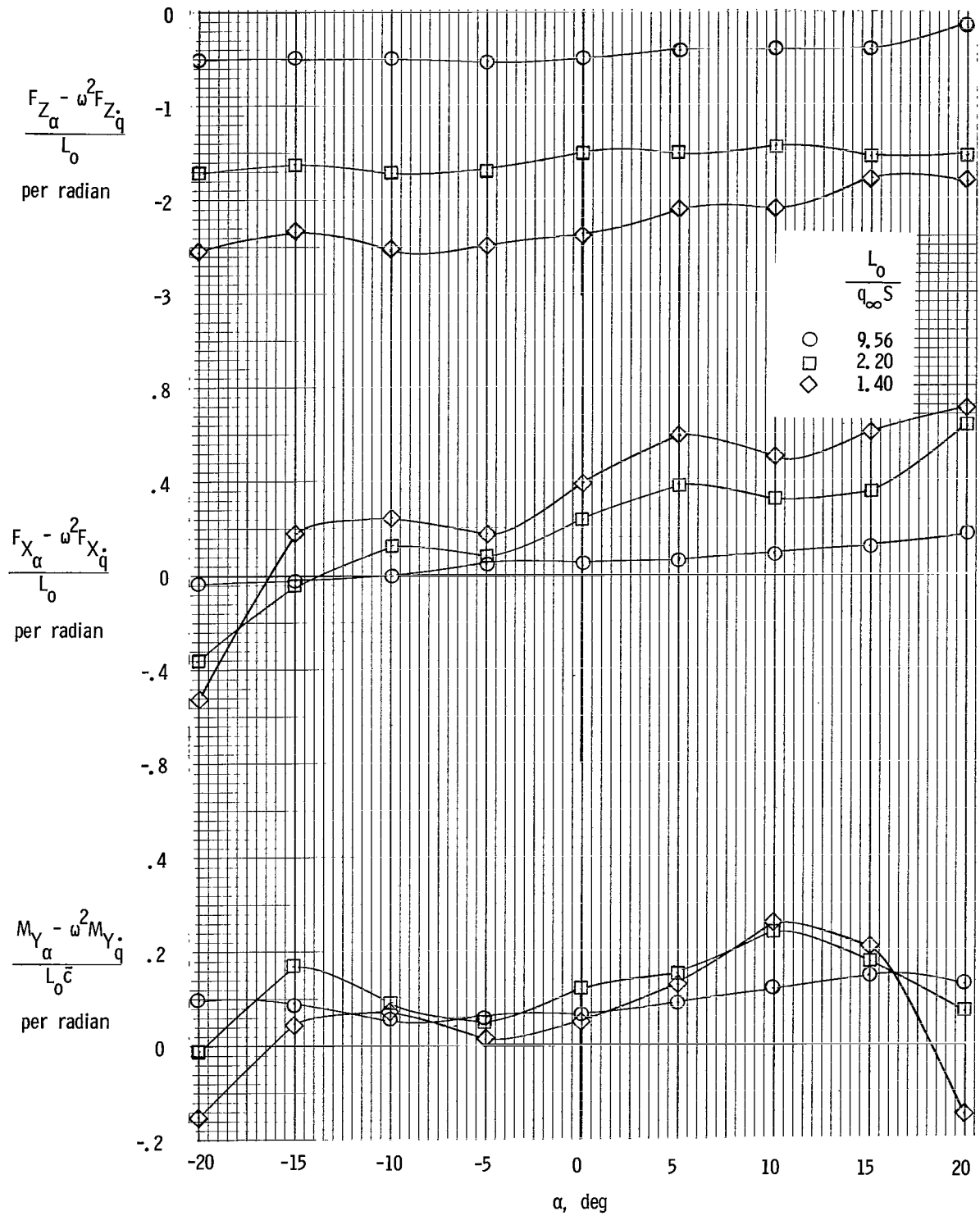


Figure 21.- Variation of the in-phase oscillatory derivatives with angle of attack. $\delta_L = 30^\circ$; $i_t = 20^\circ$.

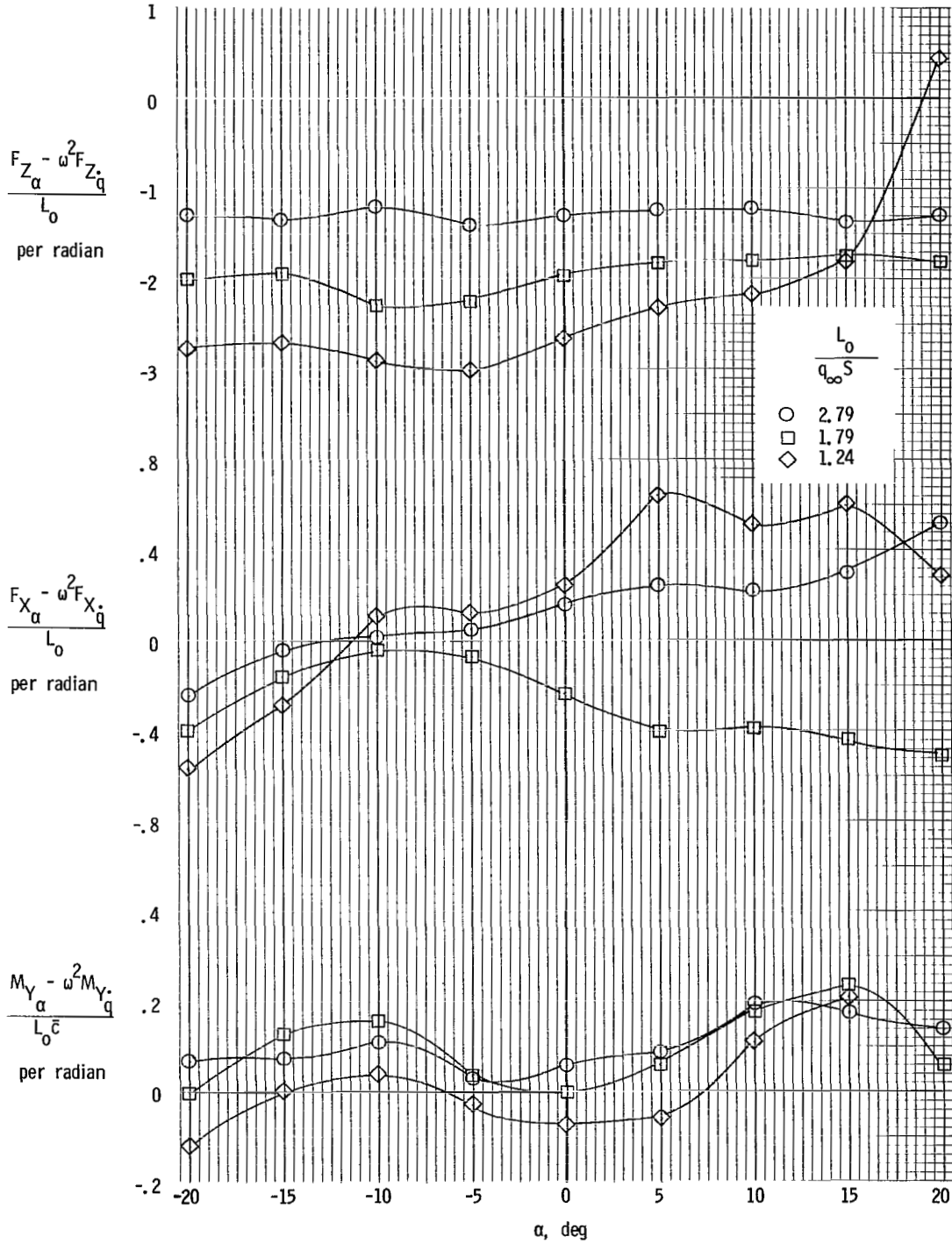


Figure 22.- Variation of the in-phase oscillatory derivatives with angle of attack. $\delta_L = 40^\circ$; $i_t = 15^\circ$.

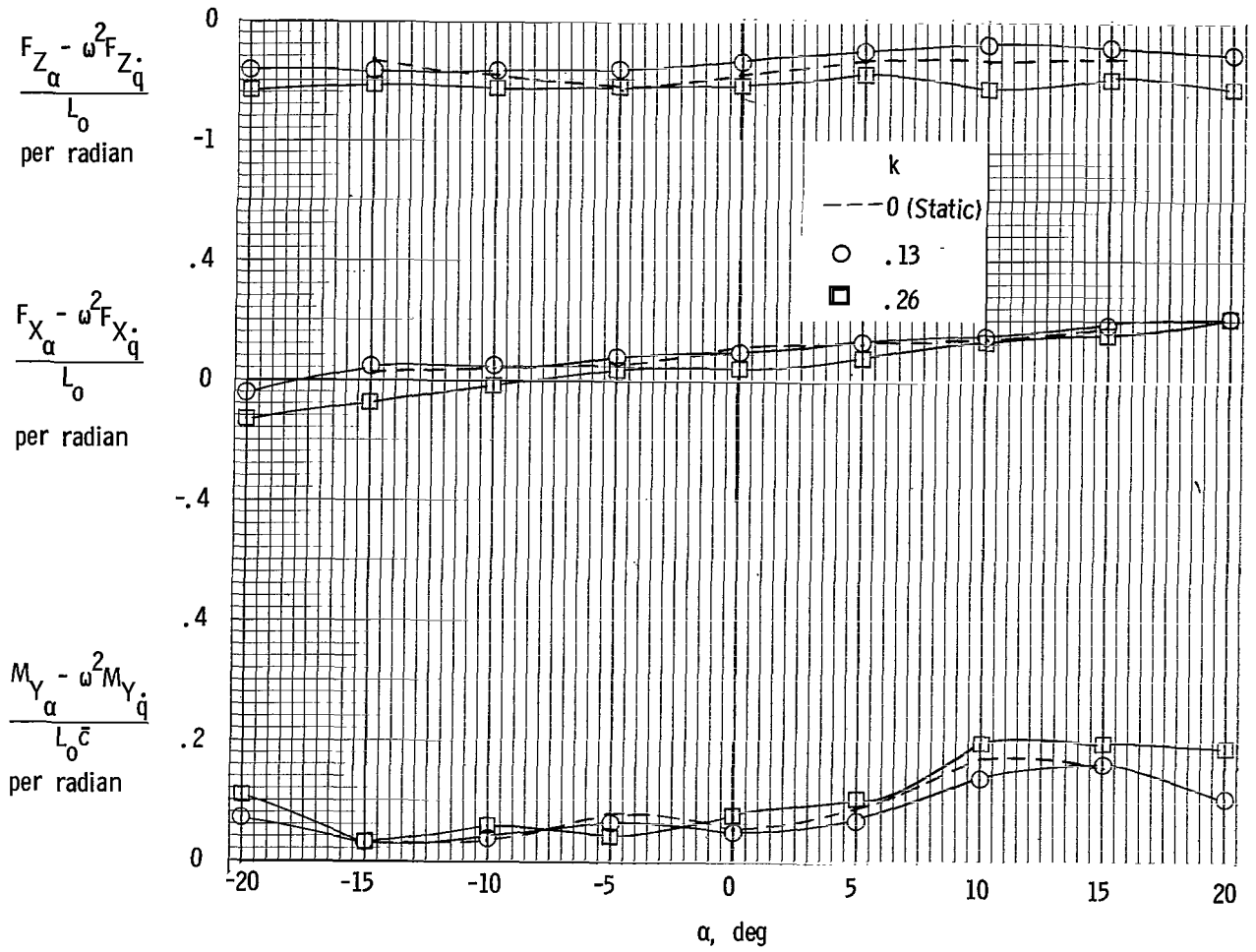


Figure 23.- Effect of frequency on in-phase oscillatory derivatives. $\delta_L = 10^\circ$; $i_t = 20^\circ$; $\frac{L_0}{q_\infty S} = 8.26$.

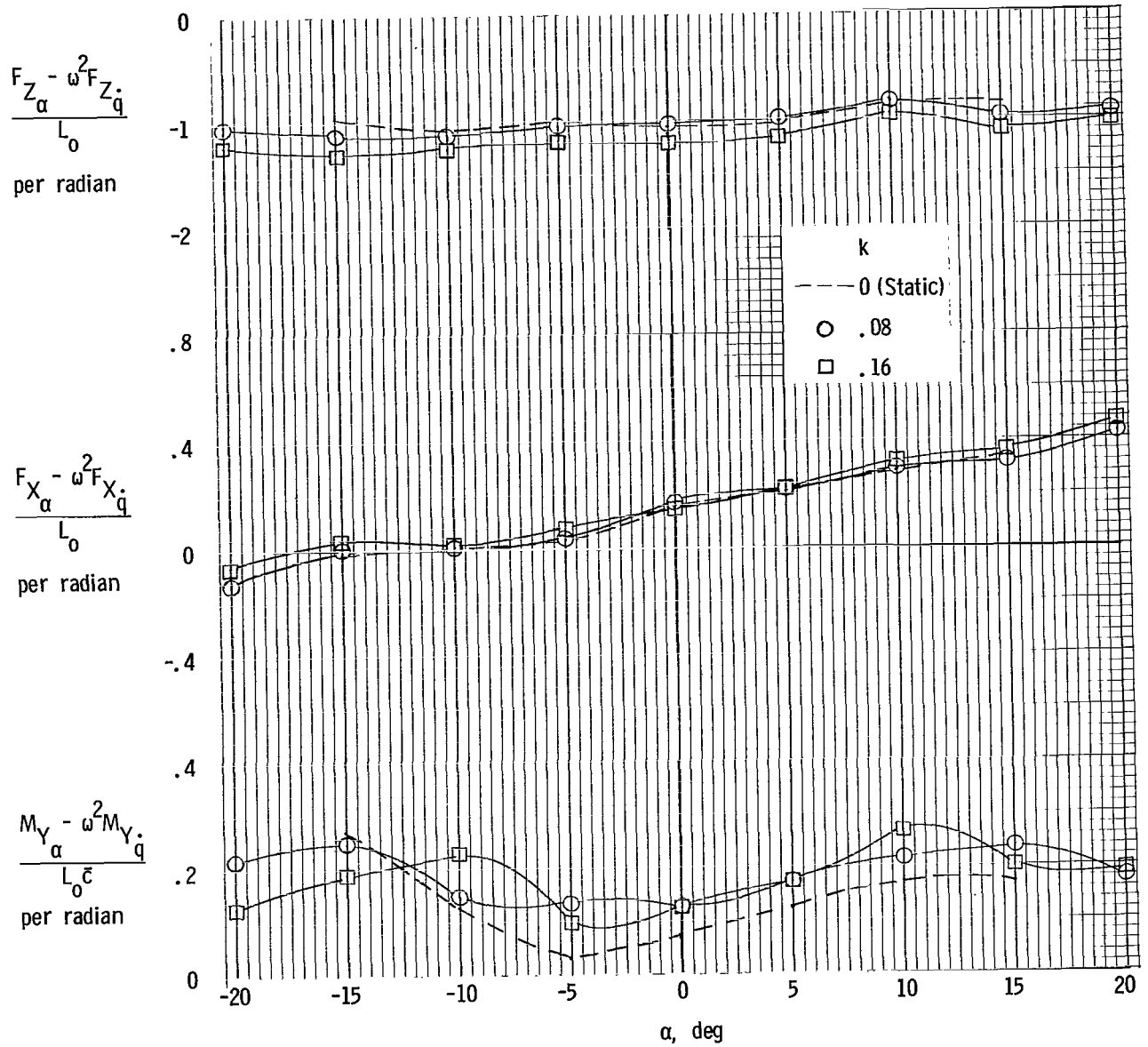


Figure 24.- Effect of frequency on in-phase oscillatory derivatives. $\delta_L = 20^\circ$; $i_t = 20^\circ$; $\frac{L_o}{q_\infty S} = 3.43$.

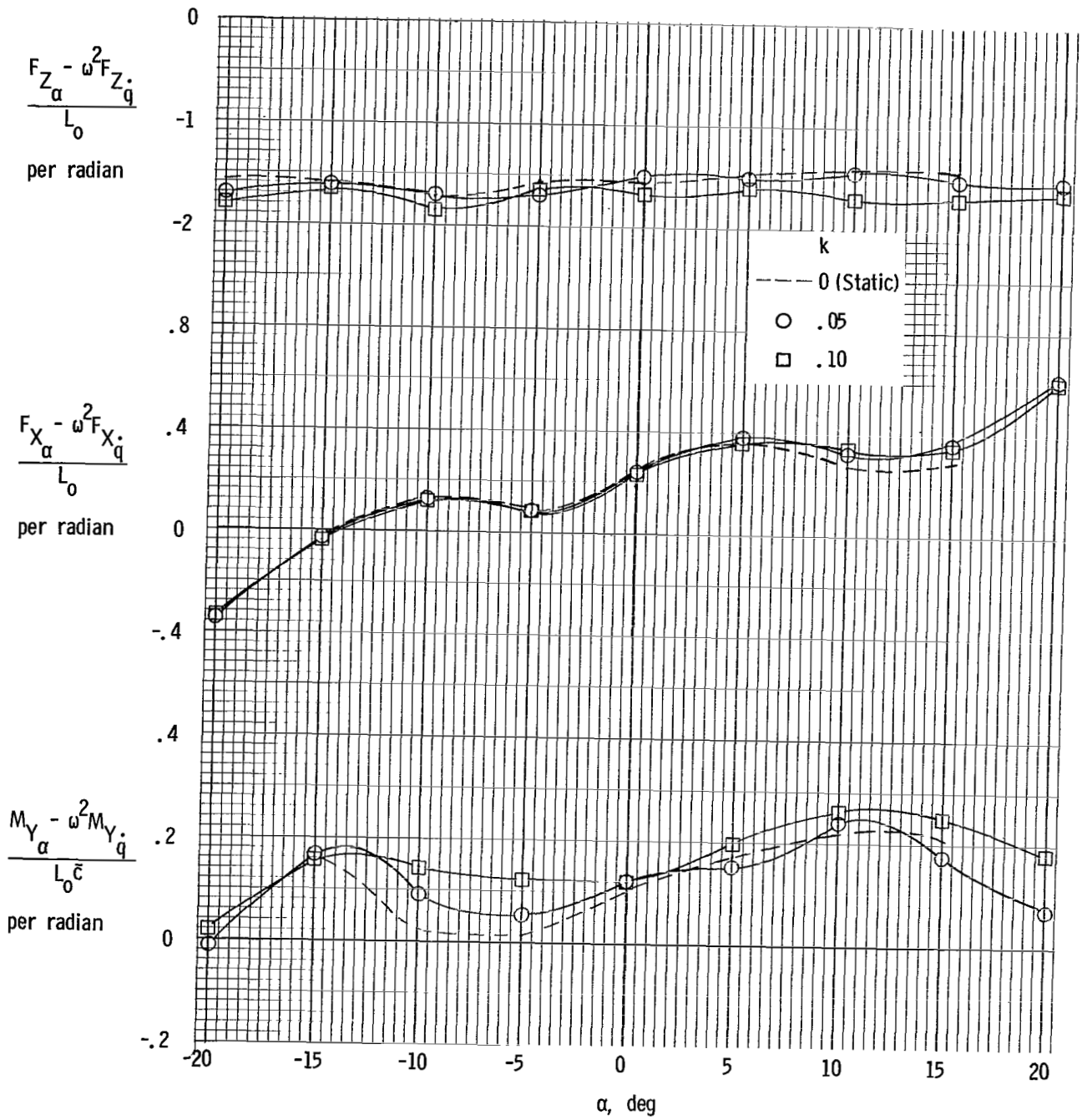


Figure 25.- Effect of frequency on in-phase oscillatory derivatives. $\delta_L = 30^\circ$; $i_t = 20^\circ$; $\frac{L_0}{q_\infty S} = 2.20$.

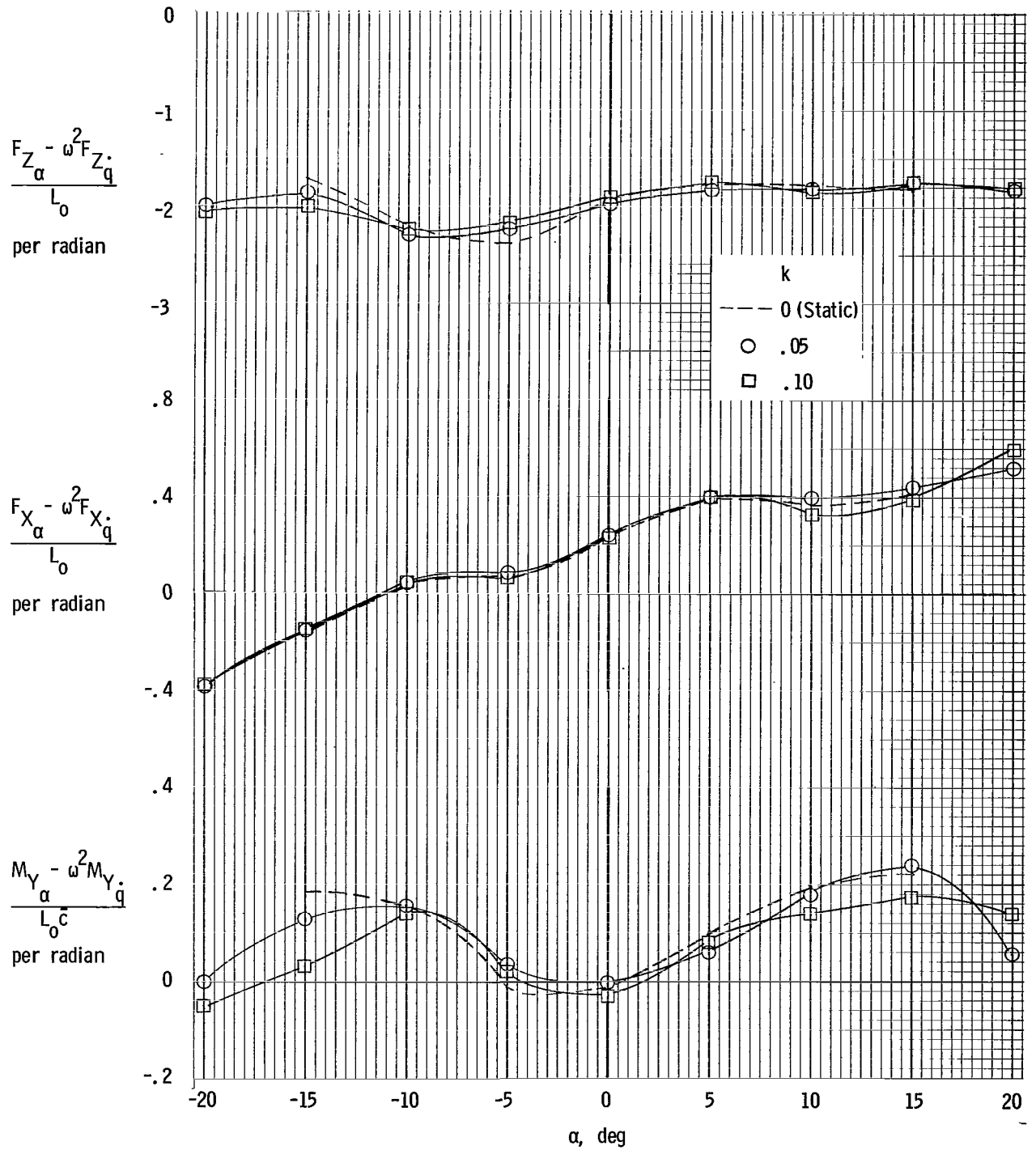


Figure 26.- Effect of frequency on in-phase oscillatory derivatives. $\delta_L = 40^\circ$; $i_t = 15^\circ$; $\frac{L_0}{q_\infty S} = 1.79$.

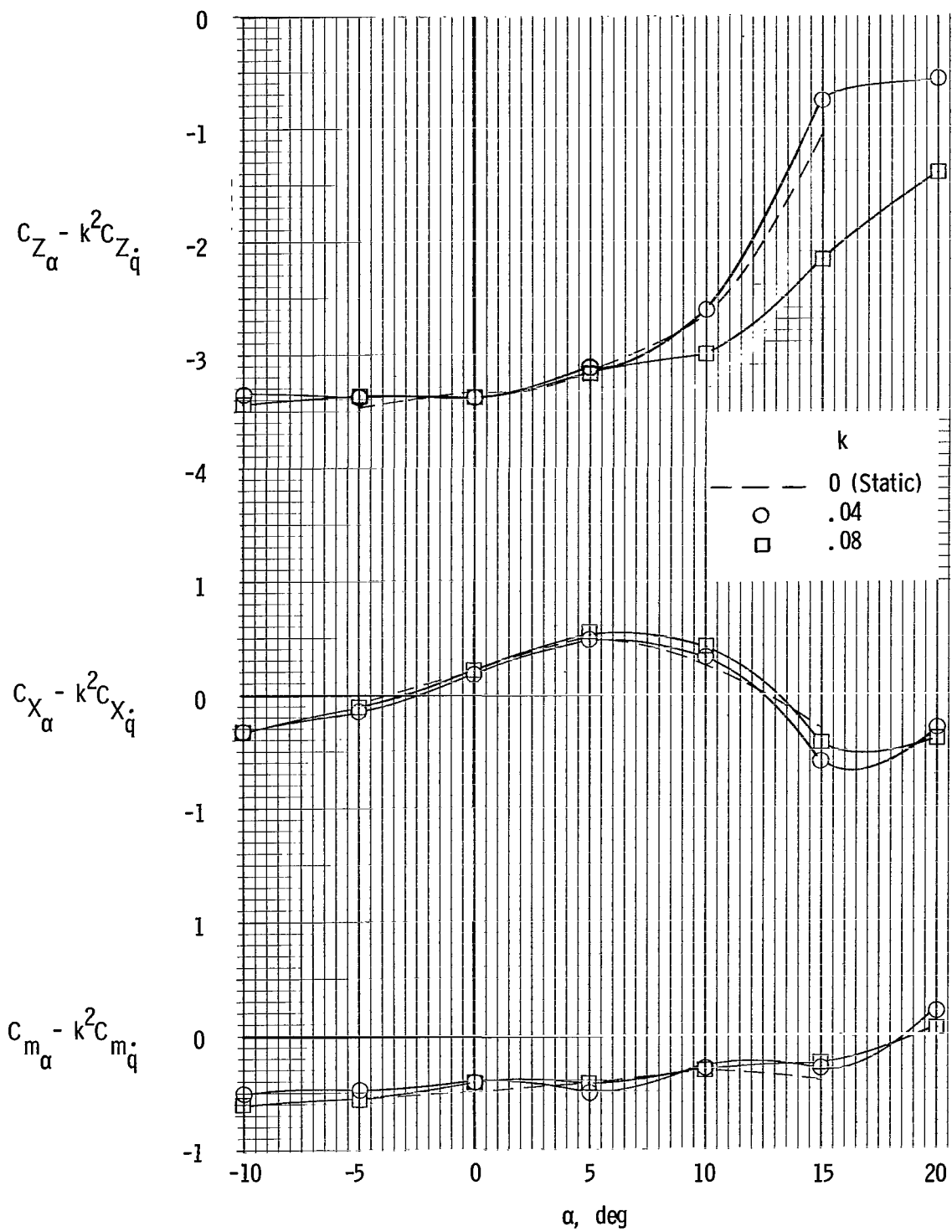


Figure 27.- Effect of frequency on in-phase oscillatory derivatives. Power off; $\delta_t = 0^\circ$; $\delta_a = 0^\circ$; $i_t = 0^\circ$.

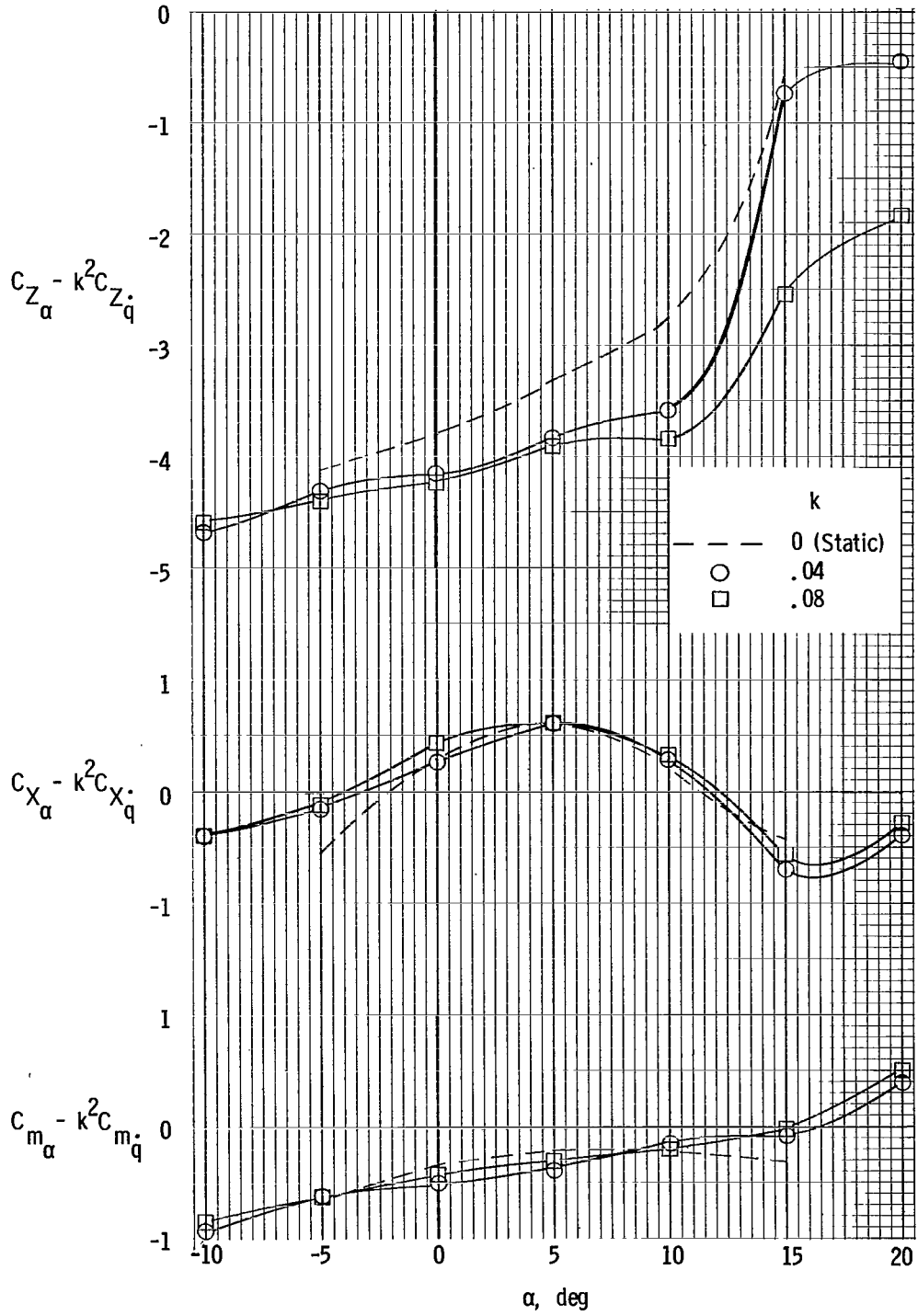


Figure 28.- Effect of frequency on in-phase oscillatory derivatives. Power off; $\delta_f = 45^\circ$; $\delta_a = 15^\circ$; $i_t = 0^\circ$.

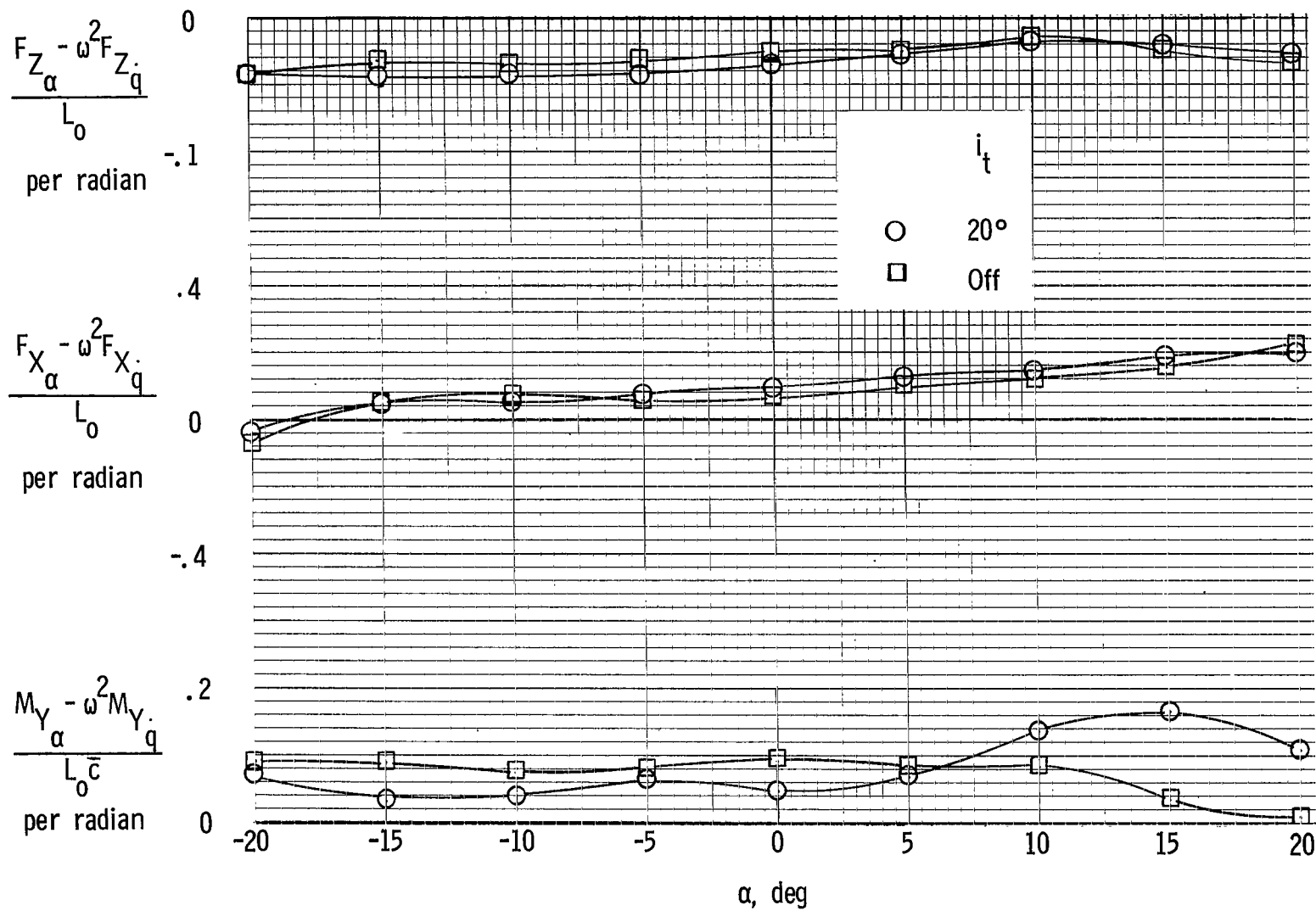


Figure 29.- Effect of horizontal tail on in-phase oscillatory derivatives. $\delta_L = 10^\circ$; $\frac{L_0}{q_\infty S} = 8.26$.

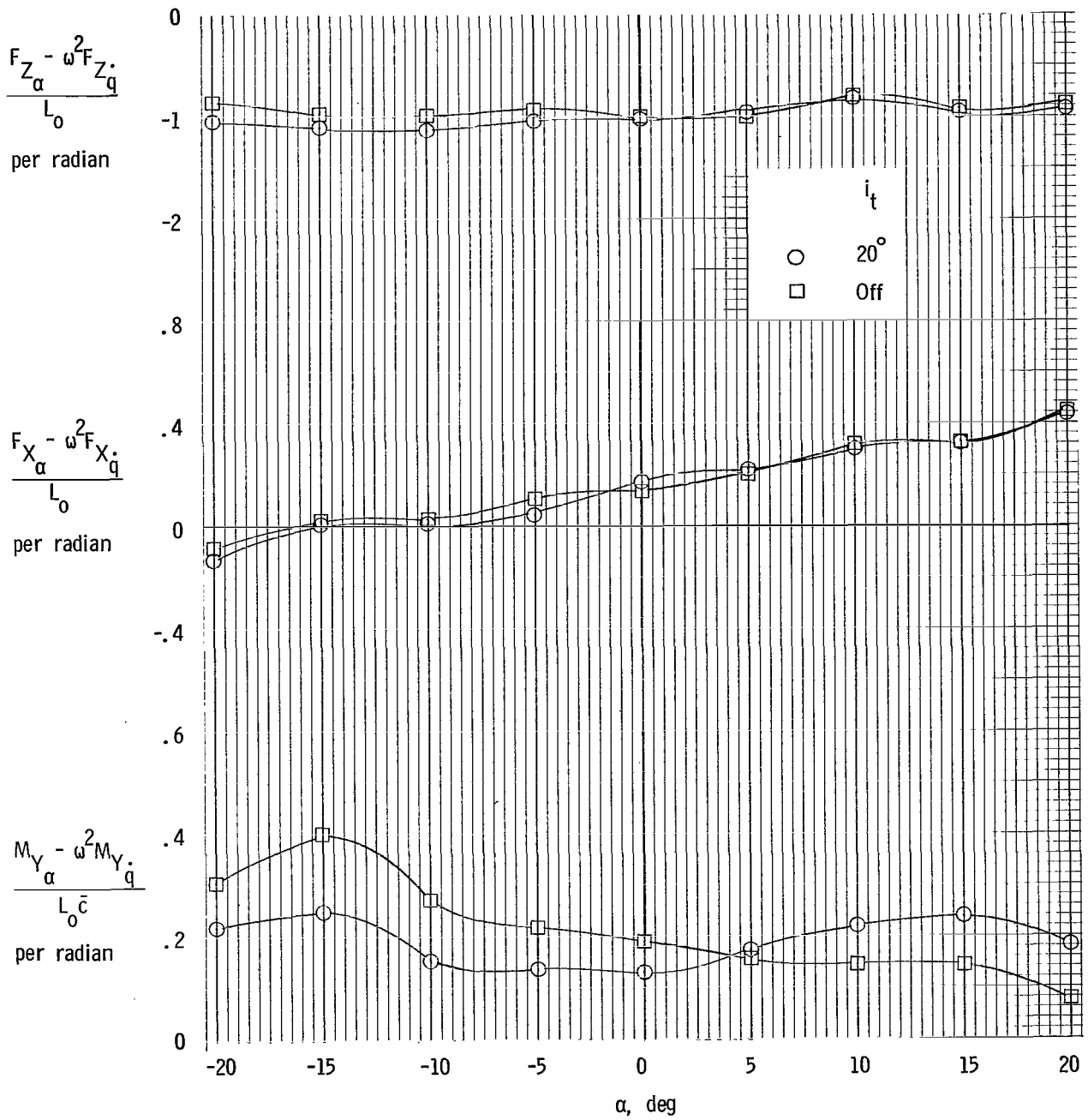


Figure 30.- Effect of horizontal tail on in-phase oscillatory derivatives. $\delta_L = 20^\circ$; $\frac{L_0}{q_\infty S} = 3.43$.

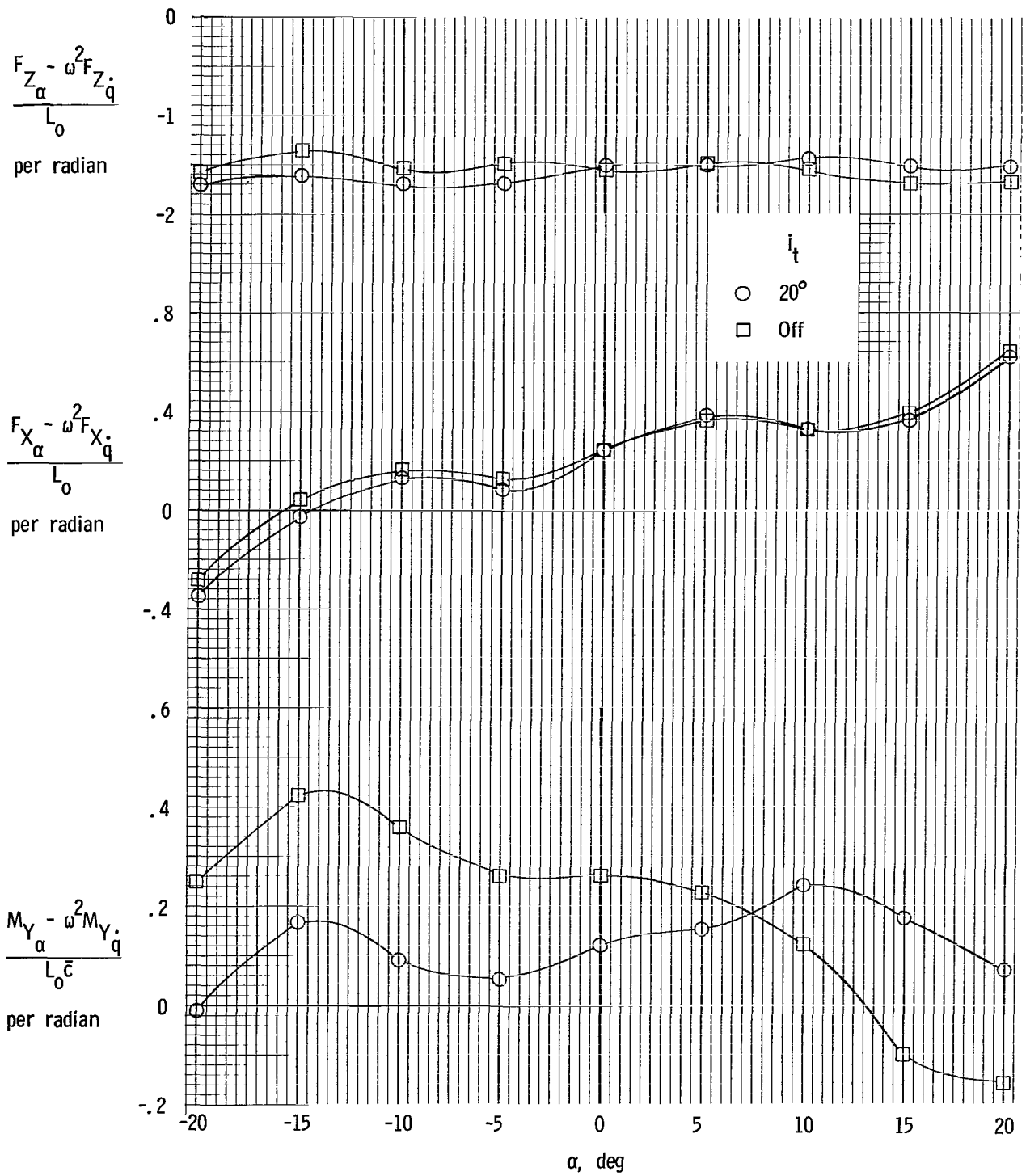


Figure 31.- Effect of horizontal tail on in-phase oscillatory derivatives. $\delta_L = 30^\circ$; $\frac{L_0}{q_\infty S} = 2.2$.

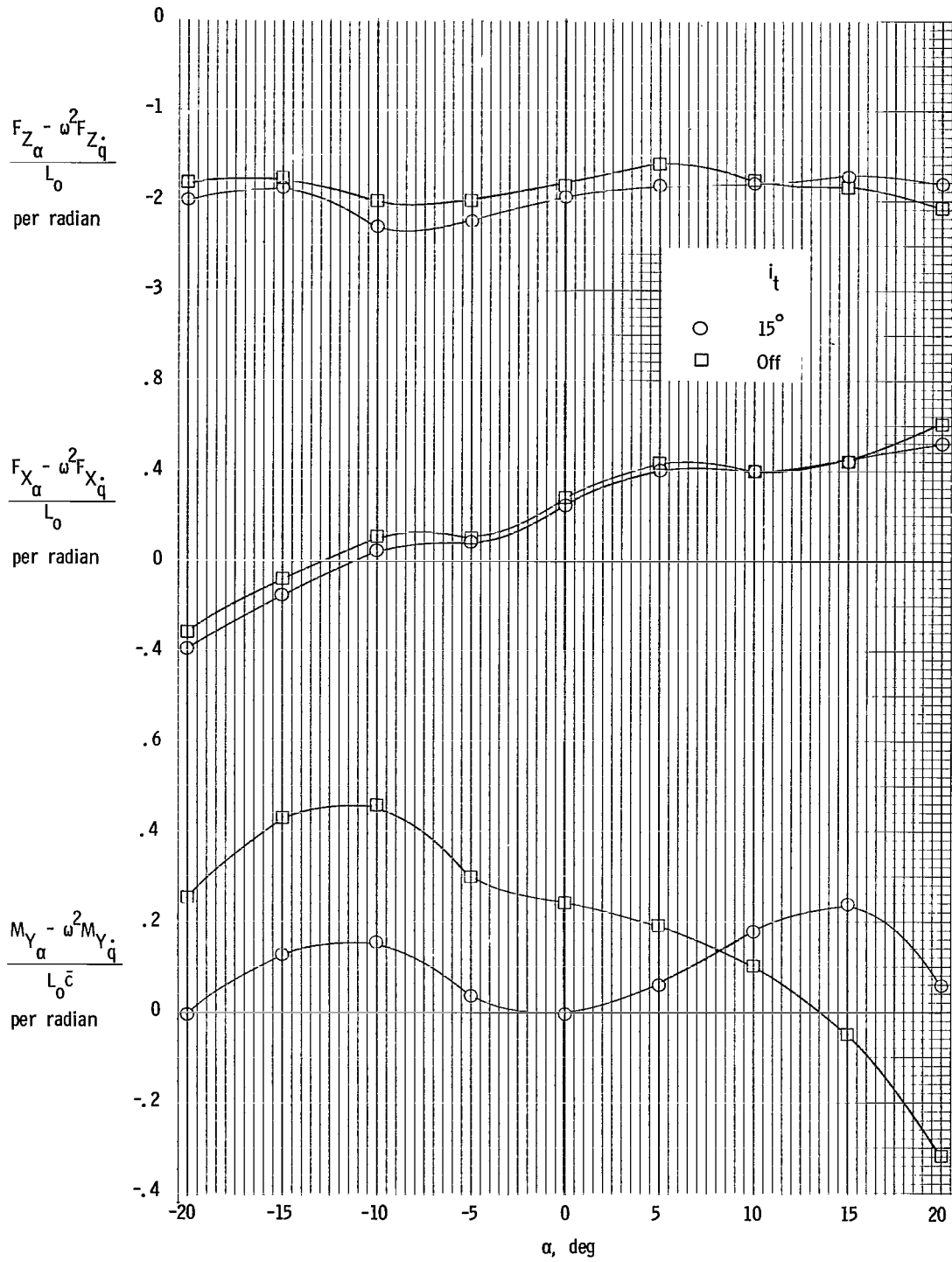


Figure 32.- Effect of horizontal tail on in-phase oscillatory derivatives. $\delta_L = 40^\circ$; $\frac{L_0}{q_\infty S} = 1.79$.

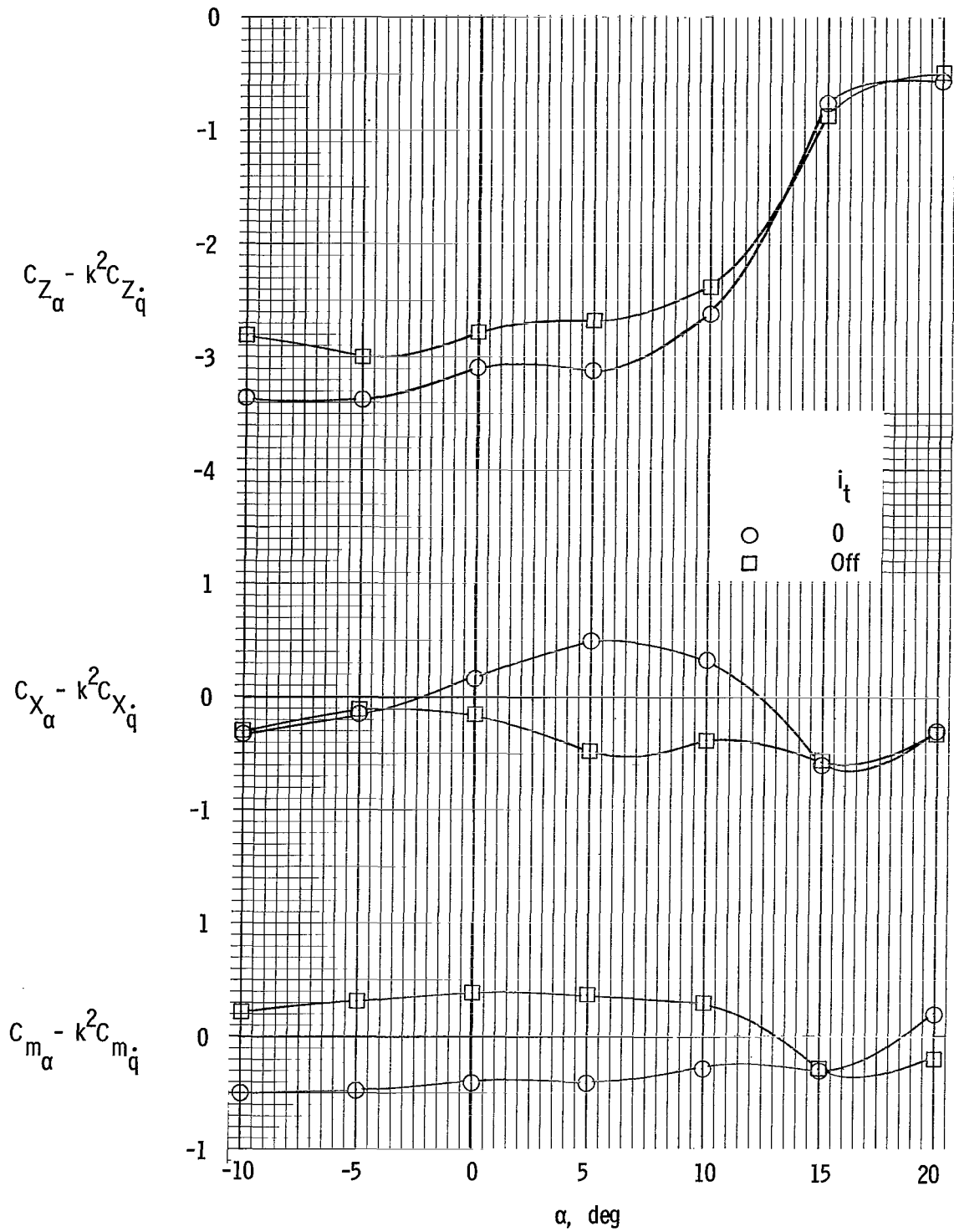


Figure 33.- Effect of horizontal tail on in-phase oscillatory derivatives. Power off; $\delta_f = 0^\circ$; $\delta_a = 0^\circ$.

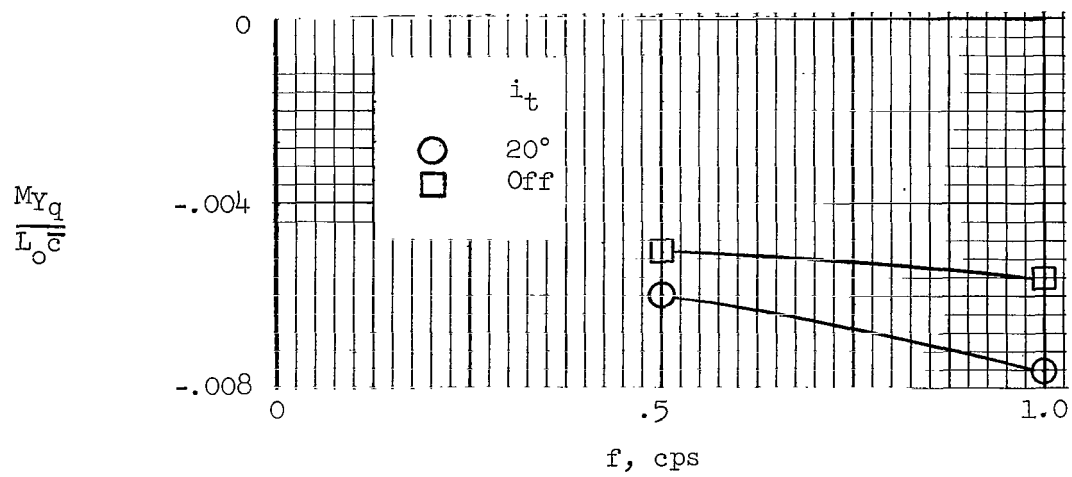


Figure 34.- Effect of oscillatory frequency on damping in pitch during hovering flight. $\delta_L = 0^\circ$; $L_0 = 50.39$ pounds (224.15 N).

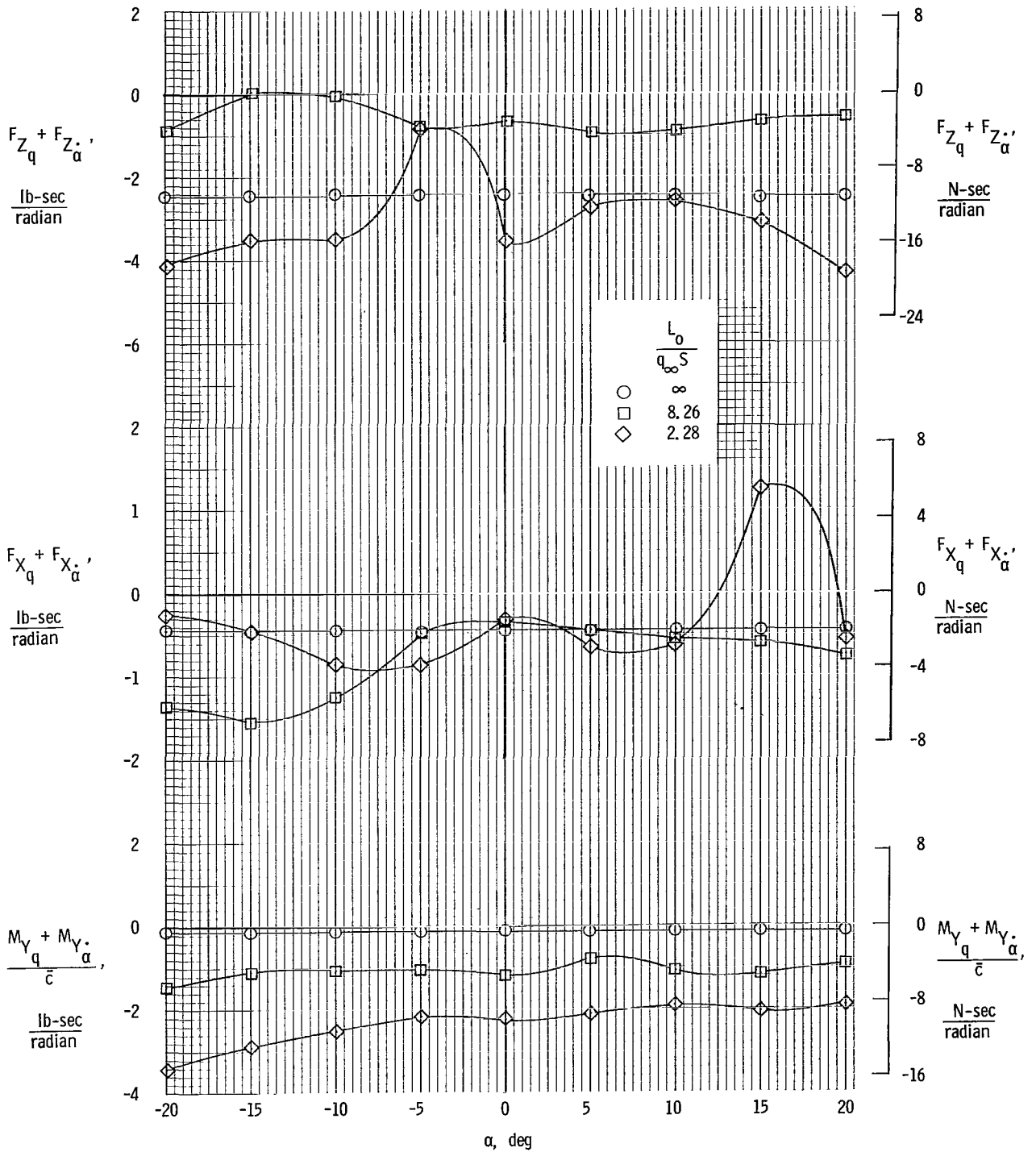


Figure 35.- Variation of the out-of-phase oscillatory derivatives with angle of attack. $\delta_L = 10^\circ$; $i_t = 20^\circ$; $L_0 = 36.5$ pounds (162.36 N).

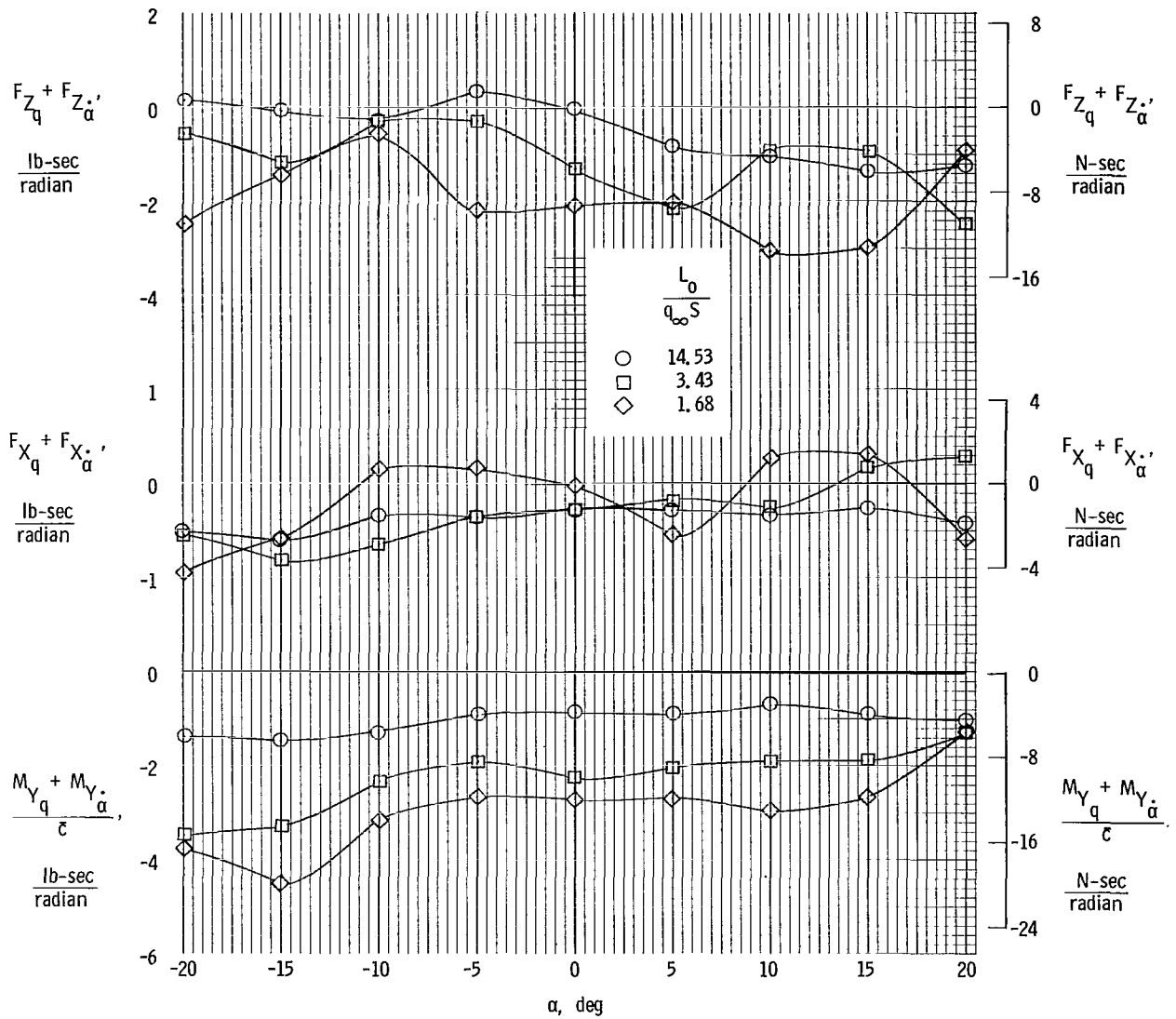


Figure 36.- Variation of the out-of-phase oscillatory derivatives with angle of attack. $\delta_L = 20^\circ$; $i_t = 20^\circ$; $L_0 = 42.11$ pounds (187.31 N).

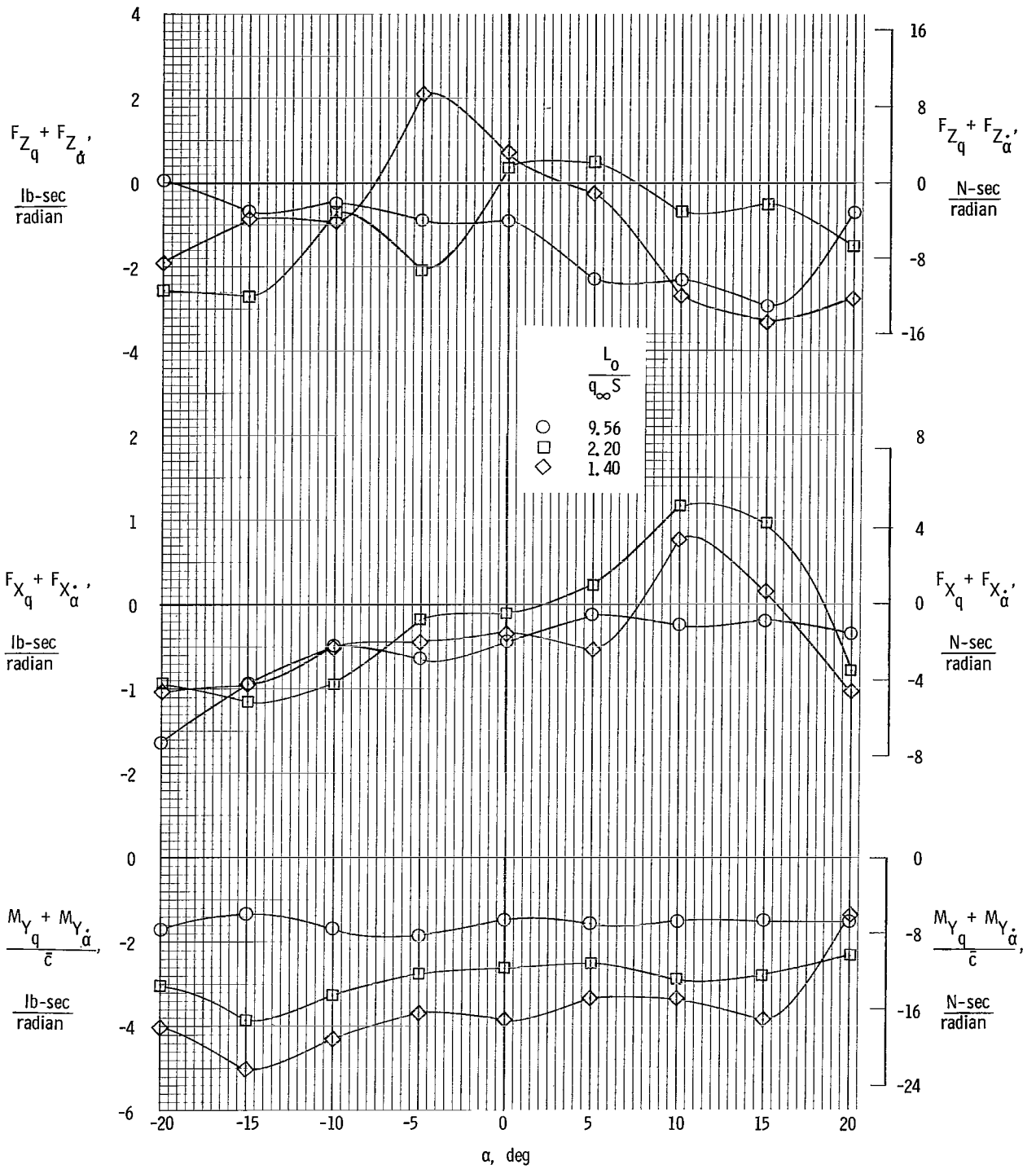


Figure 37.- Variation of the out-of-phase oscillatory derivatives with angle of attack. $\delta_L = 30^\circ$; $i_t = 30^\circ$; $L_0 = 50.73$ pounds (225.66 N).

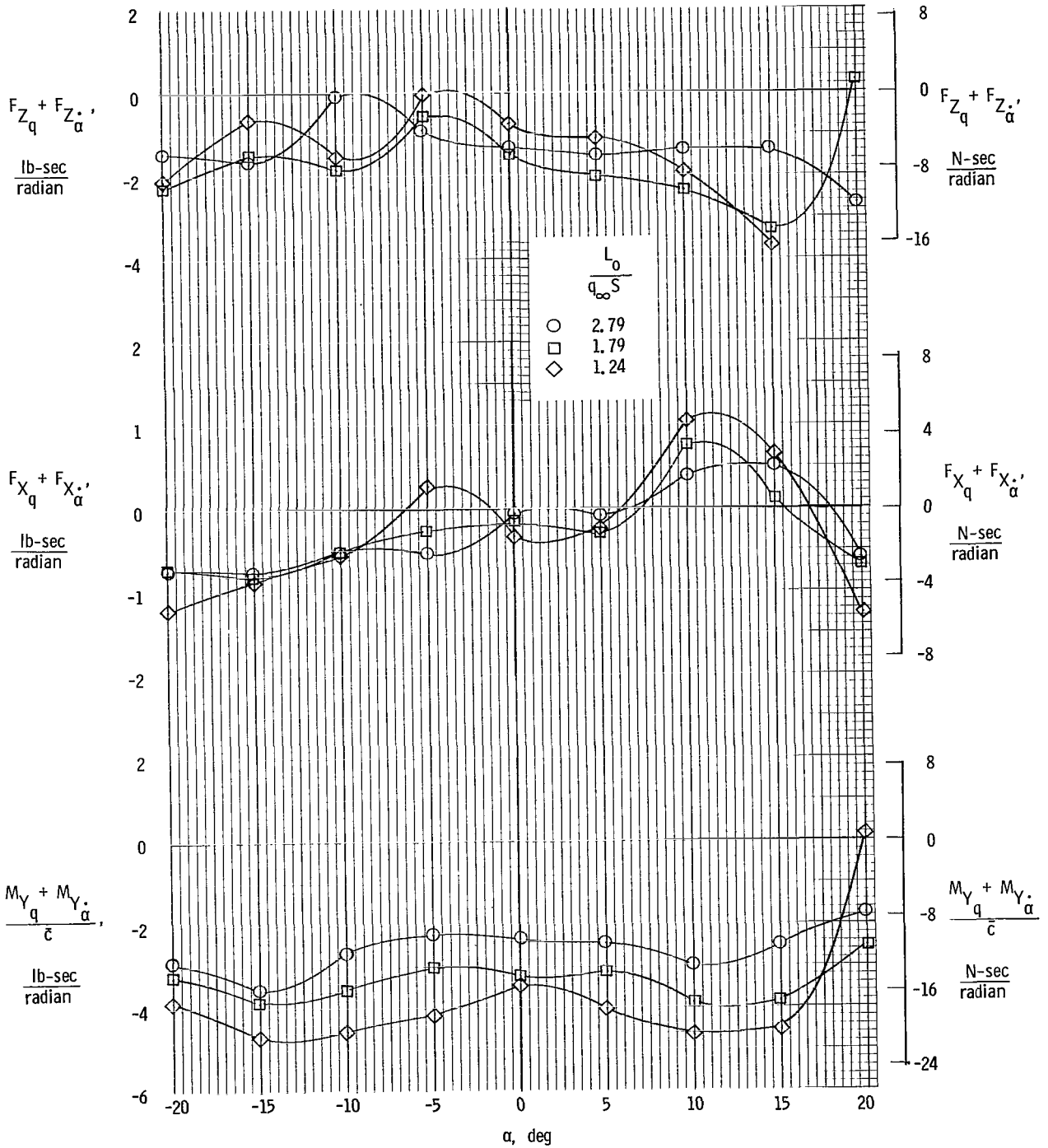


Figure 38.- Variation of the out-of-phase oscillatory derivatives with angle of attack. $\delta_L = 40^\circ$; $i_t = 15^\circ$; $L_0 = 44.81$ pounds (199.32 N).

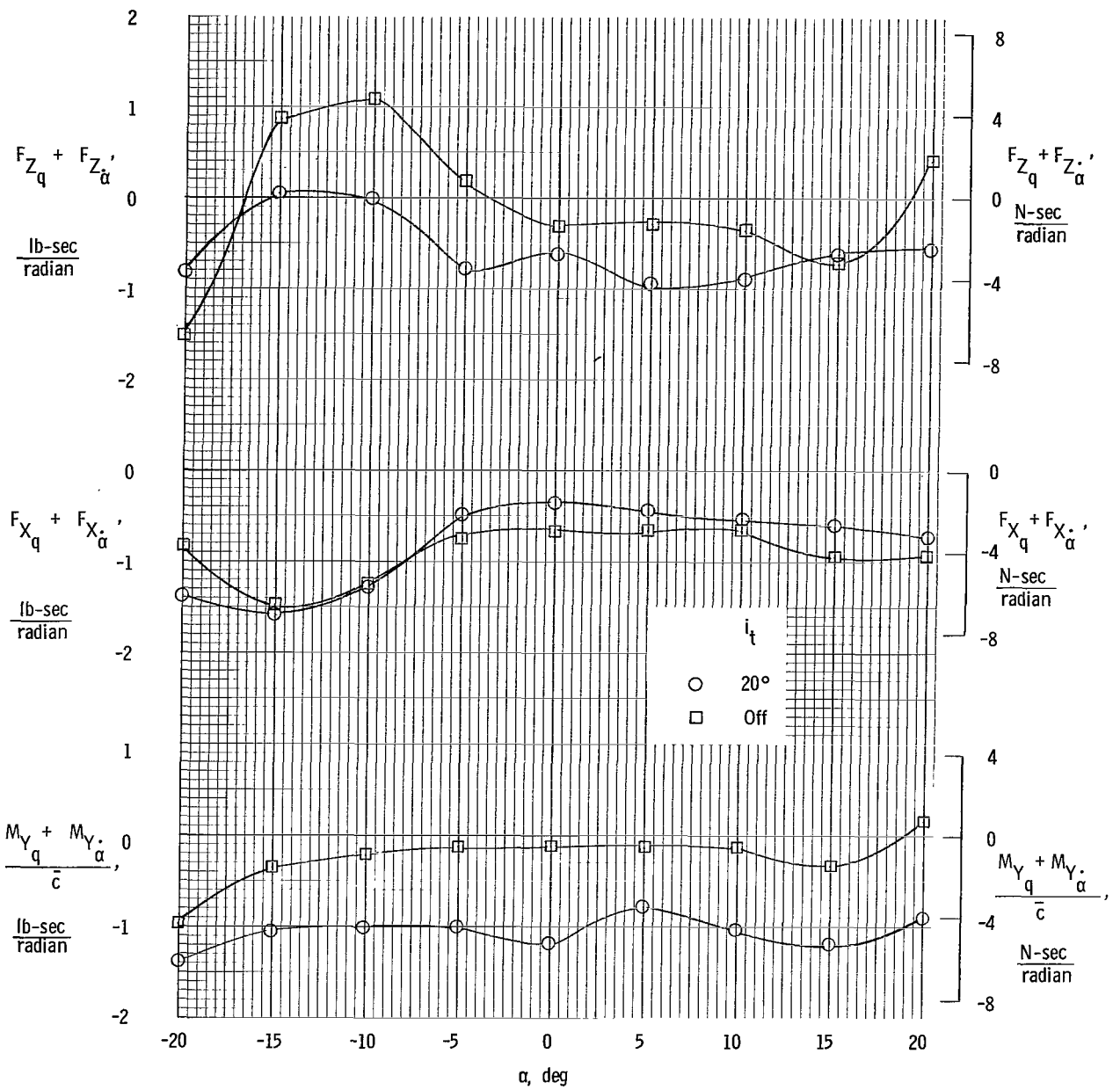


Figure 39.- Effect of horizontal tail on out-of-phase oscillatory derivatives. $\delta_L = 10^\circ$; $\frac{L_0}{q_\infty S} = 8.26$.

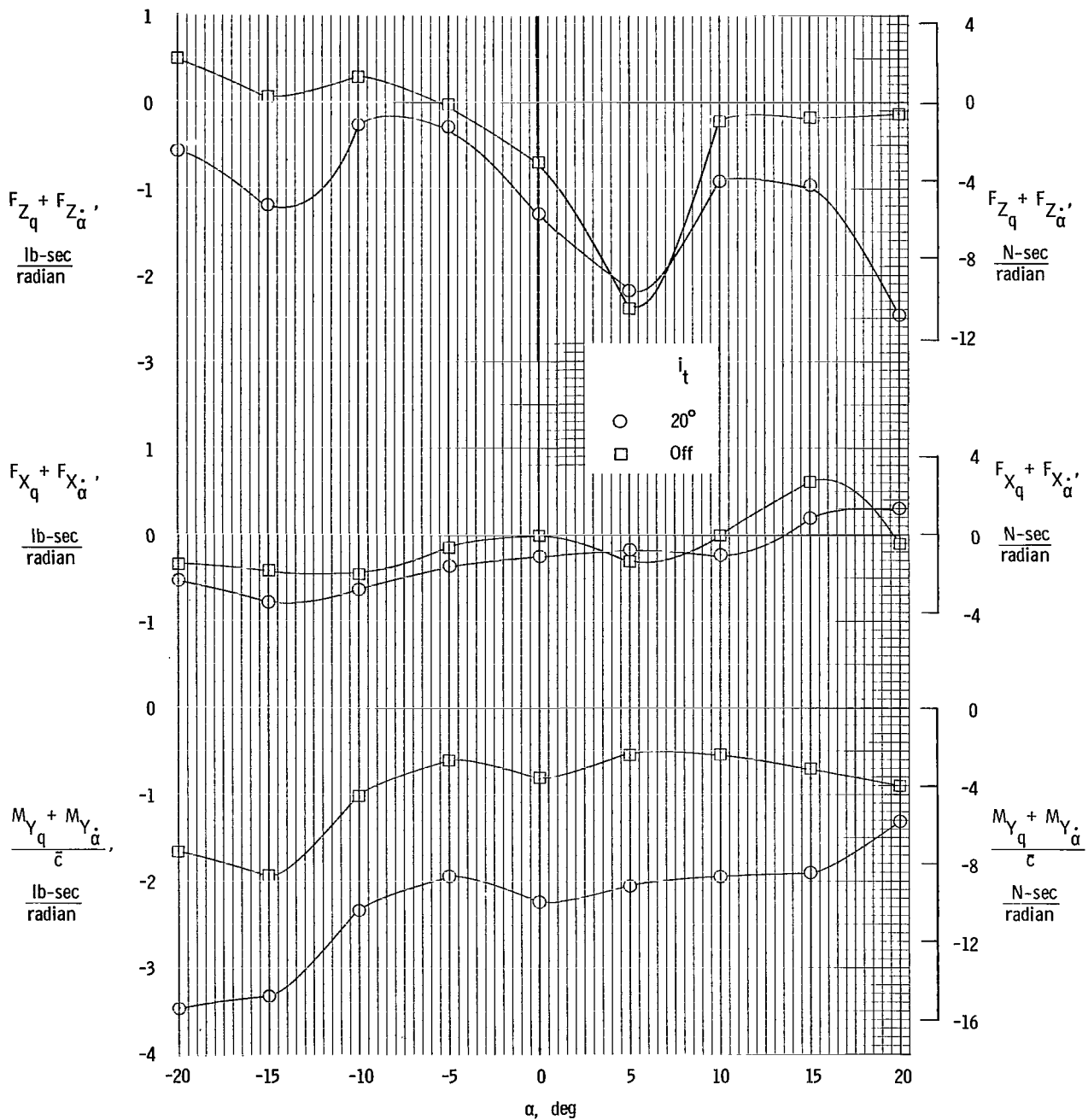


Figure 40.- Effect of horizontal tail on out-of-phase oscillatory derivatives. $\delta_L = 20^\circ$; $\frac{L_0}{q_\infty S} = 3.43$.

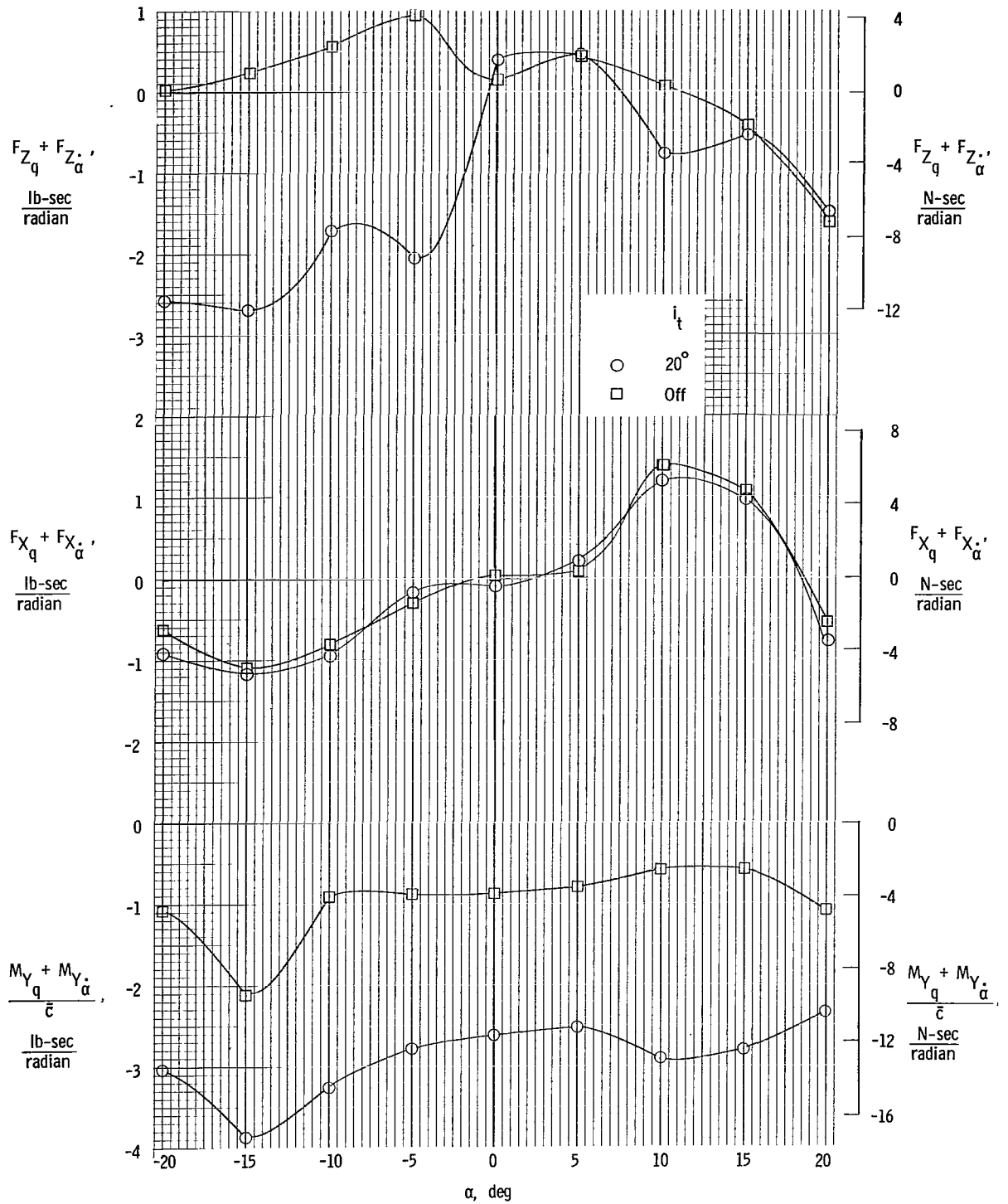


Figure 41.- Effect of horizontal tail on out-of-phase oscillatory derivatives. $\delta_L = 30^\circ$; $\frac{L_0}{q_\infty S} = 2.20$.

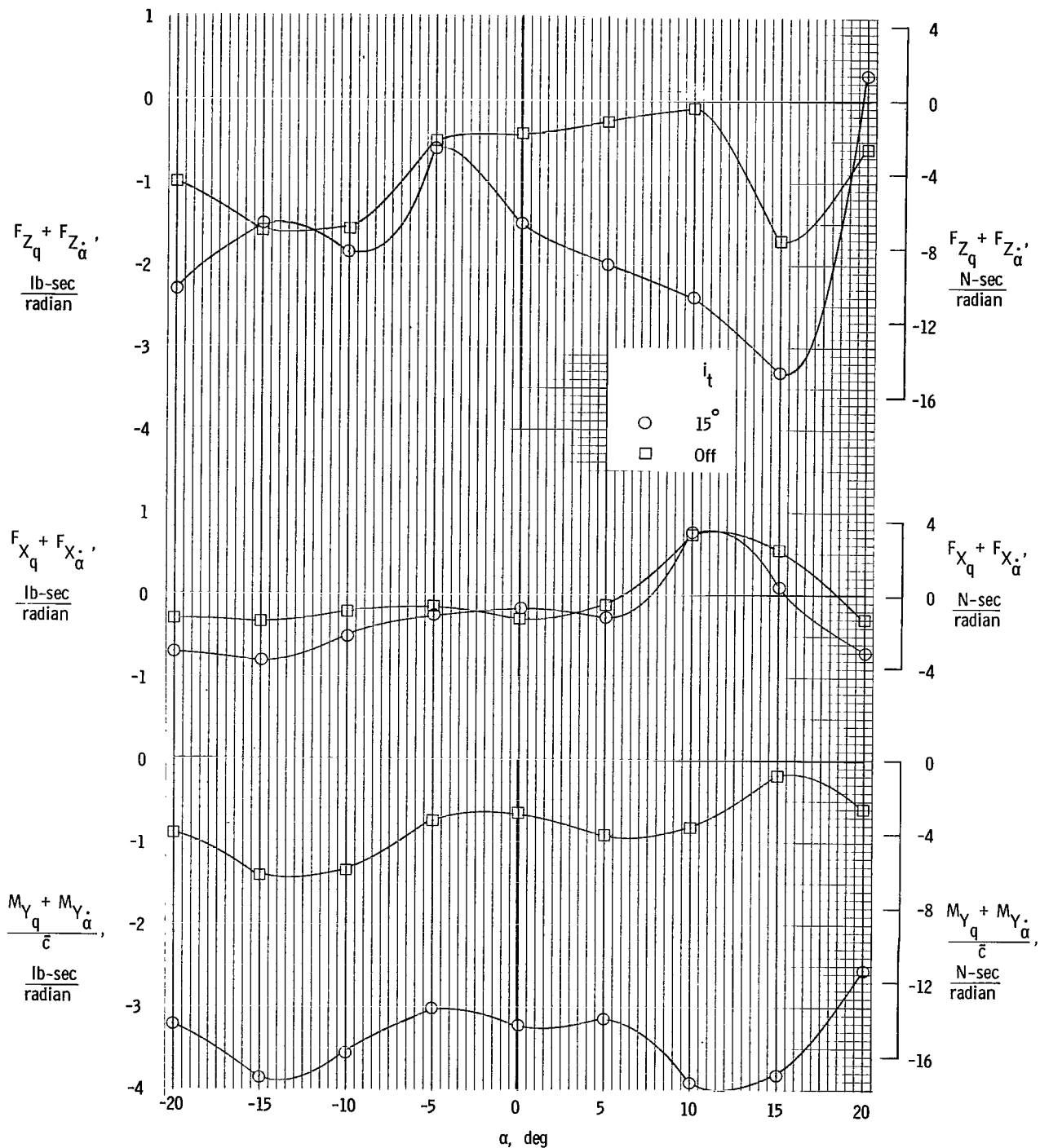


Figure 42.- Effect of horizontal tail on out-of-phase oscillatory derivatives. $\delta_L = 40^\circ$; $\frac{L_0}{q_\infty S} = 1.79$.

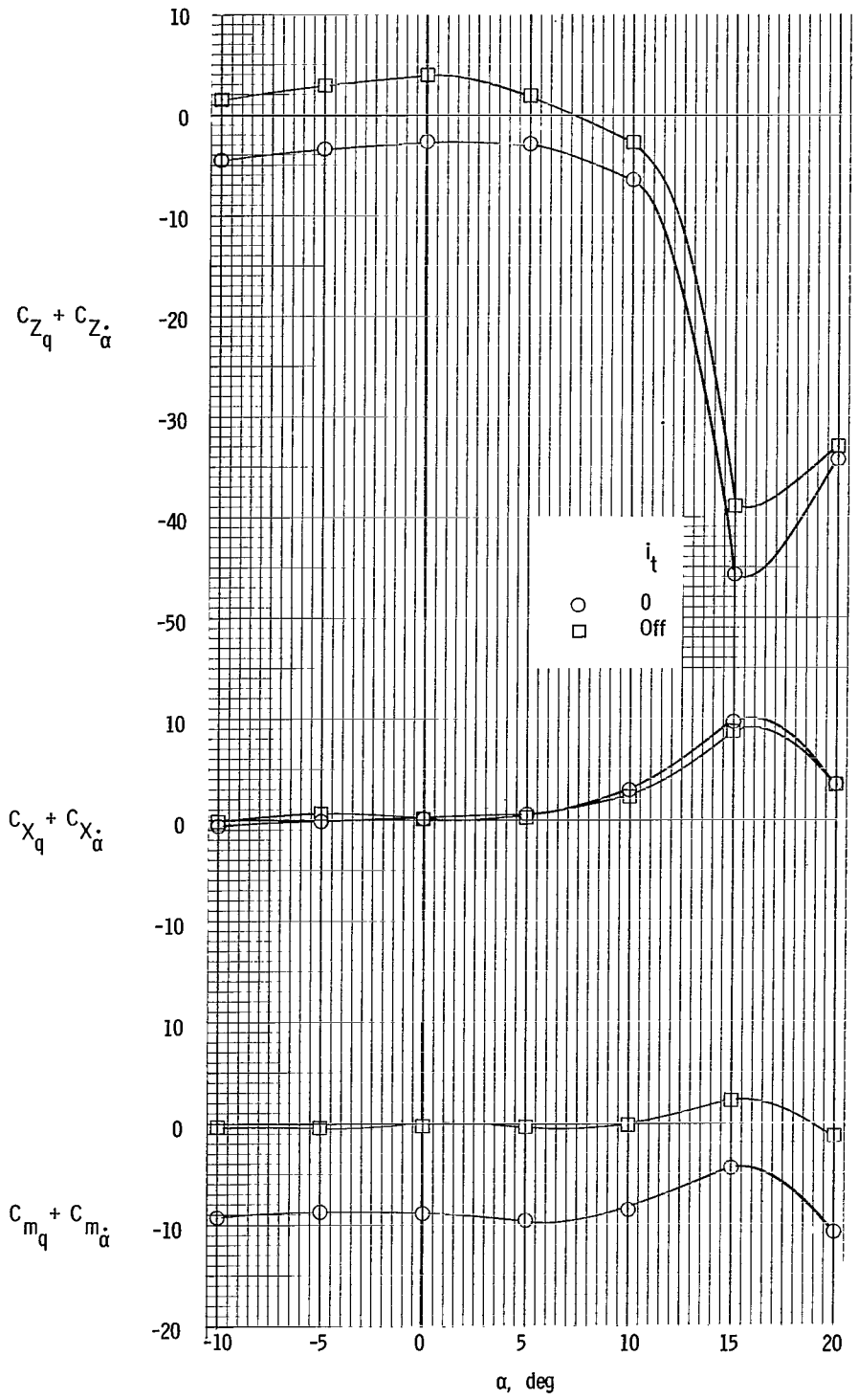


Figure 43.- Effect of horizontal tail on out-of-phase oscillatory derivatives. Power off; $\delta_f = 0^\circ$; $\delta_a = 0^\circ$.

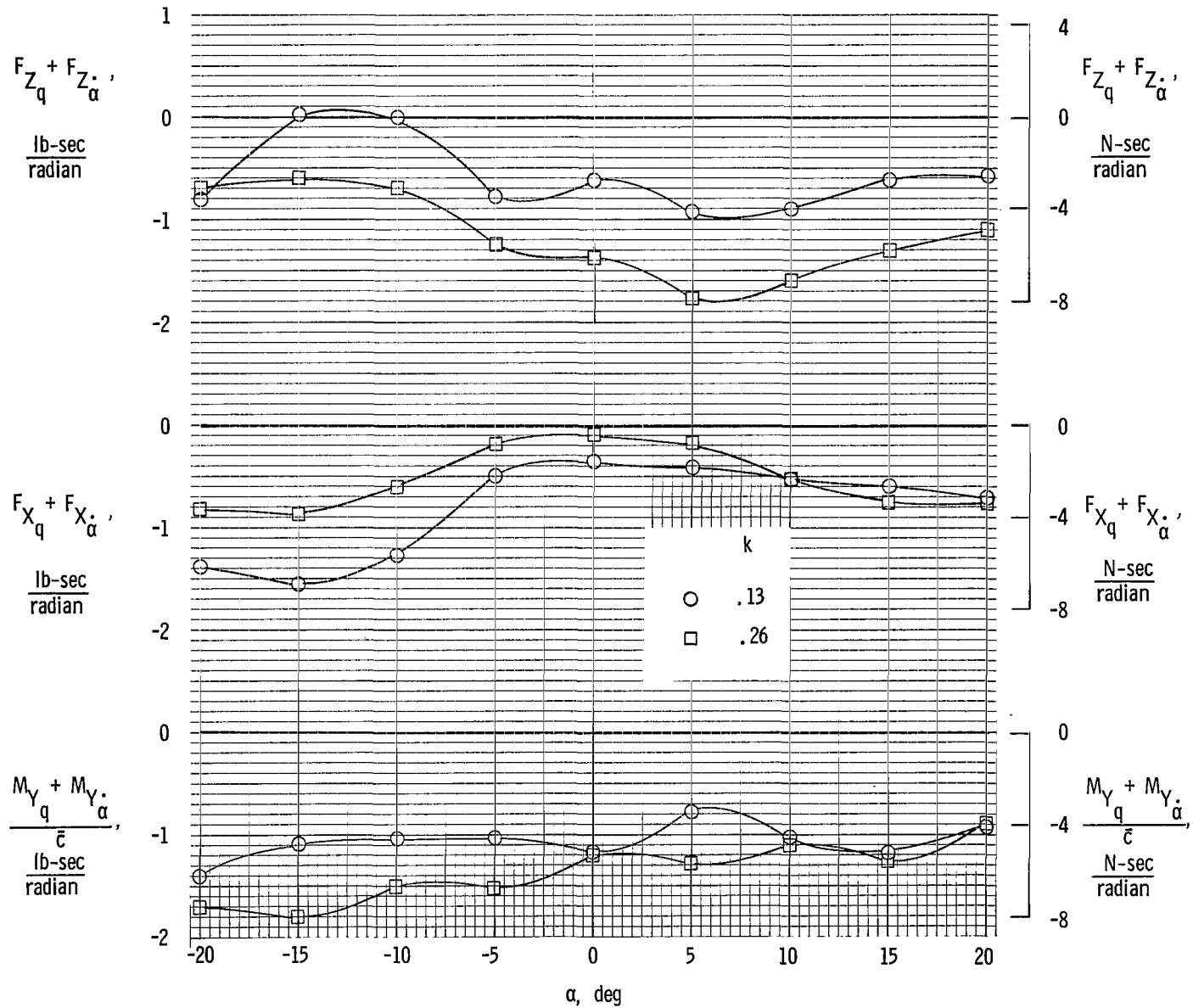


Figure 44.- Effect of frequency on out-of-phase oscillatory derivatives. $\delta_L = 10^\circ$; $i_t = 20^\circ$; $\frac{L_0}{q_\infty S} = 8.26$.

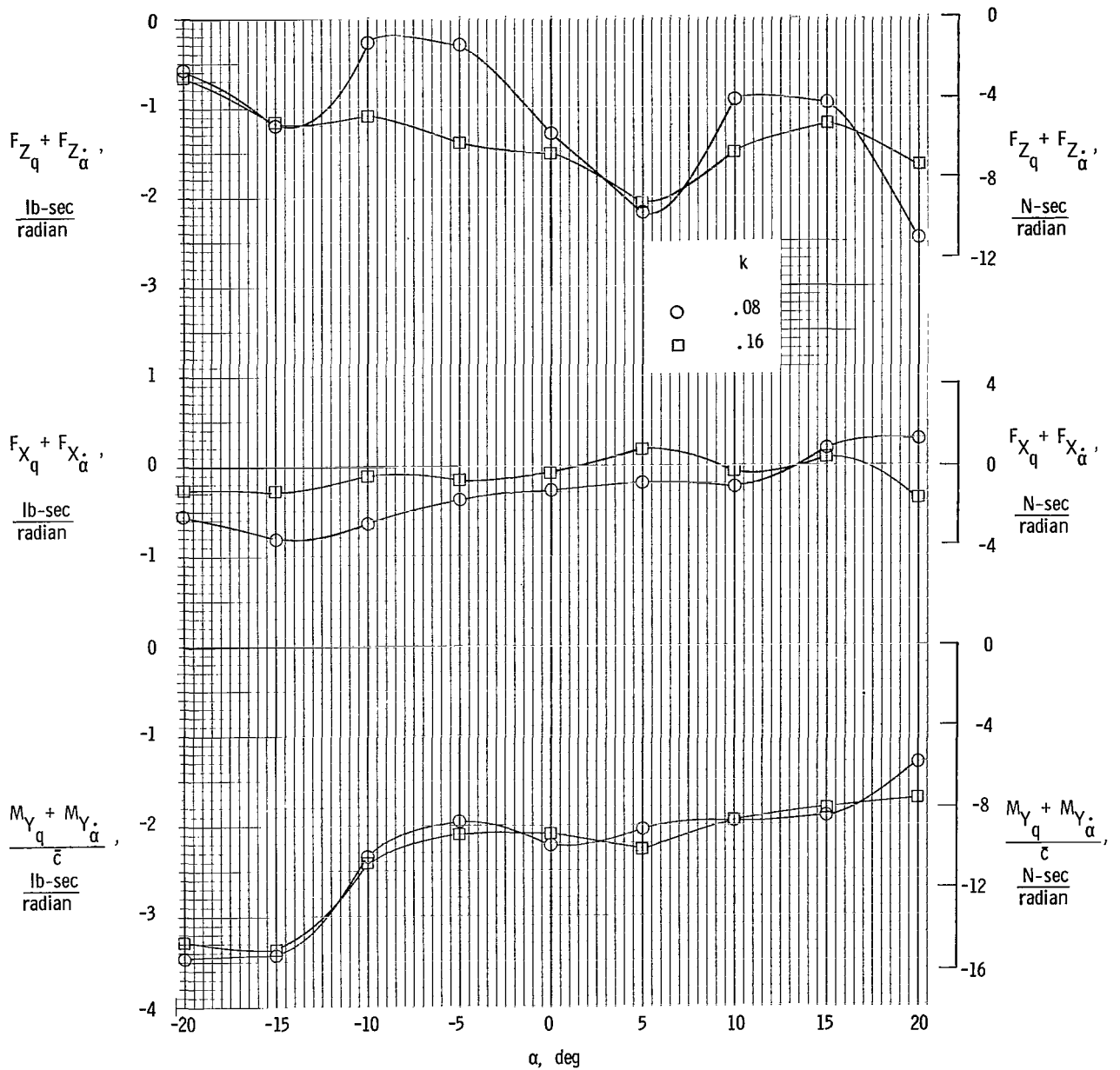


Figure 45.- Effect of frequency on out-of-phase oscillatory derivatives. $\delta_L = 20^0$; $i_t = 20^0$; $\frac{L_0}{q_{\infty} S} = 3.43$.

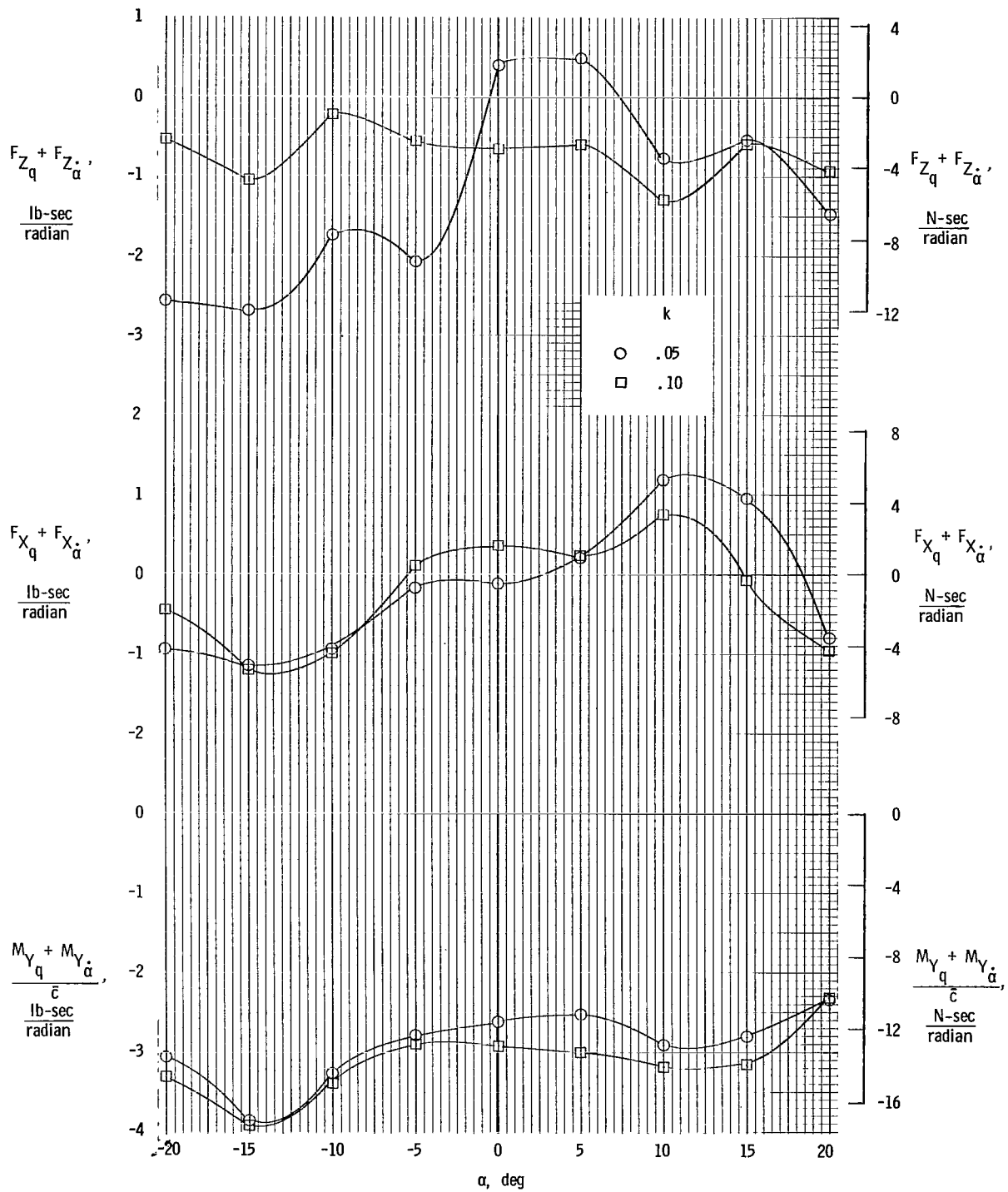


Figure 46.- Effect of frequency on out-of-phase oscillatory derivatives. $\delta_L = 30^\circ$; $i_t = 20^\circ$; $\frac{L_0}{q_\infty S} = 2.20$.

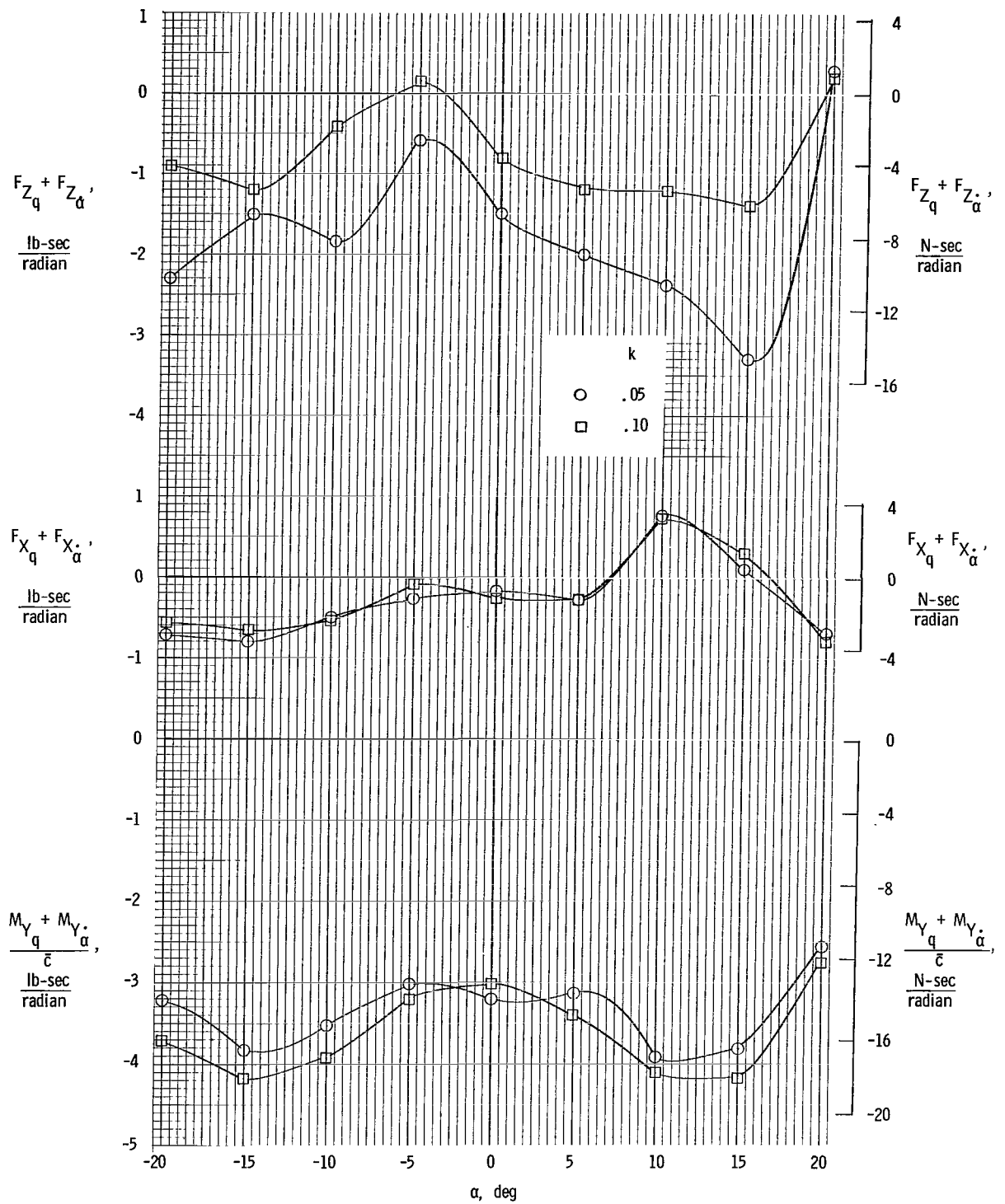


Figure 47.- Effect of frequency on out-of-phase oscillatory derivatives. $\delta_L = 40^\circ$; $i_t = 15^\circ$; $\frac{l_0}{q_\infty S} = 1.79$.

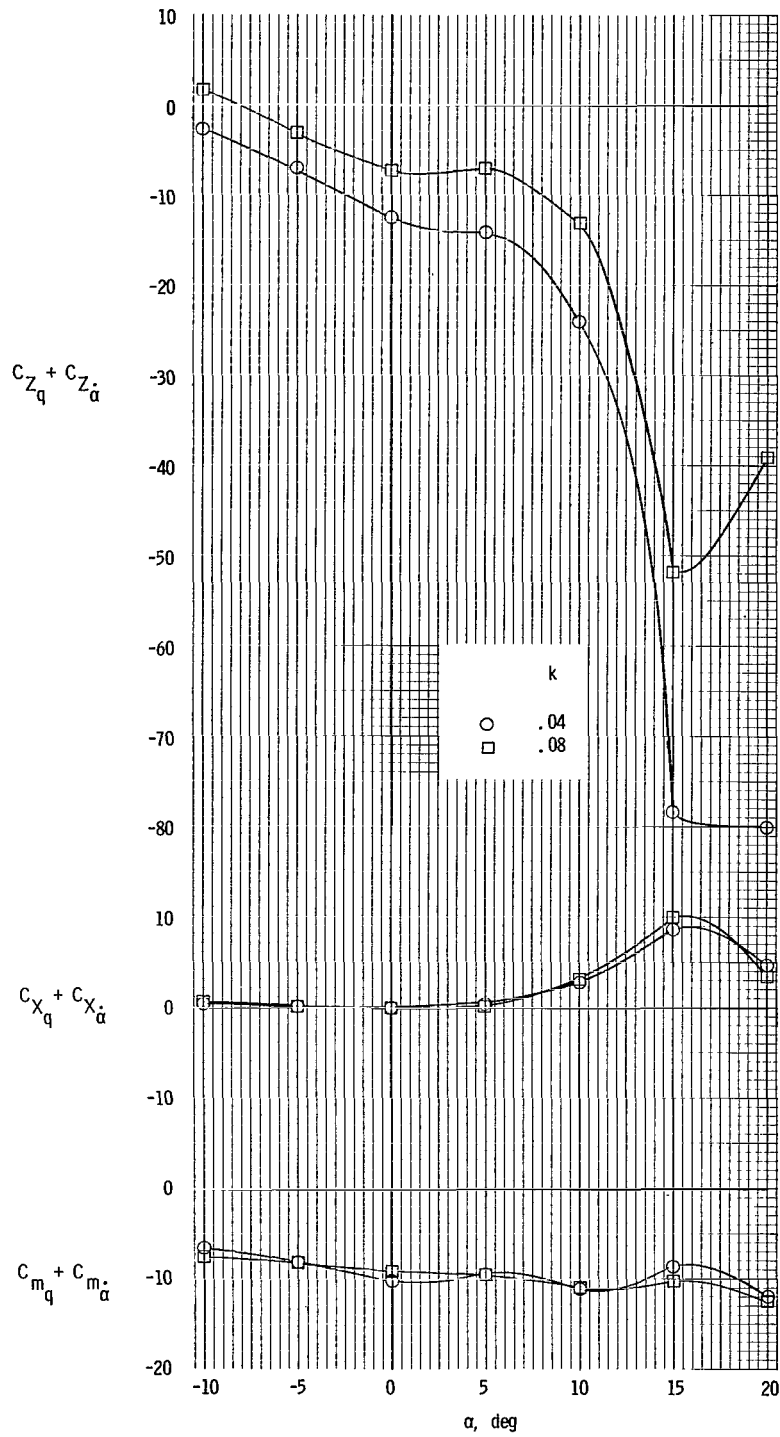


Figure 48.- Effect of frequency on the out-of-phase oscillatory derivatives. Power off; $\delta_f = 45^\circ$; $\delta_a = 15^\circ$; $i_t = 0^\circ$.

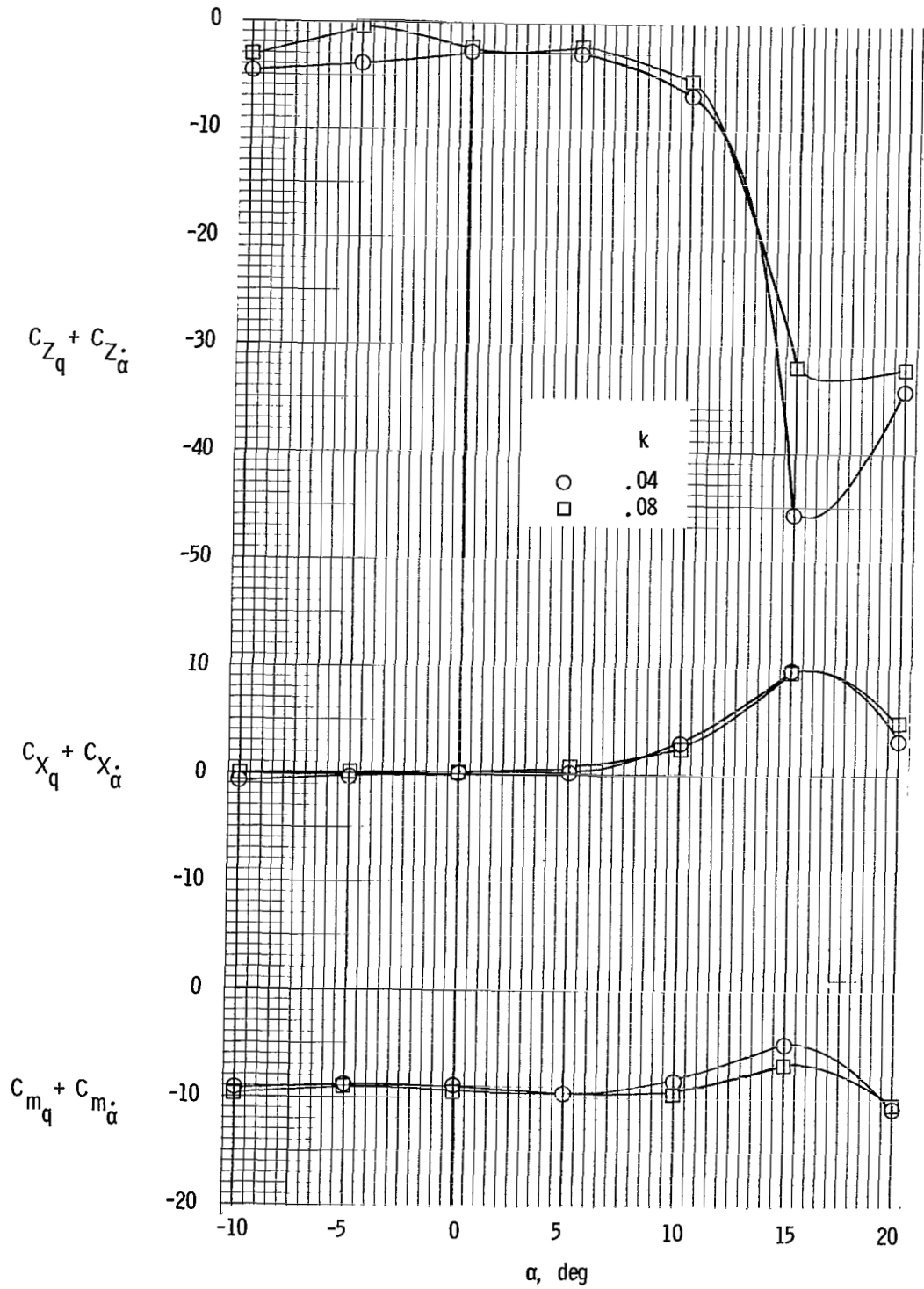


Figure 49.- Effect of frequency on the out-of-phase oscillatory derivatives. Power off; $\delta_f = 0^0$; $\delta_a = 0^0$; $i_t \approx 0^0$.

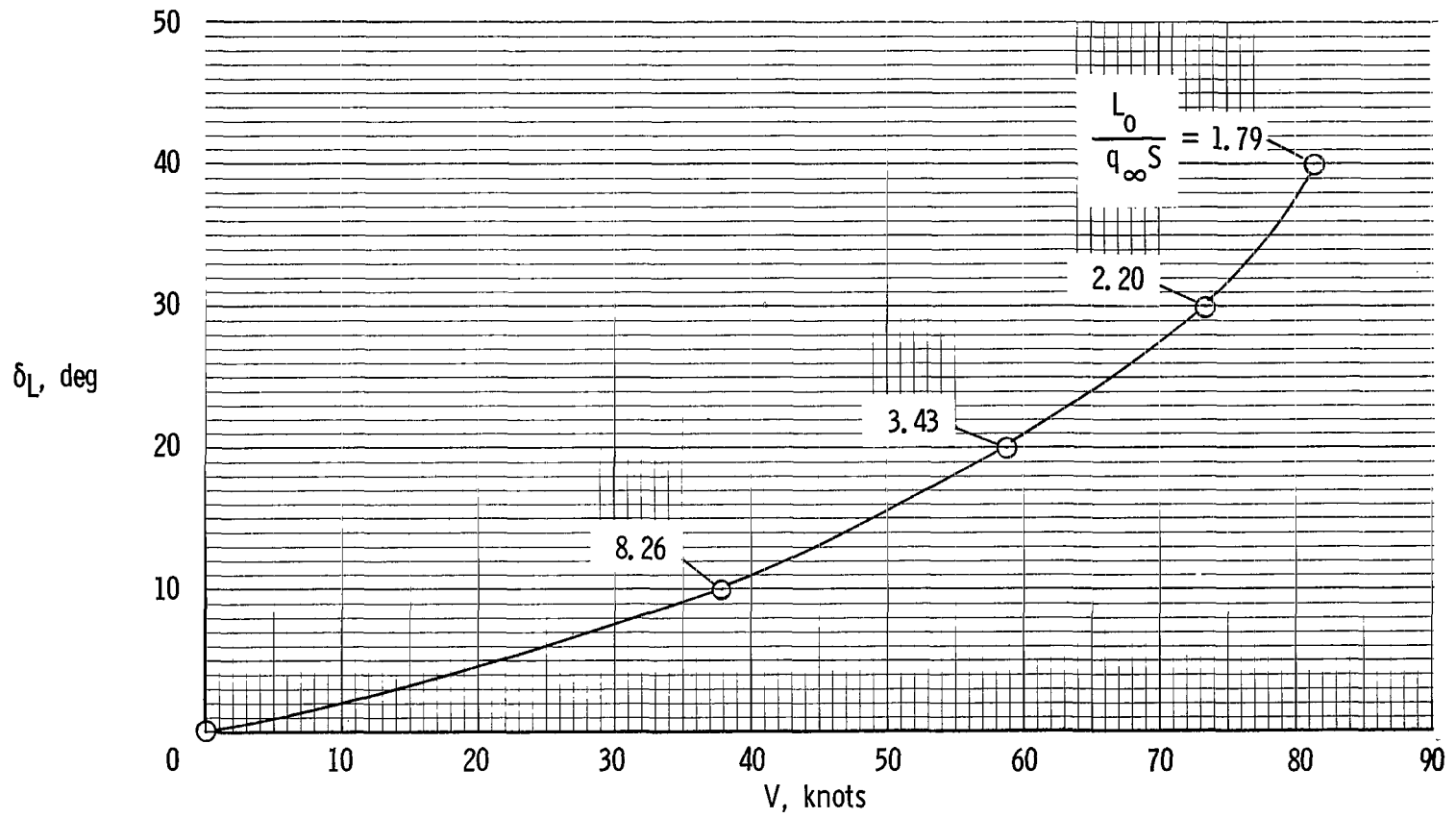


Figure 50.- Variation of exit-louver deflection with forward speed for the full-scale airplane (based on scaled-up model data). $W/S = 40 \text{ lb/ft}^2$ (1915 N/m^2).

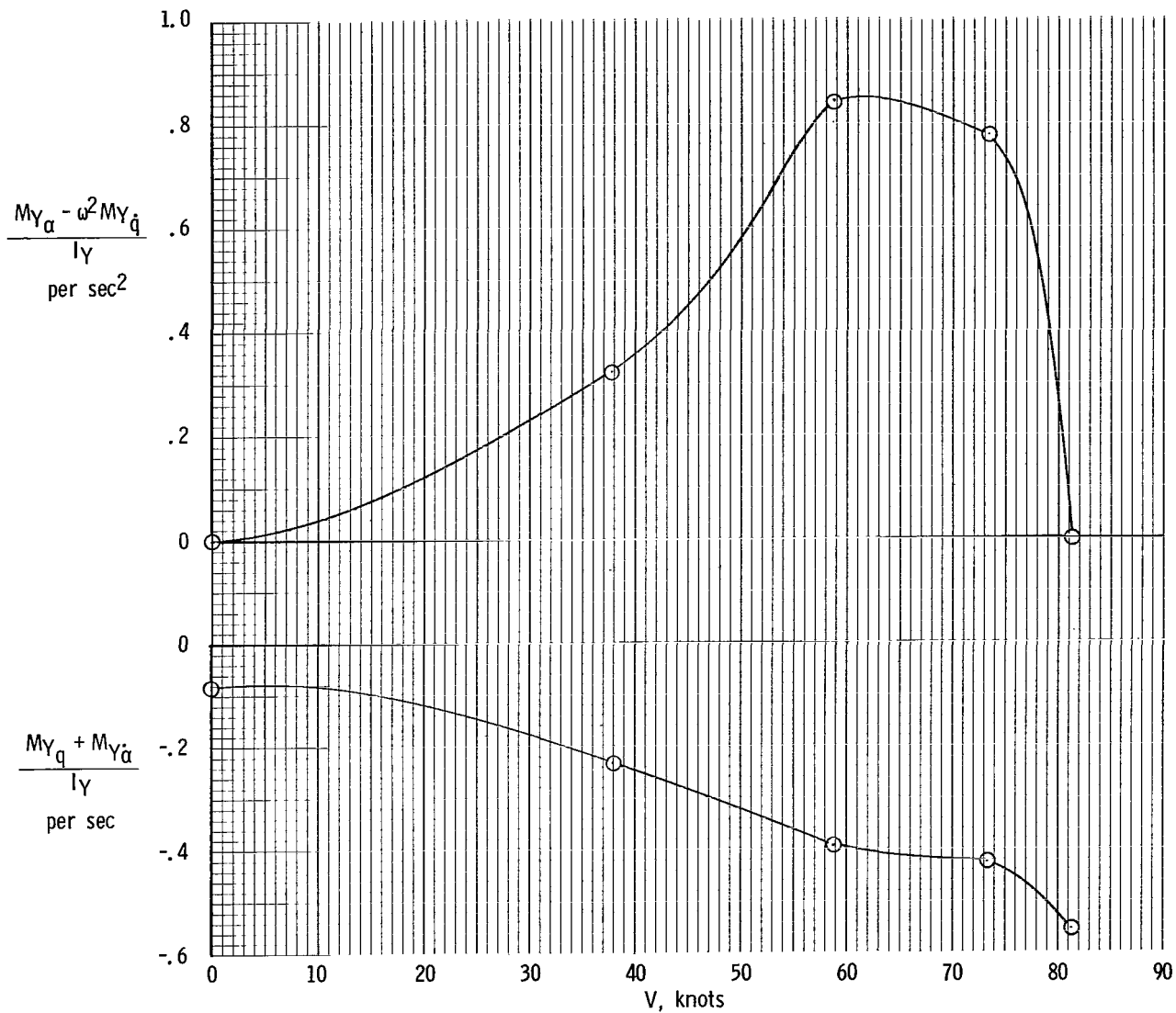


Figure 51.- Variation of static longitudinal stability parameter and damping-in-pitch parameter with forward speed for the full-scale airplane (based on scaled-up model data). $I_Y = 15\,000$ slug-ft² (20 337 kg-m²).

043 001 27 51 30S 68031 00903
AIR FORCE WEAPONS LABORATORY/AFWL/
KIRTLAND AIR FORCE BASE, NEW MEXICO 8711

DR. JAMES H. GARDNER, CHIEF TECHNICAL
LIBRARY/AFWL/

POSTMASTER: If Undeliverable (Section 158
Postal Manual) Do Not Return

"The aeronautical and space activities of the United States shall be conducted so as to contribute . . . to the expansion of human knowledge of phenomena in the atmosphere and space. The Administration shall provide for the widest practicable and appropriate dissemination of information concerning its activities and the results thereof."

—NATIONAL AERONAUTICS AND SPACE ACT OF 1958

NASA SCIENTIFIC AND TECHNICAL PUBLICATIONS

TECHNICAL REPORTS: Scientific and technical information considered important, complete, and a lasting contribution to existing knowledge.

TECHNICAL NOTES: Information less broad in scope but nevertheless of importance as a contribution to existing knowledge.

TECHNICAL MEMORANDUMS: Information receiving limited distribution because of preliminary data, security classification, or other reasons.

CONTRACTOR REPORTS: Scientific and technical information generated under a NASA contract or grant and considered an important contribution to existing knowledge.

TECHNICAL TRANSLATIONS: Information published in a foreign language considered to merit NASA distribution in English.

SPECIAL PUBLICATIONS: Information derived from or of value to NASA activities. Publications include conference proceedings, monographs, data compilations, handbooks, sourcebooks, and special bibliographies.

TECHNOLOGY UTILIZATION PUBLICATIONS: Information on technology used by NASA that may be of particular interest in commercial and other non-aerospace applications. Publications include Tech Briefs, Technology Utilization Reports and Notes, and Technology Surveys.

Details on the availability of these publications may be obtained from:

SCIENTIFIC AND TECHNICAL INFORMATION DIVISION
NATIONAL AERONAUTICS AND SPACE ADMINISTRATION

Washington, D.C. 20546